UNIVERSITÀ DEGLI STUDI DI PADOVA

DIPARTIMENTO DI INGEGNERIA DELL'INFORMAZIONE

UNIVERSITY OF PADUA

DEPARTMENT OF INFORMATION ENGINEERING

MASTER'S DEGREE IN BIOENGINEERING

"FEASIBILITY STUDY OF A ROBOTIC PROSTHETIC HAND WITH BILATERAL GRASPING ACTUATION"

Supervisor: Prof. / Dott Nicola Petrone

Candidate: Filippo Prandi

Student ID: 2130905

Co-supervisor: Eng. / Dott Emanuele Gruppioni

Co-supervisor: Eng. / Dott Marcello Valori

ACADEMIC YEAR 2025 – 2026

Graduation date: 7 July 2026

Abstract – Italian Version

La perdita di un arto superiore comporta conseguenze funzionali, psicologiche e sociali profonde, rendendo la protesica d'arto superiore un ambito di primaria importanza nella bioingegneria. Sebbene le mani protesiche robotiche moderne abbiano compiuto notevoli progressi in termini di attuazione, controllo e sensoristica, praticamente tutti i dispositivi disponibili in commercio e in ambito di ricerca si basano su un paradigma di presa unilaterale, in cui la forza di contatto è generata esclusivamente dalla chiusura delle dita verso il palmo. La superficie dorsale della mano, anche nei design underactuated, soft-robotici o con attuazione dorsale, rimane un elemento strutturale passivo che non contribuisce alla generazione della presa.

Questa tesi, sviluppata presso il Centro Protesi INAIL di Budrio, presenta uno studio di fattibilità di una mano protesica robotica capace di **presa bilaterale**, ossia di una presa attiva ottenuta tramite chiusura sia palmare che dorsale. Il lavoro estende il concetto a una mano completa a cinque dita, ciascuna azionata in modo indipendente da un motore in corrente continua dedicato, da un riduttore multistadio e un accoppiamento conico, con un pollice in grado di ruotare tra il lato palmare e quello dorsale.

Il processo di progettazione, condotto tramite Autodesk Inventor e sviluppato attraverso sei prototipi successivi, ha riguardato il sistema di trasmissione del moto, il telaio di supporto delle dita, il meccanismo di rotazione del pollice e il suo collegamento al palmo, risolvendo progressivamente problemi di interferenza cinematica, scivolamento dei cavi, allineamento, fragilità dei componenti riscontrati nella prototipazione rapida (FDM, powder-bed fusion) e la lavorazione CNC.

L'assemblaggio e i test sperimentali preliminari, condotti sul singolo dito, sul pollice e sulla sua rotazione dal lato palmare a quello dorsale, non essendo stato possibile, per vincoli di tempo e problemi legati alla stampa 3D, testare la mano completa, hanno confermato che i tempi di chiusura, la coppia e la velocità soddisfano gli obiettivi di progetto, validando il concetto di attuazione bilaterale. Sebbene non sia stato possibile completare un prototipo pienamente funzionante della mano intera entro i tempi del progetto, i risultati dimostrano la fattibilità meccanica e cinematica di un'architettura a presa bilaterale, con dimensioni comparabili a quelle di una mano adulta. Questo lavoro getta le basi per lo sviluppo futuro di mani protesiche e robotiche non antropomorfe, con possibili applicazioni che spaziano da dispositivi protesici ambidestri a sistemi di presa per l'automazione industriale.

Abstract

The loss of an upper limb has profound functional, psychological and social consequences, making upper limb prosthetics a field of primary importance in bioengineering. Although modern robotic prosthetic hands have made significant progress in terms of actuation, control and sensor technology, virtually all devices available on the market and in research are based on a unilateral grasping paradigm, in which contact force is generated exclusively by the fingers closing towards the palm. The dorsal surface of the hand, even in underactuated, soft-robotic or dorsally actuated designs, remains a passive structural element that does not contribute to the generation of the grip.

This thesis, carried out at the INAIL Prosthetics Centre in Budrio, presents a feasibility study of a robotic prosthetic hand capable of bilateral grasping, that is, an active grip achieved through both palmar and dorsal closure. The work extends this concept to a complete five-fingered hand, each finger driven independently by a dedicated DC motor, a multi-stage gearbox and a bevel gear coupling, with a thumb capable of rotating between the palmar and dorsal sides.

The design process, carried out using Autodesk Inventor and developed through six successive prototypes, focused on the motion transmission system, the finger support frame, the thumb rotation mechanism and its connection to the palm, progressively resolving issues relating to kinematic interference, cable slippage, alignment and component fragility encountered during rapid prototyping (FDM, powder-bed fusion) and CNC machining.

Assembly and preliminary experimental tests, carried out on a single finger, the thumb and its rotation from the palmar to the dorsal side, as it was not possible to test the complete hand due to time constraints and issues related to 3D printing, confirmed that the closing times, torque and speed meet the project objectives, thereby validating the concept of bilateral actuation. Although it was not possible to complete a fully functional prototype of the entire hand within the project timeline, the results demonstrate the mechanical and kinematic feasibility of a bilateral grasping architecture, with dimensions comparable to those of an adult hand. This work lays the foundations for the future development of non-anthropomorphic prosthetic and robotic hands, with potential applications ranging from ambidextrous prosthetic devices to gripping systems for industrial automation.

Table of Contents

Introduction and Objectives……………………………………………………………9

Chapter 1- Overview of the current state of the art in bilateral-grip robotic prosthetic hands……11

1.1 Introduction………………………………………………………………………………11

1.2 Grasping architectures in robotic prostheses: the unilateral paradigm……………….............11

1.3 Underactuated and soft robotic hands: increased adaptability but not bilateralism…………...13

1.4 Sysyem with rear actuation: distinction between actuation and grip…………………………14

1.5 Lack of bilateral-grip prosthetic hands……………………………………………………..15

1.6 Technological limitations…………………………………………………………………...16

1.6.1 Kinematic constrains and mechanical interferences……………………………………..17

1.6.2 Size and weight…………………………………………………………………………..17

1.6.3 Comfort and user interface……………………………………………………………… 17

1.6.4 Control complexity………………………………………………………………………18

1.6.5 Sensors and feedback……………………………………………………………………18

1.6.6 Trade-off between dexterity and stability………………………………………………..19

1.7 Research Opportunities……………………………………………………………………..19

1.7.1 Introduction of active back surfaces……………………………………………………..19

1.7.2 Hybrid architectures combining anthropomorphic hands and grippers………………….20

1.7.3 Enveloping grasping strategies…………………………………………………………..20

1.7.4 New control strategies…………………………………………………………………...20

1.7.5 Distributed sensors and feedback………………………………………………………...21

1.7.6 Potential Impact…………………………………………………………………………..21

Chapter 2 – Materials and Methods……………………………………………………………..22

2.1 Mechanical design…………………………………………………………………………..22

2.1.1 CAD Software – Autodesk Inventor Professional………………………………………..23

2.1.2 Printers used………………………………………………………………………………24

2.1.3 Three – phalanx finger models……………………………………………………………25

2.1.3.1 Description of the tendon – driven finger……………………………………………...26

2.2 Objectives……………………………………………………………………………………29

2.3 Motion trasmission system…………………………………………………………………..34

2.3.1 Brushed DC motors……………………………………………………………………..34
2.3.2 Multistage planetary gearboxes…………………………………………………………36
2.3.3 Power trasmission components…………………………………………………………38
2.3.3.1 Bevel gears and bevel gears couplings………………………………………….38
2.3.3.2 Worm gear – helican gear……………………………………………………….40
2.4 Design of the drive train…………………………………………………………….…..42

Chapter 3 – Hand Models and Prototypes Developments………..……………………………..47
3.1 First model…………………………………………………………………………………..47
3.1.1 Finger holder frame – first model………………………………………………………49
3.1.2 Fist thumb design…………………………………………………………………….....51
3.2 Second model……………………………………………………………………………..51
3.3 Third model………………………………………………………………………………….56
3.4 Fourth model………………………………………………………………………………...64
3.4.1 New connection component……………………………………………………….....69
3.4.2 Thumb………………………………………………………………………………….73
3.4.3 Connection between the thumb and the frame…………………………………………76
3.5 Fifth model…………………………………………………………………………………..79
3.5.1 Thumb………………………………………………………………………………….82
3.6 Sixth model………………………………………………………………………………….84
3.6.1 Thumb………………………………………………………………………………….86
3.6.2 Further changes………………………………………………………………………...89
3.6.3 Other components……………………………………………………………………...91

Chapter 4 – Results………………...…………………………...………………………...94
4.1 Assembly and considerations……………………………………………………………….94
4.2 Performance testing…………………………………………………………………………99

Conclusions…………………………………………………………………………………..103

Bibliography…………………………………………………………………………………105

Introduction and Objectives

The loss of an upper limb is a highly debilitating condition, with significant repercussions not only on the individual's functional ability, but also on their independence, identity and quality of life. In this context, upper limb prosthetics is a field of fundamental importance within bioengineering, aiming to restore, at least in part, the compromised motor and sensory functions. Over the last few decades, this sector has undergone significant evolution, moving from purely mechanical devices to increasingly sophisticated systems, characterised by advanced electronic components and control strategies based on biological signals.

At the same time, the development of bionics has opened up new prospects in the design of smart prostheses, introducing the concept of bidirectional interaction between human and device. Bionics, in fact, does not merely passively replicate the function of the missing limb, but aims to create functional and perceptual integration between the biological and artificial systems. This translates into the development of human-machine interfaces capable of acquiring neural or myoelectric signals to control the device and, at the same time, providing sensory feedback to the user, enhancing the sense of embodiment and the naturalness of movement.

Despite significant technological advances, there remains a considerable gap between the performance of currently available prostheses and the biomechanical and sensory complexity of the human limb. The main challenges concern the accuracy and reliability of control systems, the provision of effective sensory feedback, the miniaturisation of components, and the optimisation of the interface with biological tissues. In this context, research in bioengineering plays a central role, fostering the integration of multidisciplinary expertise ranging from electronic and mechanical engineering to neuroscience, from robotics to materials science. Based on these considerations, my Master's thesis was carried out at the INAIL Prosthetics Centre in Budrio (BO), a centre with extensive experience in the field of limb prosthetics.

The aim of this thesis was to study a robotic prosthetic hand capable of bilateral grasping, i.e. with both palmar and dorsal closure. This project paves the way for the development of devices that are not strictly anthropomorphic, presenting both opportunities and constraints in terms of design. This project was originally initiated by engineer Emanuele Gruppioni, who created an initial prototype with only two functioning fingers; the aim of this thesis, however, was to carry out a feasibility study on a complete hand, creating a new design and a new actuation system for its operation, whilst retaining only the concept of the fingers (excluding the thumb).

The first chapter will provide a review of the state of the art regarding commercially available hands and bilateral grasping mechanisms. The second chapter will describe the materials and methods used, paying particular attention to the mechanisms and couplings employed, whilst outlining the objectives set and the procedure followed. The third chapter will present the prototypes developed during this thesis project, detailing for each one the components and issues resolved in the subsequent model. Finally, in the fourth chapter, the results obtained from experimental tests will be presented, with a discussion of how the tests were carried out, the parameters compared with the calculations made, and possible solutions, before concluding.

Chapter 1

Overview of the current state of the art in bilateral-grip robotic prosthetic hands

1.1 Introduction

Modern robotic prosthetic hands aim to mimic the fundamental capabilities of the human hand, particularly its ability to grasp and manipulate objects of varying shape, volume and stiffness. Despite significant advances in actuation, control and sensing systems, almost all contemporary designs employ unilateral grasping strategies, in which force is generated exclusively by the fingers closing towards the palm.

In this context, the concept of bilateral closure, understood as the active creation of a grip using opposing surfaces, both on the palm side and the dorsal side, represents an alternative paradigm that remains largely unexplored.

1.2 Grasping architectures in robotic prostheses: the unilateral paradigm

Current robotic prosthetic hands predominantly employ grasping architectures derived from the biomechanics of the human hand, based on unilateral palmar closure mechanisms. In such configurations, the grasp is generated by the coordinated flexion of the fingers towards the palm, with the thumb playing a key role in opposing and stabilising the object [1].

The most advanced commercial solutions, developed by companies such as Ottobock, Open Bionics and Psyonic, incorporate multi-articulated fingers and various predefined grasp types, including:

- power grasp;
- precision pinch;
- lateral grasp.

These configurations are designed to cover the main modes of interaction identified in the literature on manipulation, such as the classification proposed by Cutkosky [2], which was subsequently extended to the fields of robotics and prosthetics [3].

From a mechanical point of view, these systems share certain fundamental characteristics:

- **the palm acts as the primary reaction surface**;
- the fingers generate forces directed towards the centre of the hand;
- the object's stability is achieved through the balance of internal forces between the fingers and the palm.

This paradigm has been further consolidated by the development of underactuated, synergy-based robotic hands, such as the SoftHand proposed by the Italian Institute of Technology, which utilises principles of passive adaptation to improve grip robustness [4]. In such systems, a small number of actuators control multiple degrees of freedom, enabling an automatic distribution of contact forces across the object.

Despite the advantages in terms of adaptability and ease of control, these architectures also retain an intrinsically unilateral grasping structure, in which:

- the main contact is on the palm side;
- the back of the hand does not contribute to the generation of gripping force;
- stability is limited to the fingers' ability to wrap around and press the object against the palm.

Several studies have shown that this configuration may be suboptimal when dealing with irregular or deformable objects, where a wider distribution of contact surfaces could improve stability and reduce the force required [5][6].

In particular, grasping theory shows that an increase in contact surfaces and their spatial arrangement play a crucial role in grip stability and resistance to slipping [2][5]. However, in anthropomorphic prosthetic hands, these principles are generally implemented exclusively through the action of the fingers, without involving other surfaces of the hand.

Consequently, the current state of the art reveals a heavy reliance on unilateral grasping architectures, with a notable lack of solutions that utilise configurations involving **multiple opposing surfaces**, such as in the case of bilateral palmar–dorsal closure.

1.3 Underactuated and soft robotic hands: increased adaptability but not bilateralism

In recent years, research in the field of robotic hands has seen growing interest in underactuated and soft architectures, developed with the aim of improving the adaptability and robustness of grasping whilst reducing control complexity and the number of actuators [7].

Underactuated hands are characterised by having fewer actuators than degrees of freedom, utilising passive mechanisms (such as differentials or elastic couplings) to automatically distribute motion and forces among the fingers. This approach allows the hand to adapt to the object's geometry without requiring explicit control of each joint [8].

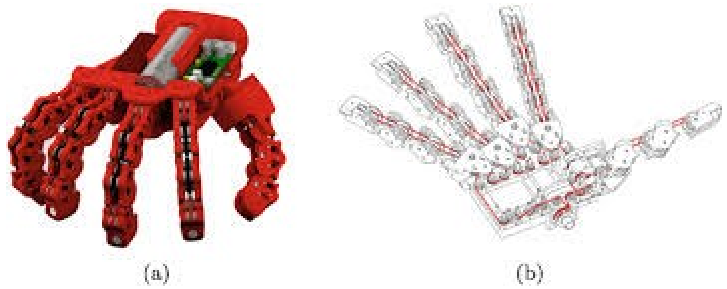

Figure 1: Pisa/IIT SoftHand

A notable example is the SoftHand, a hand already mentioned in the previous sub-section [4]. This paradigm enables robust grips even in the presence of uncertainties regarding the object's shape and position.

At the same time, the development of soft technologies has introduced the use of deformable materials and pneumatic or cable actuators, enabling the creation of highly compliant hands that interact safely with the environment [9]. Such systems are particularly effective in handling fragile or irregular objects, thanks to their ability to distribute pressure across large contact surfaces.

Despite these significant advances, underactuated and soft architectures retain one fundamental characteristic: the grip remains **inherently unilateral**. Specifically:

- the main contact is on the palm side;
- the fingers curl towards the palm in a flexed position;
- the back of the hand does not contribute to the active generation of grip force.

Even when the hand forms an 'enveloping' grasp, the object is still stabilised against the palm, whilst the dorsal side does not contribute to restraining the object.

Several studies have shown that passive adaptability improves grip quality but does not alter the interaction paradigm, which remains based on a single reaction surface [10] [6]. In other words, these systems optimise the efficiency of unilateral gripping but do not introduce a genuine **spatial redistribution of contact surfaces.**

Consequently, although they represent one of the main advances in the state of the art of robotic hands, underactuated and soft architectures do not implement bilateral closure configurations, leaving open the possibility of exploring new solutions based on opposing gripping surfaces.

1.4 Systems with rear actuation: distinction between actuation and grip

As regards technologies relevant to robotic and prosthetic hands, several configurations feature actuators and transmission systems positioned on the dorsal side of the hand. This design choice is widely adopted in rehabilitation exoskeletons and in certain robotic systems, primarily because it leaves the palmar surface free for interaction with the environment [11].

However, it is essential to clearly distinguish between two concepts that are often confused:

- Dorsal actuation, which refers to the positioning of actuators or transmission mechanisms on the back of the hand;
- Dorsal grip, which involves the active engagement of the dorsal surface in generating contact force on an object.

In the vast majority of current devices, the back of the hand serves solely as a mechanical support and a means of transmitting movement. For example, in exoskeletons used for hand rehabilitation:

- Actuators or cables are mounted on the back;
- Finger flexion and extension are mechanically assisted;
- The palm remains the primary interface surface for contact with objects [12].

This configuration is preferred for ergonomic and functional reasons, as it avoids interference with grasping operations and improves user comfort. However, this does not imply that the back of the hand actively contributes to stabilising the object.

Similarly, in some tendon-driven robotic hands, the extensor tendons are routed along the dorsal side of the fingers, contributing to movement control but not to the direct generation of gripping force [13]. In these cases too, the back of the hand does not act as an active contact surface.

From the perspective of grasping mechanics, contact force is generated by the fingers towards the palm; the palm acts as a reaction surface, whilst the dorsal surface does not contribute to the closure around the object.

In the scientific literature, grip stability is generally analysed in terms of the distribution of contact forces and the geometry of contact points [14]. In this context, the absence of a dorsal contribution implies that the entire gripping system is limited to a configuration with a single reaction surface, reducing the potential for geometric confinement of the object.

Consequently, despite the widespread use of dorsal implementation, it can be stated that:

the systems currently available on the market do not implement true bilateral grasping, as the back of the hand does not actively contribute to the generation of contact forces.
This distinction is essential to avoid terminological confusion and to correctly situate the contribution of the various technological solutions within the state of the art.

1.5 Lack of bilateral-grip prosthetic hands

A joint analysis of the scientific literature and currently available technological solutions reveals that robotic prosthetic hands are almost exclusively based on unilateral, palmar-type grasping architectures. In such systems, object stability is achieved by generating forces between the fingers and the palm, without the active involvement of dorsal surfaces.

The main commercial platforms, developed by Ottobock, Open Bionics and Psyonic, do not incorporate grasping mechanisms based on opposing palmar–dorsal surfaces. Similarly, the most advanced academic solutions, including underactuated and soft hands, maintain an interaction paradigm in which the back of the hand does not actively contribute to the generation of grip force [4][6].

Even in systems featuring active dorsal elements, as discussed in the previous paragraph, these components are used exclusively for the transmission of motion or for structural support, and not as contact surfaces that serve to stabilise the object [12].

At the same time, in the field of manipulation robotics, there are numerous examples of grippers based on opposing surfaces, which demonstrate the effectiveness of the principle of object confinement through balanced forces [15]. However, such solutions have not been significantly transferred to the field of anthropomorphic prostheses, mainly due to constraints related to morphology, size, weight and usability.

In light of these considerations, it can be stated that:

at the current state of research and technology, there are no robotic prosthetic hands in the literature or on the market that implement a true active bilateral palmar–dorsal closure.

This absence is not due to a lack of theoretical principles or analogous solutions in other fields of robotics, but rather to the complexity of integrating such concepts into an anthropomorphic prosthetic system.

Consequently, bilateral closure remains an open area of research, with the potential for significant impact in terms of:

- increased grip stability;
- better distribution of contact pressures;
- greater adaptability to complex or deformable objects.

The identification of this technological gap forms the basis for exploring new prosthetic hand architectures capable of overcoming the limitations of current solutions.

1.6 Technological limitations

Despite the potential benefits associated with the introduction of bilateral grasping in robotic prosthetic hands, the absence of such solutions in the current state of the art can be attributed to a number of **technological and design constraints** that make their implementation complex.

1.6.1 Kinematic constraints and mechanical interferences

The integration of an active dorsal surface involves the inclusion of additional moving parts within the space already occupied by the fingers during closure. This entails:

- potential interference between fingers and the back structure;
- restrictions in the range of joint motion;
- increased complexity of the kinematic structure.

Anthropomorphic robotic hands are already characterised by high mechanical complexity, and the introduction of additional degrees of freedom may compromise the system's reliability and controllability [8].

1.6.2 Size and weight

In upper limb prostheses, weight and size are critical factors affecting user acceptance. The addition of:

- additional actuators;
- movable dorsal structures;
- dedicated transmission systems

can lead to a significant increase in distal mass, with negative effects on:

- comfort;
- fatigue;
- daily usability [16].

1.6.3 Comfort and user interface

The back of the hand is a particularly sensitive area and is close to the interface with the prosthetic socket. The introduction of active elements in this area raises issues relating to:

- pressure distribution;
- the risk of discomfort or pain;
- the need for compliant and safe materials.

The design must therefore ensure a balance between mechanical functionality and ergonomic comfort, a crucial aspect for the clinical adoption of prostheses [17].

1.6.4 Control complexity

A bilateral grip requires coordination between:

- fingers (palm closure);
- any active dorsal surfaces;
- distribution of contact forces.

This introduces issues related to:

- multi-input multi-output (MIMO) control;
- force and stability management;
- synchronisation between active components.

Given that prosthetic control is often based on noisy and limited myoelectric signals, the increased complexity of the system can reduce the robustness and intuitiveness of the control [18].

1.6.5 Sensors and feedback

To make effective use of bilateral grasping, it would be necessary to:

- measure forces across multiple surfaces;
- detect distributed contacts;
- implement feedback-based control strategies.

However, the sensory systems currently integrated into prostheses are still limited and often do not provide comprehensive feedback to the user, making it difficult to control the grip precisely [19].

1.6.6 Trade-off between dexterity and stability

Anthropomorphic hands are designed to maximise dexterity, whereas opposing-surface grippers prioritise stability. The introduction of a bilateral grip involves a trade-off between:

- fine manipulation capability;
- grip strength;
- mechanical simplicity.

This trade-off represents one of the main challenges in the design of new hybrid architectures [13].

1.7 Research Opportunities

The review of the current state of the art has highlighted that existing robotic prosthetic hands are heavily reliant on unilateral grasping architectures, and that the concept of bilateral palmar–dorsal closure remains largely unexplored. This gap opens up a range of research opportunities, both from a mechanical perspective and in terms of control and human–machine interaction.

1.7.1 Introduction of active back surfaces

One initial approach involves the development of back structures capable of actively participating in the grip. Such surfaces could be designed as:

- articulated rigid elements;
- segmented structures;
- compliant or soft surfaces.

The use of deformable materials, already extensively studied in soft robotics [9], could enable the creation of dorsal surfaces capable of adapting to the object's geometry, improving pressure distribution and reducing comfort-related issues.

1.7.2 Hybrid architectures combining anthropomorphic hands and grippers

Another line of research involves integrating the principles of grippers with opposing surfaces into anthropomorphic structures. In particular, it is possible to envisage systems in which:

- the fingers retain their function of fine manipulation;
- a dorsal surface contributes to overall stabilisation.

This integration could make it possible to combine:

- the dexterity of anthropomorphic hands;
- the stability of industrial grippers.

Similar approaches have been explored in robotics to improve grip robustness, but have not yet been transferred to the field of prosthetics [6].

1.7.3 Enveloping grasping strategies

Bilateral closure naturally enables grasping strategies based on confining the object, similar to those observed in soft grippers. In such configurations:

- the object is enveloped by multiple surfaces;
- forces are distributed over larger areas;
- stability does not depend solely on local friction.

This approach is particularly advantageous when handling:

- deformable objects;
- fragile objects;
- complex or irregular geometries [20].

1.7.4 New control strategies

The introduction of a bilateral grip requires the development of dedicated control strategies capable of managing:

- coordination between the fingers and the dorsal surface;

- the distribution of contact forces;
- grip stability.

In this context, approaches based on the following show promise:

- hybrid position/force control;
- control via extended synergies;
- machine learning techniques for grip adaptation.

These methodologies have already been successfully applied to the control of complex robotic hands and could be extended to bilateral configurations [5].

1.7.5 Distributed sensors and feedback

To fully exploit the benefits of bilateral closure, it is necessary to integrate distributed sensor systems capable of detecting:

- contact forces across multiple surfaces;
- pressure distribution;
- any slippage

The development of flexible sensors that can be integrated into soft structures represents a promising avenue for enabling these functionalities [21].

1.7.6 Potential impact

The introduction of bilateral grasping in prosthetic hands could lead to significant improvements in terms of:

- grip stability;
- reduction in the force required;
- greater adaptability to complex objects;
- improved user experience.

Looking ahead, such developments could help bridge the gap between the capabilities of current prostheses and those of the biological hand, particularly with regard to safe and effective interaction with the environment.

Chapter 2

Materials and Methods

This chapter describes the materials and methods used in this thesis, which was carried out at the Research and Training Department of the INAIL Prosthetics Centre in Vigorso di Budrio. It will outline the software used to carry out the project, the main objectives and performance requirements for the robotic hand, and provide a detailed explanation of the components and mechanical couplings used. In order to perform the necessary calculations, this chapter provides a detailed explanation of how the finger works.

2.1 Mechanical Design

The aim of this thesis project is to devise a new concept for a robotic hand, which consequently also has potential applications in the field of prosthetics.

Specifically, the proposed design involves a bilaterally actuated hand, i.e. one whose fingers are capable of flexing in both directions. Consequently, for a hand of this type, it becomes impossible to define the palmar and dorsal regions a priori, thereby losing the anthropomorphic curves and directionality of the fingers found in a conventional prosthetic hand.

Autodesk Inventor Professional 3D CAD software was used to design this hand. By exporting the created files in STL format, it was possible to produce some of the components for an initial prototype of the hand using rapid additive prototyping techniques. In future, these parts will be replaced by bespoke machined components made from aluminium, ensuring greater structural rigidity and a better fit at the critical points. For those components requiring greater mechanical strength, such as the main support shaft, additional secondary shafts and the finger pins, metal components were instead chosen. The main shaft and the purchased mechanical components underwent further machining, thanks to collaboration with the DII at the University of Padua, in order to achieve the required fits, using technical drawings generated by CAD and machined by CNC machines.

2.1.1 CAD Software – Autodesk Inventor Professional

Autodesk Inventor Professional is a 3D CAD software package developed by Autodesk, used primarily for mechanical design, parametric modelling and the development of industrial products. The programme enables users to create 3D solid models, complex assemblies and 2D technical drawings, whilst incorporating tools for simulation, mechanical analysis and technical documentation.

The software is based on a parametric modelling approach, which allows geometries and dimensional relationships to be defined in such a way that they can be modified at any stage of the project. This feature makes it possible to automatically update components, assemblies and technical drawings following design changes, thereby improving the efficiency of the development process.

In the field of robotics and prosthetics design, Autodesk Inventor Professional is used to create complex mechanical components, verify kinematic linkages and simulate the behaviour of assembled systems. Furthermore, the software allows models to be exported in various formats compatible with digital manufacturing technologies, including the STL format, commonly used in 3D printing and rapid prototyping processes.

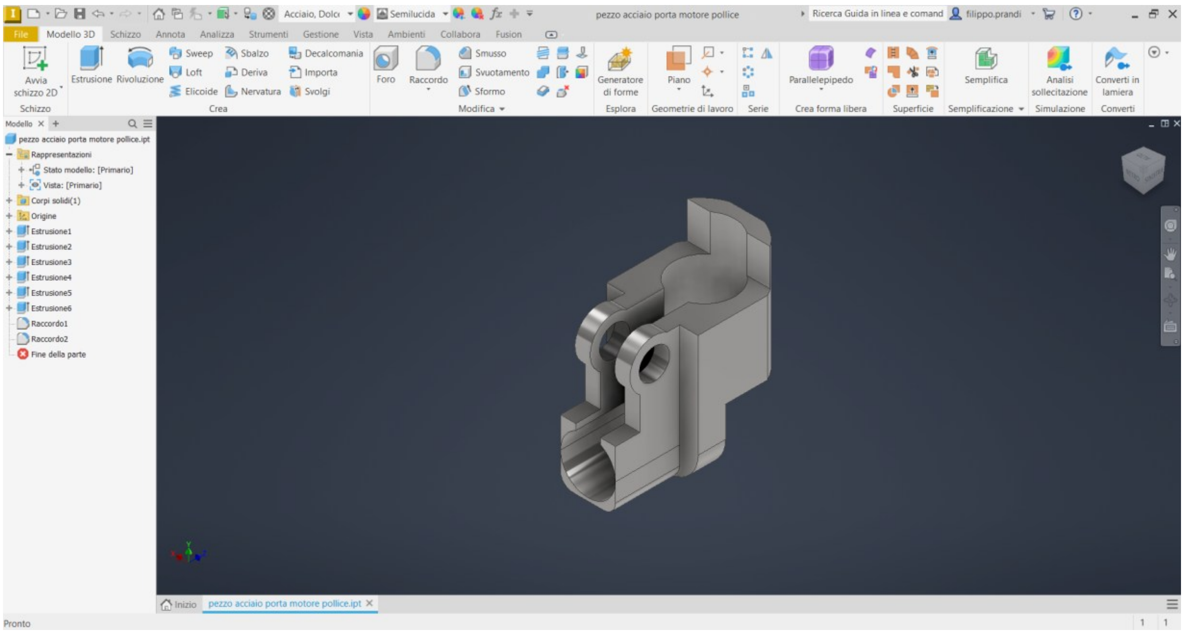

Figure 1: An example of a part created in Autodesk Inventor

Key features of the software include parametric 3D modelling, the design of mechanical assemblies, the automatic generation of technical drawings, kinematic and structural simulations, the management of materials and physical properties, and export to CAM systems and additive manufacturing technologies.

Thanks to these features, Autodesk Inventor Professional is a widely used tool in the fields of mechanical engineering and industrial design, making it particularly suitable for the development of functional prototypes and complex mechatronic devices.

2.1.2 Printers used

During the course of this thesis, a number of tests were carried out using rapid prototyping techniques, which were employed both to produce various frames for the final prototype and to assess the actual dimensions and structural challenges of certain components during the design phase. The HP Jet Fusion 580 Colour printer was used extensively; this is an all-in-one industrial system from HP designed for the production of functional prototypes and final parts in full colour (CMYK spectrum) with engineering-grade mechanical properties. It utilises HP's proprietary Multi Jet Fusion (MJF) technology, which enables the production of polyamide (PA12) parts with excellent mechanical properties, high dimensional accuracy and colours integrated directly during the printing process. Thanks to colour control at the voxel level (the three-dimensional equivalent of a pixel), the machine is capable of producing models with graphic details, textures and lettering directly incorporated into the part, reducing the need for post-processing. Compared to larger MJF systems in the range (such as the 4200 or 5200 series), the 580 integrates the build chamber, material mixing and automatic powder recovery into a single compact unit. The Multi Jet Fusion technique belongs to the family of powder bed technologies. A thin layer of polymer powder is spread over the build platform, and special inkjet heads selectively deposit fusing agents, details and colour. Subsequently, a heat source fuses only the relevant areas, consolidating the material layer by layer until the final component is achieved. This process allows complex geometries to be produced without support structures, ensuring high productivity, a good surface finish and uniform mechanical properties throughout the part.

During the printing of a model to test the required torque and speed specifications, the pulley wheels were produced using filament-based 3D printing. Fused filament fabrication (FFF), also known as Fused Deposition Modelling (FDM), is an additive manufacturing technology that creates three-dimensional objects through the controlled deposition of a molten thermoplastic filament. The material, wound onto a spool, is fed into an extruder which heats it to its melting point and deposits it layer by layer, following the path defined by the digital model. Each layer adheres to the previous one until the complete part is formed. This technique is among the most widely used thanks to its low cost, ease of use and the wide availability of materials, such as PLA, ABS, PETG and nylon, making it particularly suitable for rapid prototyping, concept models and the production of customised components.

2.1.3 Three-phalanx finger models

During this project, the first phase involved brainstorming numerous ideas for the design of the robotic prosthetic hand, evaluating various actuation systems, which led to different gripping mechanisms, each with their own possible finger prototypes. The main solutions considered led to the development of a prototype that enabled gripping via rigid links, whilst another prototype enabled gripping via cables.

Robotic grippers with rigid links are articulated systems consisting of mechanical segments connected to one another via rotary joints or hinges. The bending motion is transmitted via a kinematic chain comprising levers and rigid links, driven directly by electric motors or other mechanical actuators.

This configuration allows for precise control of the position and trajectory of the phalanges, ensuring high structural rigidity and good force transmission capacity. Furthermore, rigid-link mechanisms are generally more robust and predictable from a kinematic point of view, facilitating modelling and control operations.

However, such systems can present greater mechanical complexity and an increase in the overall weight of the robotic hand, especially when the actuators are integrated directly within the fingers.

In contrast, robotic fingers that close using cables, also known as tendon-driven fingers, use cables or flexible wires to transmit motion from the actuators to the finger joints, in a manner similar to how the tendons in the human hand function.
In this configuration, flexion is achieved by pulling the wires, whilst extension can be achieved using springs, elastic elements or, as in this case, a second system of opposing cables. The actuators can be positioned outside the hand, thereby reducing the bulk and mass of the fingers.
This approach allows for the creation of lighter, more compact and biomimetic structures, as well as conforming naturally to the object’s geometry during the grasping phase, distributing contact forces

more evenly. On the other hand, wire-based systems can be subject to elasticity, wear and loss of tension, which make motion control more complex compared to rigid-link mechanisms.

To reduce the complexity of the model and incorporate an adaptive grip, it was decided to proceed with the tendon-driven model.

2.1.3.1 Description of the tendon-driven finger

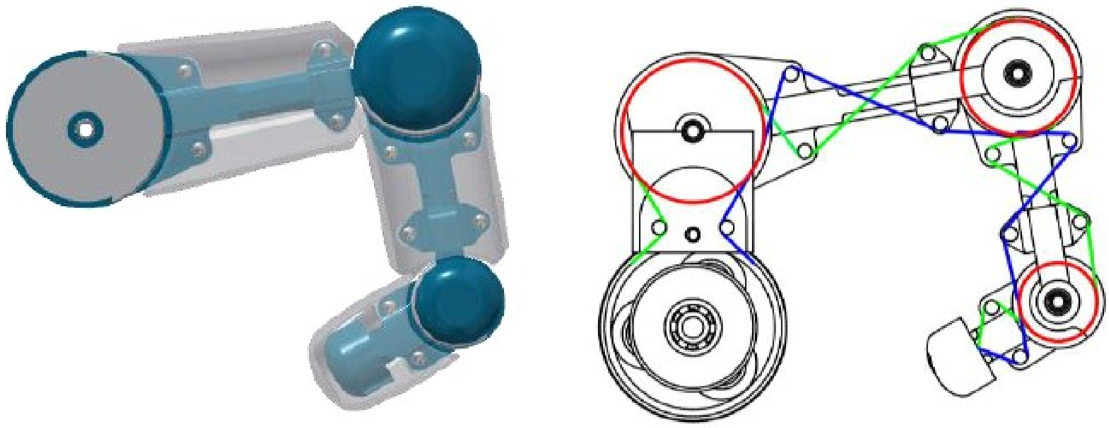

Figure 2: Model of the three-phalanx finger

The finger model used reflects the anatomical dimensions and proportions of a normal index finger. For this first hand prototype, it was decided that the four three-phalanx fingers would all be based on the same model.

The movement of the structure is achieved by a pair of Dyneema cables (one for each direction of flexion), each wrapped around a pulley located proximally and secured to the distal phalanx; the actuation acts on the pulleys, tensioning one of the two cables and thus generating a torque around the joints that causes the phalanges to move. The instantaneous balance between the driving torque, resulting from the tensile force and the joint radii, and the resisting torque, due to the elements opposing the movement (including elastic components), determines the specific sequence in which the phalanges flex. During operation, it is essential that the length of cable wrapped around one pulley corresponds exactly to the length of cable unwound from the other pulley. The limit switches have been designed so that the metacarpophalangeal joint and the proximal interphalangeal joint reach a flexion of 90° (on both sides), whilst the distal joint is limited to 45°.

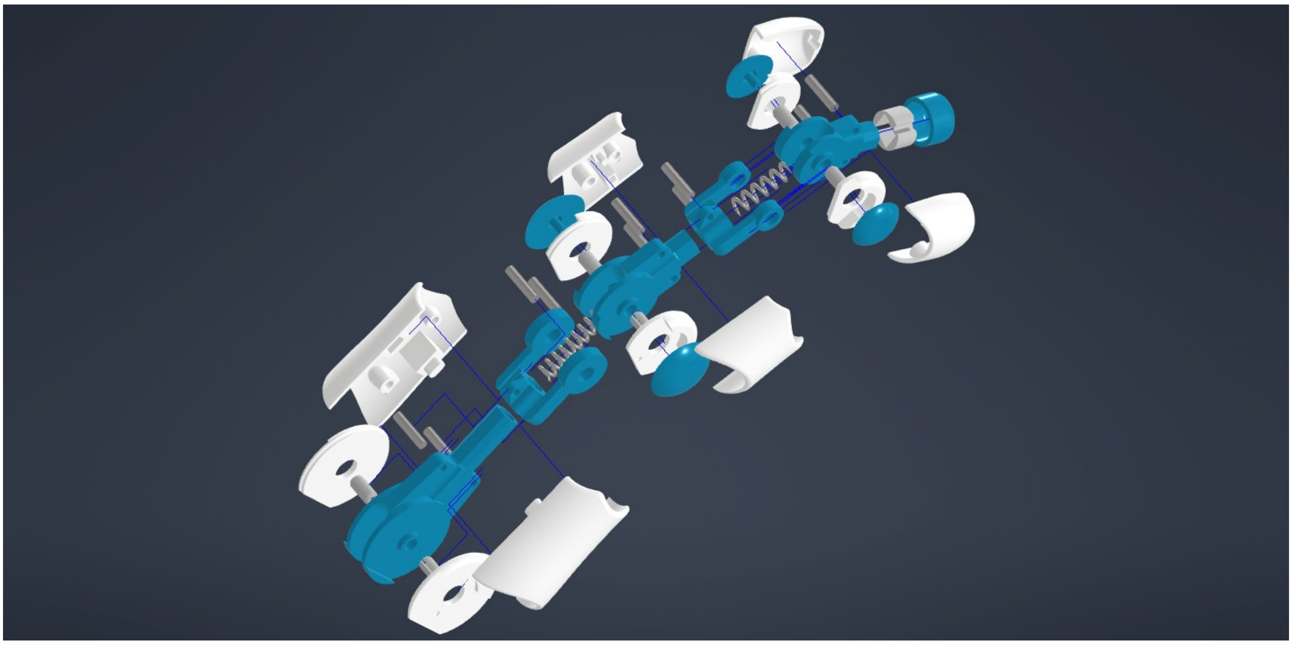

Figure 3: exploded view of the finger

The structure features three springs, one for each joint, inserted proximally into the fork and distally into the shank (the first spring, located between the fork and the finger holder, is shown in the final prototype). The use of springs and the perforation of the stems allowed for the creation of a cavity running the entire length of the finger; this feature was designed to provide the finger with sensor capability, as the sensor cables would be housed within it without interfering with the mechanisms.

The model consists of three main parts: a proximal phalanx, an intermediate phalanx and a distal phalanx. Each phalanx is divided into further components for assembly purposes; as can be seen from the figure, each phalanx features a central body and a connecting section for the next phalanx (both hollow to allow the cables to pass through), the pins that allow the cables to pass through, and the springs that form the elastic part of the prototype. Each phalanx is fitted with a pulley over which the cables will pass, creating a symmetrical path for the cables that will join at the grey/blue cap shown on the distal phalanx. It is important to ensure that the cables are of equal length on both sides and that they are correctly tensioned to prevent unwanted slackening, which could cause the cables to slip out of their guides and interrupt movement. Finally, covers were created to cover all three phalanges; this gave the finger a symmetrical structure and shape. As its function is to close from both the dorsal and palmar sides, it was decided to omit details typical of an anthropomorphic finger, such as nails and curves, as this would compromise its bilateral function [22].

The proximal phalanx has a total length of 43.5 mm (the distance between the centres of the first and second phalanges), the middle phalanx 27.5 mm and the distal phalanx 20 mm, resulting in a maximum cross-sectional thickness of 20 mm; these measurements are based on the anthropometric values of an adult male's index finger.

The white inner pulleys have diameters of 10 mm, 7.5 mm and 6 mm respectively; we will need these values later to calculate the torque and speed requirements for the finger, so any change to them will necessitate a recalculation of the specifications. These 28omponent salso serve another function, namely that of a physical limit switch; as mentioned earlier, each joint has its own range of motion (90° for the first two and 45° for the last).

The cable used has a Dyneema SK75® core and a polyester sheath, and has a diameter of 0.9 mm. Dyneema SK75® is a highly durable and lightweight material used in the marine sector for ropes and nets, as well as in a wide range of industrial applications. The molecular structure of the fibres is derived from a solvent spinning process of Ultra-High Molecular Weight Polyethylene (UHMWP), which gives the fibres excellent alignment and a high degree of crystallinity.

The springs in the joints help the mechanism return from the closed position to the open position, a task already performed by the cables, as they balance each other out.

2.2 Objectives

One of the first aspects considered during the design of this bilateral hand was the requirements it would need to meet.

In Engineer Gruppioni's prototype, a drive system comprising a Faulhaber 1717 012 SR brushed DC motor (rated at 2.2 mNm and 6650 rpm), with a cyclo reduction first stage, a synchronous pulley second stage and a differential epicycloidal third/fourth stage, which allows two fingers to be moved simultaneously by the same motor [22].

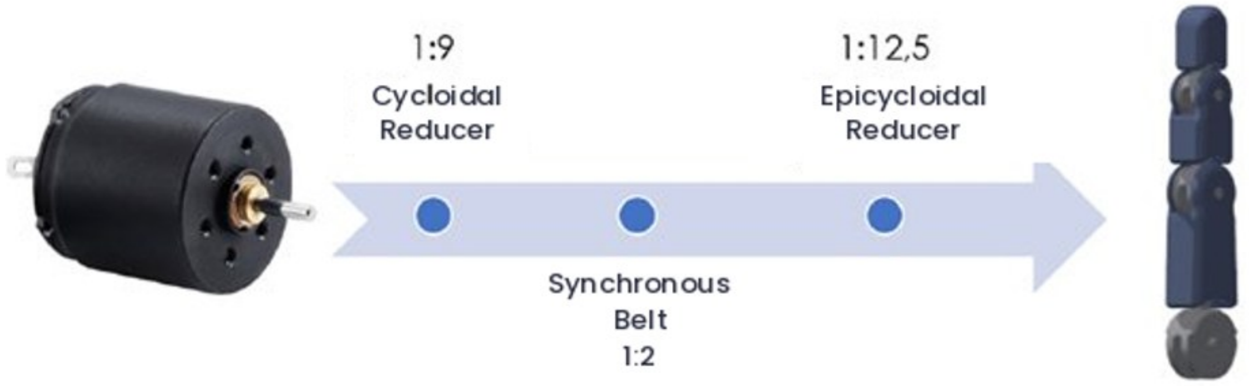

Figure 4: implementation and reduction system

This prototype was limited to the development of an actuation system for just two fingers, whereas the new prototype was intended to incorporate the remaining three fingers, including the thumb, which presented a number of issues that we will examine in the following sections.

Initially, we started from the basis of this work, integrating additional actuation systems to complete the hand; however, following further evaluation, we opted for a different approach, namely to make all five fingers independent and controlled by a single motor each. Consequently, the old actuation system was no longer a viable option due to a number of factors which we will discuss later.

It was decided that this bilateral hand must meet certain torque and speed requirements, with priority given to the latter.

As a bilateral-closing hand, it must achieve a greater range of motion than an anthropomorphic hand equipped with palmar closure only; therefore, a total closing time of $t = 1$ s was adopted, i.e. a closing time from the open configuration to complete palmar/dorsal closure of 0.5 s.

The subsequent calculations were based on the choice of finger outlined in the previous sub-section, as different choices would have been required depending on the prototype used. These calculations are the result of numerous trials and tests, involving various prototypes which we will examine in the following chapters. Another crucial factor is the availability of materials; in fact, for this project, some materials were sourced from the INAIL centre in Budrio, such as the motor and its attached multi-stage gearbox, whilst others were commercially available. Consequently, a balance had to be struck between the specifications and the materials available. Below, we will examine the final calculations, commenting on them and illustrating the issues that led to these results.

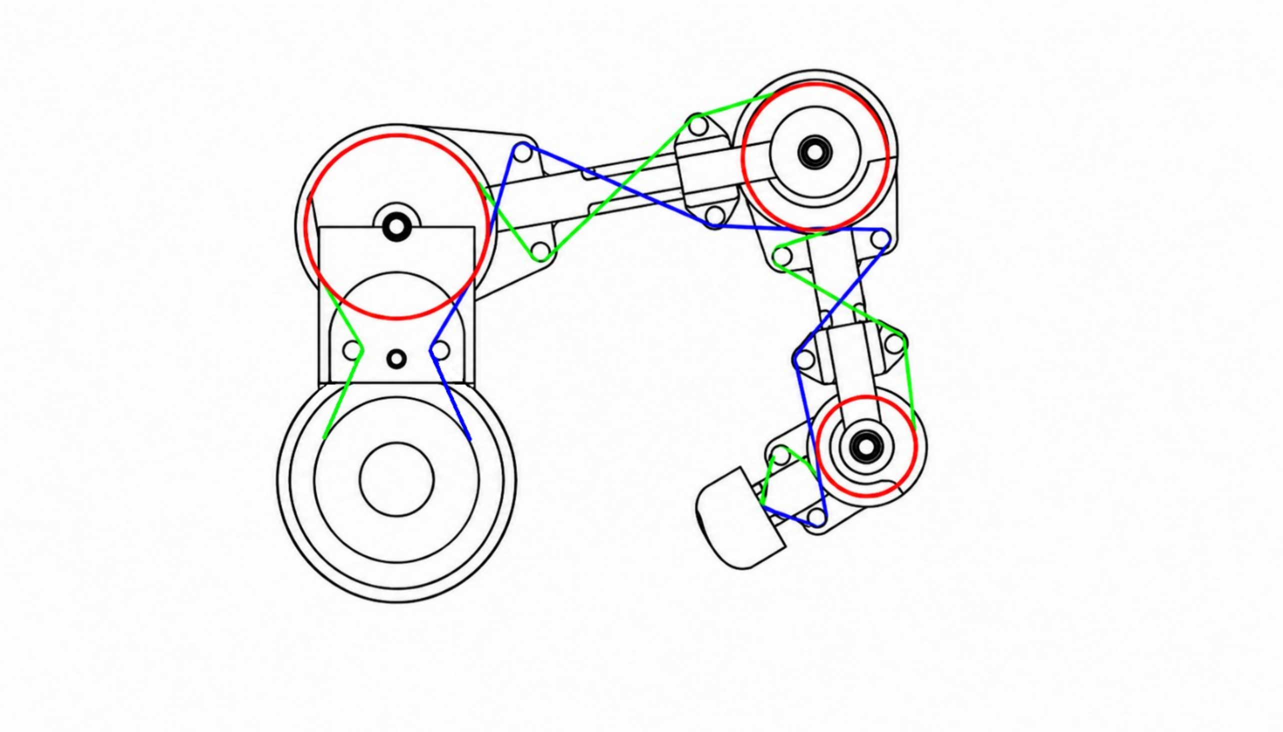

Let's start with the most important calculation, namely the closing time given above:

metacarpophalangeal joint pulley: r1=10 mm
proximal interphalangeal joint pulley: r2=7.5 mm
distal interphalangeal joint pulley: r3=6 mm
cable-winding pulley: R = 7 mm

To ensure the closing time of 0.5 s is met, we need to know the RPM at which the cable reel at the base of the finger must operate. Based on this, we need to calculate the change in rope length on each of the pulleys of the finger (arc) from the open to the closed configuration.
Formula for calculating the arc of the circumference:

$$L = \alpha \times r$$

Where:

L: length of the arc

r: radius of the circle

α: central angle subtended by the arc (rad)

Given the physical constraints imposed in the finger prototype for each joint (90° for the first two joints and 45° for the last joint), we can easily calculate the total change in the length of the string resting on the pulleys.

$$L_{tot} = r1 \times \frac{\pi}{2} + r2 \times \frac{\pi}{2} + r3 \times \frac{\pi}{4}$$

with L_{tot} = 32.2 mm

This length represents the total length of string that will be wound by the string winder once the finger is fully closed. From this, we calculate the angle subtended by the arc using the inverse formula.

$$\theta = \frac{\text{Ltot}}{R}$$

with $\theta = 4.6$ rad ≈ 263°

If I therefore consider a closing time of t = 0.5 s:

I work out the angular velocity $\omega = \frac{\theta}{t} = 9.2 \frac{rad}{s}$

Finally, I work out the frequency and, consequently, the RPM required to meet the specification:

$$f = \frac{\omega}{2\pi} = 1.46 \frac{revs}{s}$$

$$RPM = f \times 60 \text{ s} = 87 \text{ rpm}$$

The next step was to calculate the torque required on the cable-winding pulley to keep the finger in certain critical positions under load.

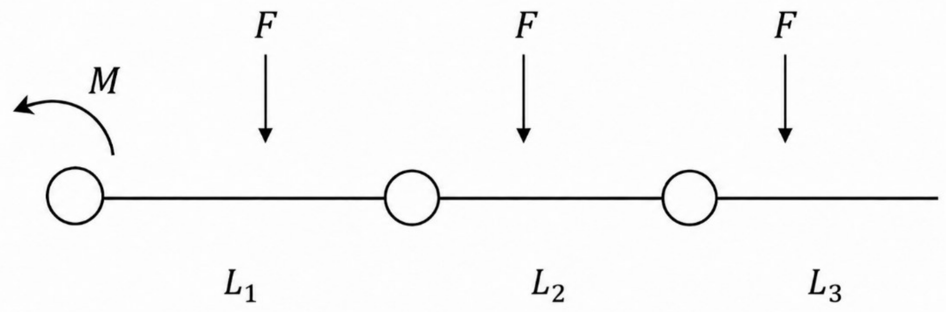

Given that the finger is subject to numerous configurations with varying distributed forces, to calculate the torque, we considered the configuration in which the finger was completely horizontal and subjected to a vertical load, so that we could calculate the maximum torque required for the finger to support the weight P in this most unfavourable configuration. Obviously, the calculation of this torque will allow for the lifting of heavier weights in configurations with more advantageous leverages.

Following an initial approach, it was decided to use a mass of 1 kg per finger, but this required a high torque that could not be achieved by the motor and reduction systems whilst maintaining the required RPM. A mass of 0.8 kg was chosen for the final calculations.

In the model shown here, to simplify the calculations, instead of using a distributed force, it was decided to use a concentrated force at the centres of the various phalanges.

Data:

length of proximal phalanx: L1 = 43.5 mm
length of middle phalanx: L2 = 27.5 mm
length of distal phalanx: L3 = 18.5 mm
m = 0.8 kg

$$Ftot = m \times g \approx 7.8\ N \qquad F = \frac{Ftot}{3} = 2.6\ N$$

Once the force and the necessary parameters had been calculated, we proceeded to solve a simple biomechanical problem. The aim was to calculate the torque M acting on the first pulley; we know that the finger is traversed by a specific sequence of cables, as shown in the previous chapters, and consequently the tension T acting on the pulley was calculated to create a state of equilibrium in the system.

$$M = F \times \frac{L1}{2} + F \times (L1 + \frac{L2}{2}) + F \times (L1 + L2 + \frac{L3}{2})$$

with $M = 414\ Nmm$

From this, we can calculate the voltage T using the inverse formula:

$$T = \frac{M}{r1} = 41.4\ N$$

This tension T represents the tension in the section of cable connecting the first pulley on the finger to the cable-winding pulley from which the motion originates; consequently, to determine the torque C acting on the cable reel, we simply need to calculate the moment acting on it.

$$C = T \times R$$

with $C = 290\ Nmm$

In conclusion, under the most critical conditions, the drive system must generate a torque of C = 290 N·mm and a speed of 87 rpm near the cable drum. It is assumed that this limit condition will never be reached, thereby providing the robotic arm with higher loads and better performance due to more favourable configurations and lever ratios.

2.3 Motion Transmission System

The previous sections have described the structure of the finger used, its operation, and the technical and performance requirements that the robotic hand must meet. This section, however, will describe in detail the actuation and motion transmission system used to achieve the required objective.

2.3.1 Brushed DC Motors

A brushed DC motor is a rotating electric machine that converts electrical energy into mechanical energy through the interaction between a fixed magnetic field (stator) and a current flowing through the rotor winding (armature). The operating principle is based on the Lorentz force: a conductor carrying a current, when immersed in a magnetic field, experiences a force that generates torque.

Structure and operating principle

The stator consists of permanent magnets (or electromagnets) that generate the excitation field B. The rotor, known as the armature, carries a winding connected to the mechanical commutator, over which graphite brushes slide. These automatically reverse the direction of the current in the conductors as the rotor turns, maintaining the force in the same direction at all times and thus providing a continuous, unidirectional torque.

Key equations

The back-EMF generated by the rotating rotor:

$$\varepsilon = K_e \cdot \phi \cdot \omega$$

where K_e is the back-EMF constant, ϕ is the magnetic flux per pole, and ω is the angular velocity of the rotor [rad/s].

The **electrical circuit equation** for the armature:

$$V = \varepsilon + R_a \cdot I_a + L_a \cdot \frac{dI_a}{dt}$$

where V is the applied voltage, R_a is the armature resistance, L_a is the armature inductance, and I_a is the armature current. In steady-state operation, the inductive term cancels out.

The **electromagnetic torque** generated:

$$C_{em} = K_t \cdot \phi \cdot I_a$$

where K_t is the torque constant. In SI units and for a constant flow rate, $K_t = K_e$.

The **steady-state velocity** is obtained by combining the two equations:

$$\omega = \frac{V - R_a \cdot I_a}{K_e \cdot \phi}$$

Mechanical power at the shaft (ignoring mechanical losses):

$$P_{mec} = C_{em} \cdot \omega = \varepsilon \cdot I_a$$

Motor efficiency:

$$\eta = \frac{P_{mec}}{P_{el}} = \frac{C_{em} \cdot \omega}{V \cdot I_a}$$

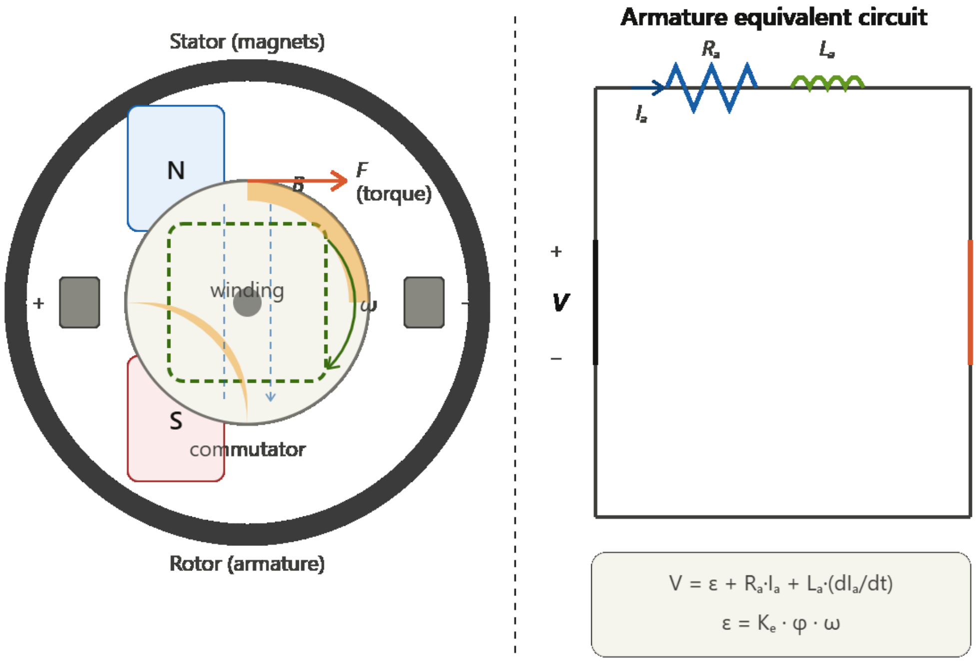

Operating Characteristics

The mechanical characteristic of a brushed DC motor (torque-speed) is **linear**: as the load increases (and thus I_a), the speed decreases proportionally. The no-load speed is $\omega_0 = V/(K_e \cdot \phi)$, while the starting torque (with the rotor locked, ω=0) is $C_{sp} = K_t \cdot \phi \cdot V/Ra$. Among the **structural limitations** of the brushed motor are brush and commutator wear, sparking (arcing) at high speeds or under heavy loads, and the need for periodic maintenance. These factors make it less suitable than brushless motors in high-reliability or high-speed applications, although it retains the advantages of circuit simplicity and direct torque control through the sole adjustment of V or I_a.

2.3.2 Multistage Planetary Gearboxes

A planetary gearbox, also known as an epicyclic gearbox, is a transmission mechanism in which multiple gears (planetary gears) rotate around a central gear (sun gear), meshing simultaneously with it and with an outer ring gear. The set of satellites is carried by an element called a planet carrier, which typically constitutes the output shaft. The coaxiality between the input and output, the distribution of the load across multiple simultaneous meshing points, and the compact design make this architecture superior to ordinary fixed-gear reducers for high reduction ratios and high power density.

The choice of which component to lock determines the behavior of the gearbox. In the most common configuration, the ring gear is locked, motion is applied to the sun gear, and the output is taken from the planet carrier. In this case, the reduction ratio of the stage is simply
$i = 1 + z_r/z_s$, that is, one plus the ratio of the ring gear's teeth to the sun gear's teeth: the larger the ring gear is relative to the sun gear, the higher the reduction ratio. Typically, a single planetary stage covers ratios ranging from 3 to 10.

This relationship follows from Willis's formula, which is the formal way to describe the kinematic link between the three elements: it states that the difference in speed between the sun gear and the planet carrier, divided by the difference between the ring gear and the planet carrier, is equal to the basic transmission ratio $i0 = z_r/z_s$. It is a linear equation in the three speeds, which means that fixing one completely determines the other two.

$$\frac{\omega_s - \omega_c}{\omega_r - \omega_c} = -i_0$$

One significant geometric consideration concerns how the number of teeth should be chosen: the sun gear must have exactly the same number of teeth as the sun gear plus twice the number of the planet gear (tangency condition), and the planet gears must be able to be positioned evenly distributed around the axis without interfering with one another. These are not mere design rules but precise mathematical constraints that limit the possible combinations of z_s, z_r, and the number of satellites N_p.

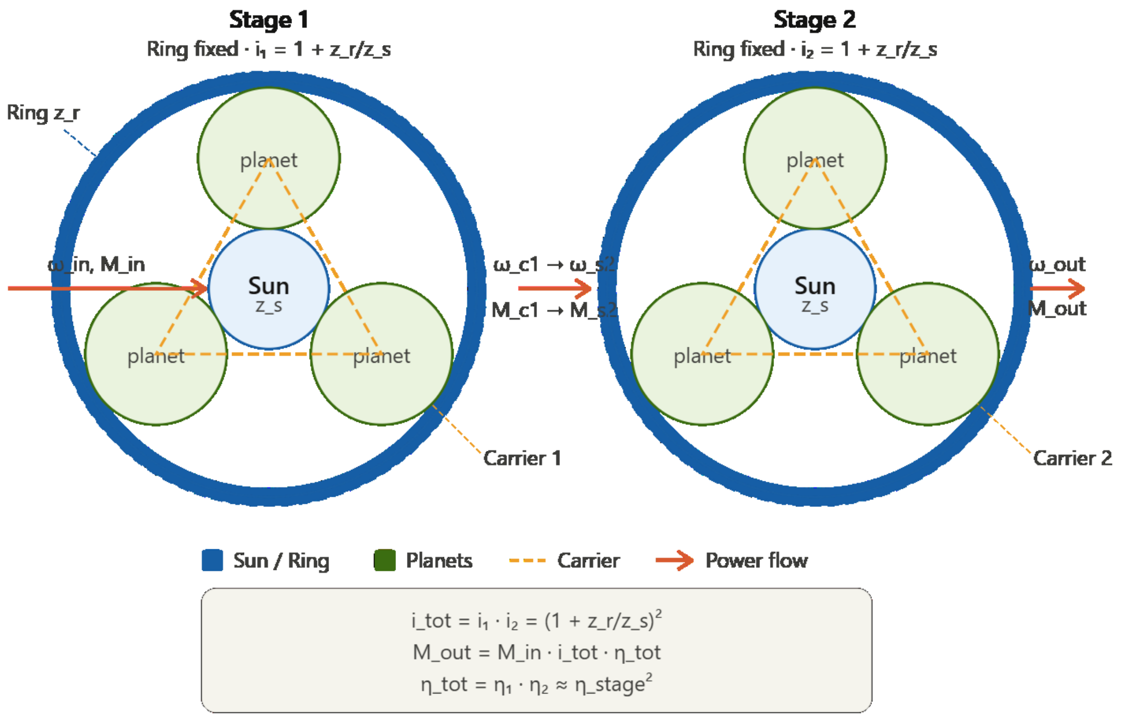

Increased performance is achieved by connecting multiple stages in series to form a multistage gearbox. The planet carrier of the first stage becomes the input shaft of the second, and so on. The total reduction ratio is the product of the partial ratios: two stages with a ratio of 5 yield 25, three stages with a ratio of 5 yield 125, and so on in a multiplicative manner. This is why multistage planetary gearboxes can achieve ratios of 100, 500, or even 1000 in a very compact space.

Torque behaves in a manner opposite to speed: it multiplies at each stage, net of friction losses. These losses are relatively modest; each stage typically has an efficiency between 0.97 and 0.99, but in a multistage gearbox they too multiply, so with four or five stages the overall efficiency can drop significantly. For this reason, whenever possible, it is preferable to minimize the number of stages while maintaining the same total ratio, optimizing the distribution of the ratio among the stages.

2.3.3 Power Transmission Components

This subsection will examine the main power transmission components. mechanical parts used to transfer motion and power from a drive source (such as an electric motor) to a load (a machine, a wheel, a pump, etc.), as used in the design.

2.3.3.1 Bevel gears and bevel gear couplings

Figure 5: pair of straight-toothed bevel gears

Bevel gears are motion transmission components used to transmit torque and power between **non-parallel shafts**, typically at a 90° angle. The geometric principle is based on two primitive cones in tangent contact at their common apex: the toothed surfaces are machined onto these cones, ensuring power transmission through meshing.

Each gear is characterized by its own **semi-angle of the primitive cone δ**, which is simply the inclination of the cone relative to the axis of rotation. In the classic case of 90° axes, the two half-angles are complementary (δ1 + δ2 = 90°) and depend directly on the gear ratio: a small gear meshing with a large one will have a very "sharp" cone, while the large gear will have a "flatter" cone. The gear ratio is simply expressed as the ratio of the numbers of teeth z_2/z_1, where z_2 and z_1 are the number of teeth on the wheel and the pinion, respectively, exactly as in ordinary cylindrical gears.

The geometry of the tooth is, however, more complex than in cylindrical gears, because the dimensions vary along the length of the tooth itself: the module, pitch and height are at their maximum at the **wide base** of the cone (outer section) and decrease towards the apex. For this reason, the **external module** m_e is always used as a reference, from which the external pitch radius $Re = m_e \cdot z/2$ and the generatrix length $L = R_e/\sin\delta$ are derived, representing the distance from the apex to the large base.

When the teeth are in mesh, the contact force between the flanks does not act in a single direction, but is broken down into three components that act on the shaft and bearings in very different ways. The **tangential component** W_t is the one that actually generates the useful torque and is proportional to the transmitted torque divided by the mean radius. The **radial component** W_r and the **axial component** W_a are both related to the pressure angle α and the cone half-angle, and tend to separate the wheels or push them along their respective axes: this is why the shafts of a bevel gear transmission always require bearings capable of withstanding axial loads, such as tapered roller bearings or axial-radial combinations.

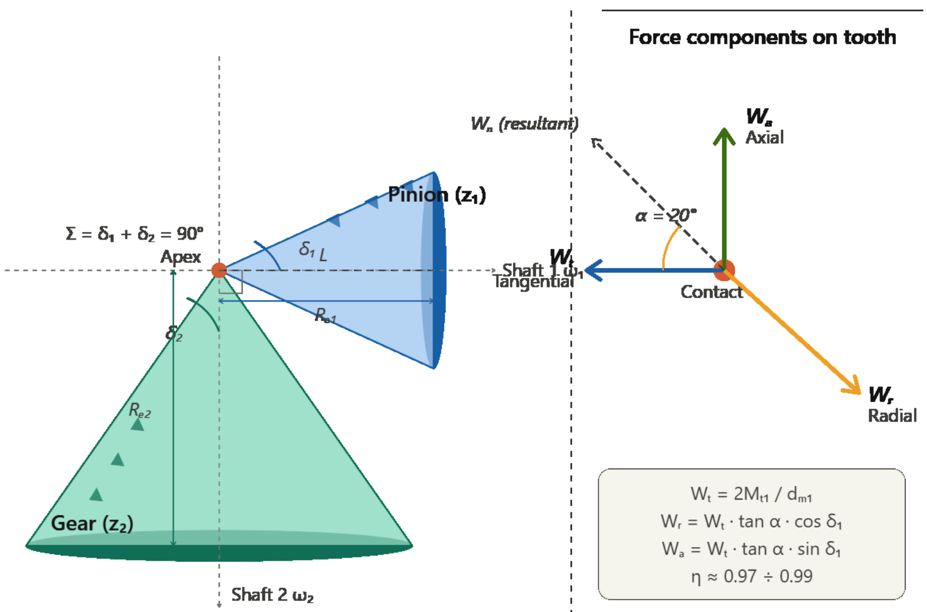

In terms of efficiency, bevel gears perform very well: their efficiency typically ranges between 0.97 and 0.99, which is comparable to that of helical gears. The main losses are due to sliding between the tooth flanks and friction in the thrust bearings, which in bevel gears are subjected to particularly high loads precisely because of the forces described above.

Types

Bevel gears are classified according to tooth geometry: **straight-toothed bevel gears**, in which the flanks converge at the apex of the cone, are the simplest to manufacture but generate noise at high speeds; **helical-toothed bevel gears** (such as the Gleason or Klingelnberg system), with teeth inclined at a helix angle β_m typically between 25° and 35°, ensure quieter operation and higher load capacity thanks to progressive meshing. By taking the helix to the extreme and offsetting the axes, hypoid gears are obtained, where the two axes do not meet but are skewed.

2.3.3.2 Worm gear – helical gear

The worm gear–helical gear combination is a transmission system that converts rotary motion between two **offset shafts**, typically at right angles, enabling very high reduction ratios within a compact space. The worm is a helical threaded element that meshes with a curved-tooth gear, the **helical gear**, partially wrapping around it. The geometry is similar to that of a screw and nut, with the difference that contact occurs along an arc of the gear rather than at a single point.

Geometry and kinematics

The fundamental geometric parameter is the **axial pitch** p_x of the worm, i.e. the axial travel per complete revolution. The **number of threads** z_w (threads of the worm) and the **number of teeth** z_g of the gear determine the transmission ratio:

$$i = \frac{\omega_w}{\omega_g} = \frac{z_g}{z_w}$$

With $z_w = 1$ (single-start screw), the highest gear ratios are achieved; with $z_w = 2.4$, the gear ratio is reduced but efficiency is improved. The helix angle λ of the screw, measured on the pitch cylinder of radius r_w, is related to the pitch:

$$\tan \lambda = \frac{z_w \cdot m_x}{2r_w} = \frac{l}{\pi d_w}$$

where $l = z_w \cdot p_x$ is the total lead, mx is the axial module and dw is the pitch diameter of the screw. The pitch diameter of the gear is given by: $d_g = m_x \cdot z_g$

The **helix angle** λ is the inclination of the screw thread relative to the plane perpendicular to its axis, and plays a central role in both the efficiency and behaviour of the system. A small angle means that the thread is almost perpendicular to the screw's axis: the mechanism tends to self-lock, because the force component that would tend to turn the screw backwards cannot overcome the friction. A large angle, on the other hand, means a more inclined thread, easier rotation in both directions, and higher efficiency. This balance between self-braking and efficiency is the fundamental trade-off of the system.

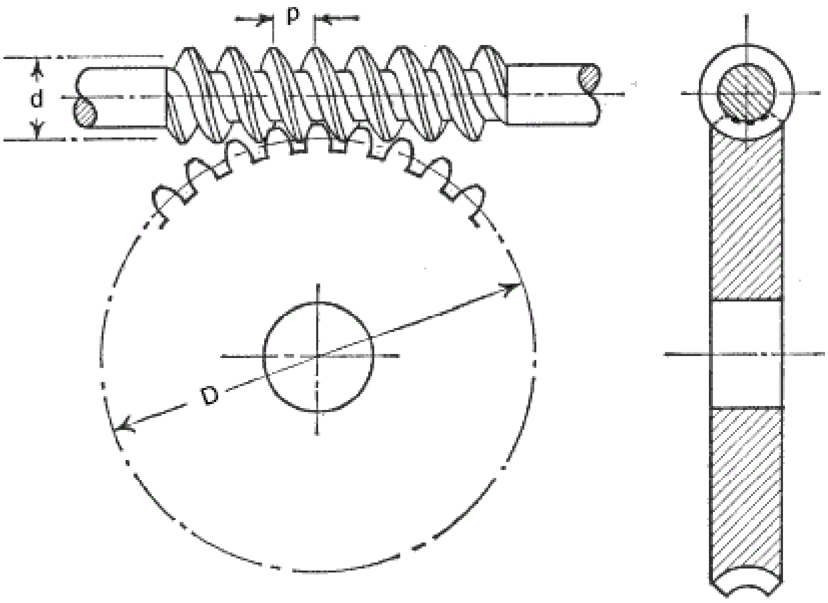

Figure 6: Worm gear and helical gear coupling diagram

Efficiency and irreversibility

Efficiency is strongly influenced by the helix angle λ and the coefficient of friction μ between the teeth (high relative sliding):

$$\eta_{w \to g} = \frac{\tan \lambda}{\tan(\lambda + \varphi)} \qquad \varphi = \arctan \mu$$

where φ is the **friction angle**. When $\lambda < \varphi$, the transmission is **irreversible** (self-locking), and the wheel is unable to drive the screw. This property is utilised in safety applications (winches, jacks, locking systems). The inverse efficiency is given by:

$$\eta_{g \to w} = \frac{\tan(\lambda - \varphi)}{\tan \lambda}$$

which becomes negative (irreversibility) for $\lambda \leq \varphi$. In practice, the direct efficiency varies between 0.5 and 0.9 depending on the propeller angle, with higher values for multi-blade propellers.

2.4 Design of the drive train

The first step in the mechanical design of the hand's drive components was the study of the drive train. This consists of a multi-stage planetary gearbox, bevel gears and pulleys.

A total of six motors were used for this project, five of which were sourced from the motors of a Bebionic® robotic hand (a prosthetic hand manufactured by Ottobock), whilst the final motor was taken from a disused thumb of an I-Limb®Access robotic hand (a prosthetic hand manufactured by Ossur).

These motors were chosen because, for an initial experiment, it was decided to use materials available in the laboratory from other prosthetic hands, on the assumption that the performance of the other hands would also be optimal for this prototype, a conclusion later confirmed by the calculations outlined above.

For this robotic hand, the decision was made to make each finger independent; consequently, the space available to create a separate actuation system for each finger was severely limited. The total space available was a 95mm x 95mm cuboid with a thickness of 23mm. Based on this available space and the calculations carried out, the actuation system was then designed.

As explained in the previous paragraph, the aim is to achieve the required specifications (82 RPM and 290 N·mm of torque) on the cable-winding pulley so that the finger moves efficiently.

We therefore started with a Faulhaber 1524T006SR DC micromotor, with a nominal voltage of 6V and a nominal power of 5W, with a diameter of 15mm and a length of 24mm.

A multi-stage planetary gearbox was fitted to the motor; this was subsequently dismantled and tested, confirming that it comprised three reduction stages. It is a Faulhaber 15/10 planetary gearbox with a reduction ratio of 37:1, a diameter of 15 mm and a length of 18 mm. With a total length of 42 mm, it offers an excellent balance between space requirements and torque output.

Following calculations, an additional reduction stage of 2.6:1 was required to achieve the target; another issue was the layout, as a connection had to be made between the output shaft of the gearbox and the cable-winding pulley, which was itself supported by a shaft positioned perpendicular to the first shaft mentioned. As for the possibility of a non-reversible system, a helical gear and worm gear combination was considered; however, the available space was insufficient, as it would have exceeded the 23mm thickness of the hand by a considerable margin; consequently, this option was ruled out.

It was therefore decided to use a straight-toothed bevel gear pair (as the loads and performance requirements did not necessitate the use of helical teeth). In the initial design, a pinion with z1 = 10 teeth and a wheel with z2 = 26 teeth were created, with a module m = 1. As it was confirmed that the wire-cut and powder-bed machines available in the laboratory could not be used, given the number of cycles and the precision required for this coupling, it was decided to search for a supplier via specialist websites. The search revealed that this coupling was not available on a large scale from major manufacturers; it would have had to be a 'custom' product made to order, exponentially increasing the cost and production time, which was an option rarely considered for a prototype.

Another problem was the mechanical coupling between the gearbox shaft and the pinion. This issue required further evaluation, leading to the rejection of potential tapered couplings due to the pinion's bore. The output shaft from the gearbox has a diameter of 3 mm, with a keyway to ensure the coupling. A pinion with a 3 mm bore diameter was required to ensure a correct fit; different dimensions would have caused problems with instability and correct alignment, leading to the subsequent drive chain jamming.

The choice therefore fell on a bevel gear pair purchased from the manufacturer Misumi. This is a coupling with a reduction ratio of 2:1; the pinion has $Z_1 = 20$ teeth whilst the wheel has $Z_2 = 40$ teeth, with a module m = 0.8; manufactured from carbon steel (ISO C45), ensuring sufficient coupling and strength to withstand the imposed loads.

マイタギヤ / ベベルギヤ
MITER AND BEVEL GEARS

モジュール **0.5** MODULE

圧力角 20°　歯数比 1：1、1：2
1：1 and 1：2 Ratio 20° PRESSURE ANGLE

JIS B1704　3 級
System of accuracy : JIS B1704 Class 3

New ねじを２箇所（120°配）にしました。
New item with two threaded holes (120°)

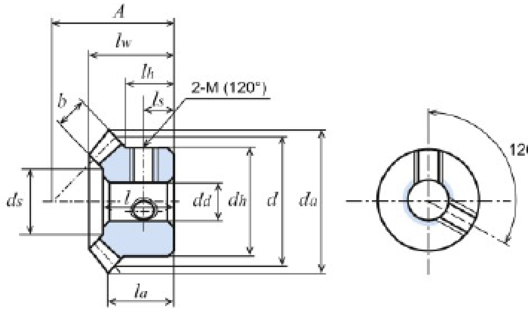

S45C 機械構造用炭素鋼
Material : Carbon Steel (ISO C45)

単位：mm
Dimensions：mm

商品記号 Catalogue Number	歯数比 Ratio u	歯数 Number of Teeth z	基準円直径 Reference Diameter d	歯先円直径 Tip Diameter da	組立距離 Locating Distance A	穴径 Bore Diameter dd(H8)	ハブ外径 Hub Diameter dh	ハブ長さ Hub Projection lh	穴長さ Bore Length l	全長 Overall Length lw	Tip Distance la	歯幅 Face Width b	ねじ Set Screw 2-M(120°)	ls	歯先角 Face Angle δa	ds	重量 Weight W(g)
M50S 20 − 1103	1	20	ϕ10	ϕ10.71	11	ϕ3	ϕ 8	5	7	8	6.35	2.5	-	-	49° 3′	ϕ 4.9	2.7
M50S 25 − 1204	1	25	ϕ12.5	ϕ13.21	12	ϕ4	ϕ11	5	7	8.11	6.10	3.0	-	-	48°14′	ϕ 6.5	5.2
M50S 30 − 1404	1	30	ϕ15	ϕ15.71	14	ϕ4	ϕ12	5	8	9.21	6.85	3.5	-	-	47°42′	ϕ 9.1	7.4
M50S 20 ∗ 1103	1	20	ϕ10	ϕ10.71	11	ϕ3	ϕ 8	5	7	8	6.35	2.5	2-M2.5	2.5	49° 3′	ϕ 4.9	2.5
M50S 25 ∗ 1204	1	25	ϕ12.5	ϕ13.21	12	ϕ4	ϕ11	5	7	8.11	6.10	3.0	2-M3	3	48°14′	ϕ 6.5	4.6
M50S 30 ∗ 1404	1	30	ϕ15	ϕ15.71	14	ϕ4	ϕ12	5	8	9.21	6.85	3.5	2-M3	3	47°42′	ϕ 9.1	7.0
B50S 20	2	20	ϕ10	ϕ10.89	15.52	ϕ3	ϕ 8	5	8	8.54	5.74	3.2	-	-	29° 8′	ϕ 5.6	3.0
B50S 40	2	40	ϕ20	ϕ20.45	10.56	ϕ4	ϕ12	4	6.3	7.31	6.01	3.2	-	-	66° 0′	ϕ13.5	8.2
B50S 20 ∗ 3	2	20	ϕ10	ϕ10.89	15.52	ϕ3	ϕ 8	5	8	8.54	5.74	3.2	2-M2.5	2.5	29° 8′	ϕ 5.6	2.8
B50S 40 ∗ 4	2	40	ϕ20	ϕ20.45	10.56	ϕ4	ϕ12	4	6.3	7.31	6.01	3.2	2-M3	2	66° 0′	ϕ13.5	7.8

【∗】(アスタ)にはセットスクリューが２個付いております。
[∗] : Gear with two threaded holes / with two set screws.

Figure 7: Technical data sheet for Misumi bevel gears used

The B50S20 *3 and B50S40 *4 models were used for this purpose. The first model mentioned represents the pinion required for coupling with the shaft; it features a 3 mm diameter bore and a side hole with a tapped thread to ensure correct coupling via a set screw: the second model represents the wheel, which instead has a 4 mm bore, corresponding to the diameter of the shaft onto which 44 twill subsequently be mounted. The dimensions of the latter fall within the specified thickness limits, resulting in a total height of the reduction system of 70 mm, leaving ample scope for the frame design discussed in the following chapters.

The decision to opt for this combination, with specifications different from those listed above, is a compromise necessitated by the unavailability of custom wheels and the engine's performance.

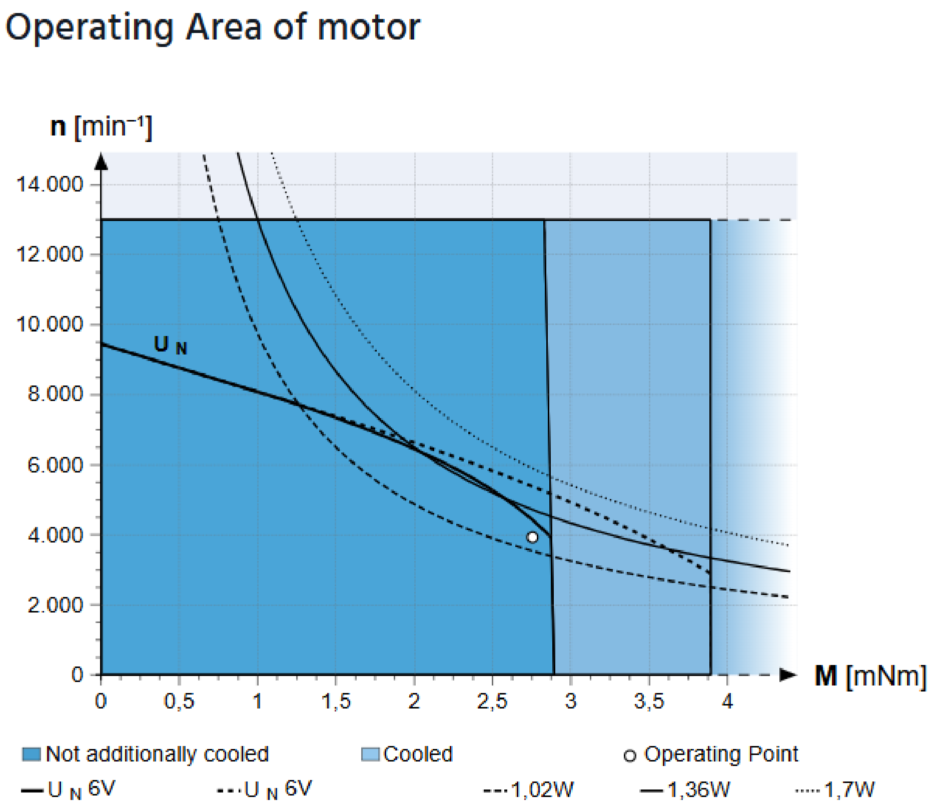

Figure 8: engine operating area

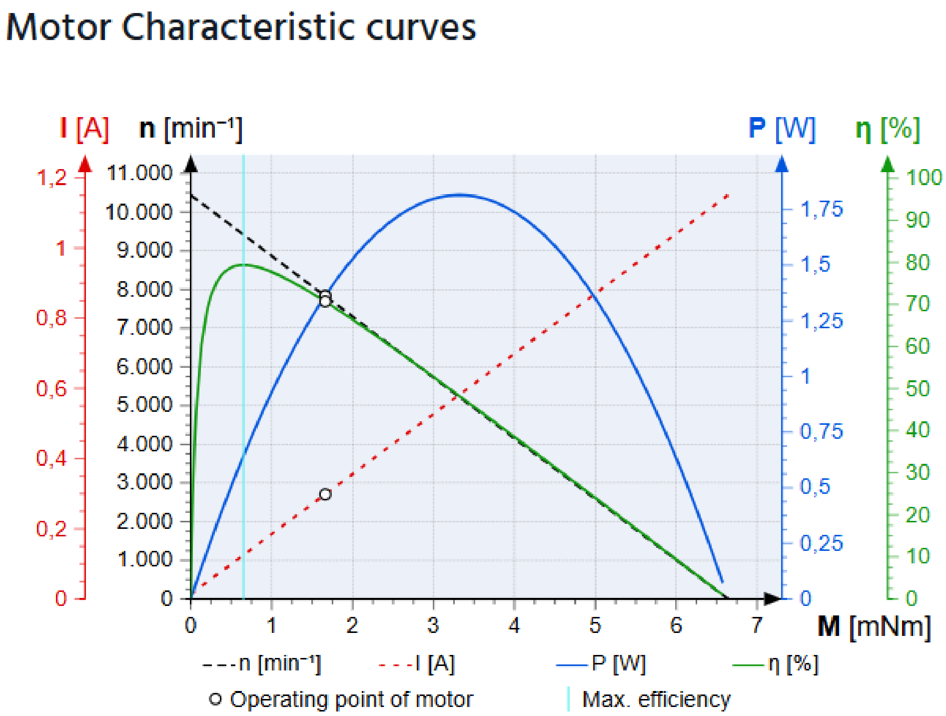

Figure 9: motor characteristic curves

As can be seen from the figures, the motor can run continuously up to a certain torque and speed; however, for our purposes, it is necessary for the motor to operate efficiently for only a time t = 0.5 s, over a relatively small number of cycles.

Results of the Load Calculation

Load current (max.)	668,75	mA
Load voltage (max.)	7,57	V
Winding temperature	30,99	°C
Housing temperature	26,79	°C
Required Speed (Motor)	6.438	min^{-1}
Required load torque	3,9	mNm
Output power	2,63	W
Efficiency (over all) ⓘ	52,36	%

Overall Dimensions

Diameter	15	mm
Total Length	23,8	mm
Mass	18	g

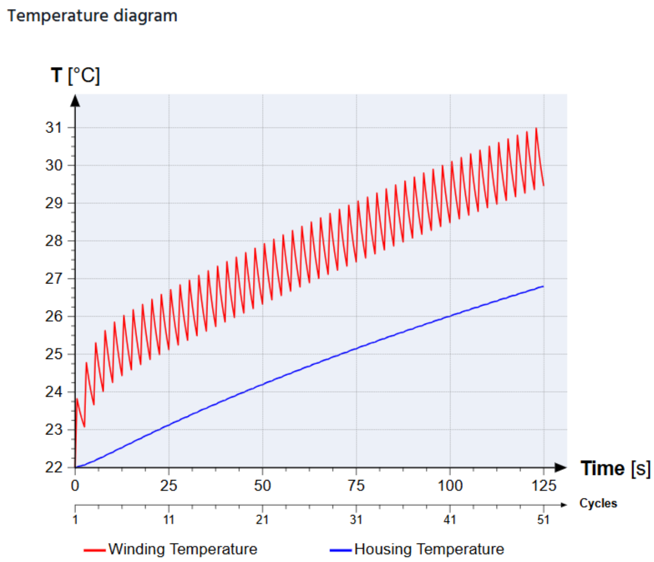

Figure 10: result of the load calculation

Consequently, the motor was set to deliver a torque of 3.9 N·mm and 6,438 revolutions per minute, thereby ensuring the performance required following the choice of the bevel gear coupling.

Finally, to complete the drive system, a connection was created between the bevel gear and the cable reel pulley by machining the former to form a keyway connection. This coupling will be explained in the following chapters alongside the thumb model.

The actuation system described represents the mechanism for moving a single finger, allowing its extension and flexion in the palmar and dorsal regions of the hand. However, the fifth actuation system itself will perform the task of rotating the thumb block, moving it from a palmar to a dorsal configuration. It is positioned below the other four motors, filling the space between them and the wrist block. This will also be analysed in the various prototypes in the following chapters.

Chapter 3

Hand models and Prototypes developments

In this chapter, following a detailed description of the objectives and materials used, we will describe the hand models designed using CAD, outlining their characteristics and challenges right through to the final complete model.

3.1 First model

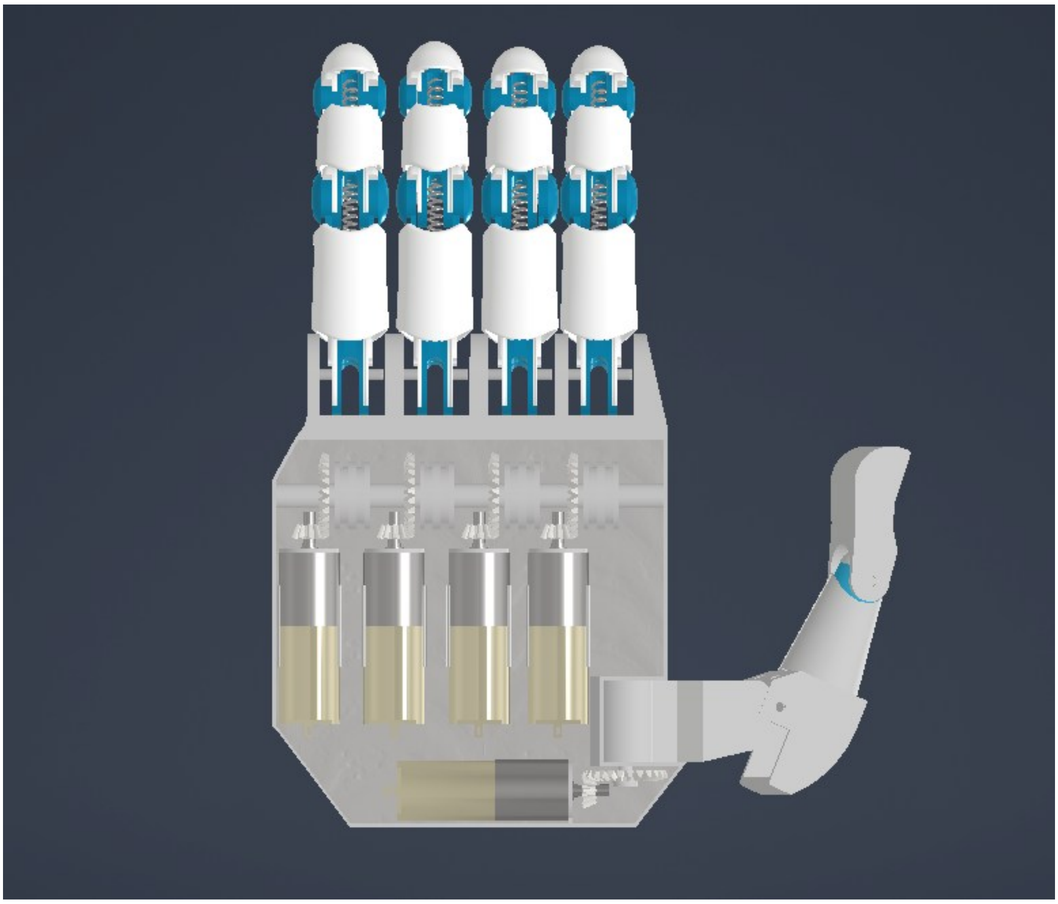

Figure 11: internal view of the hand

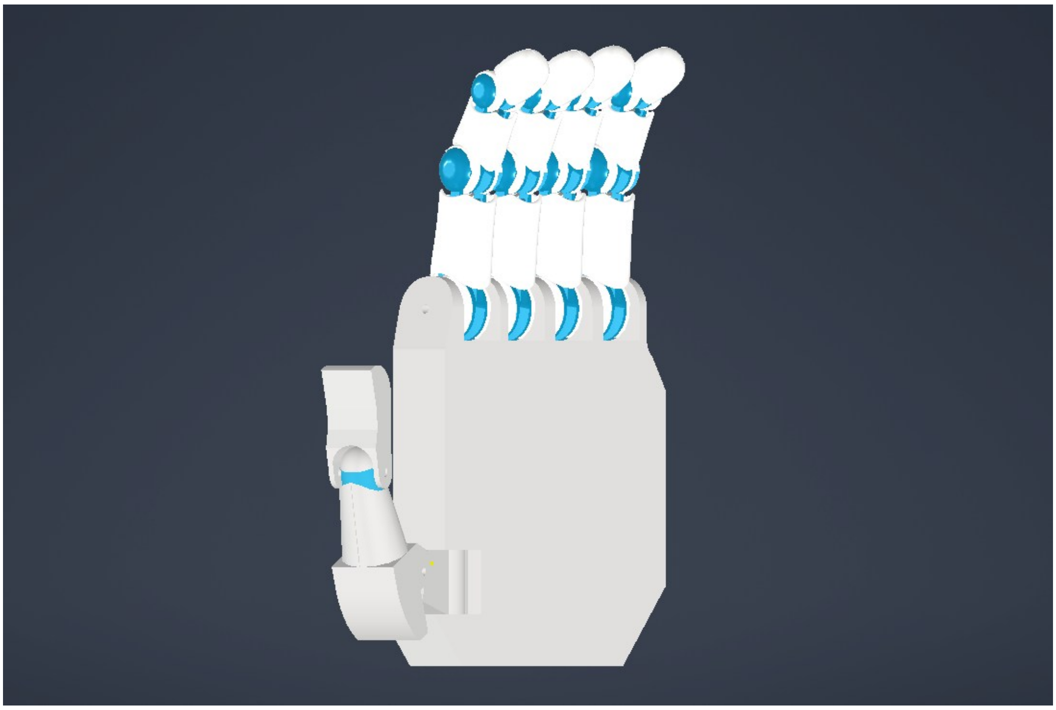

Figure 12: external view of the hand

The figures above illustrate the first hand model proposed following an initial experimental draft. In the figure 11 the internal structure of the hand's central body can be seen, whilst in the figure 12 the hand's structure is shown from the outside.

In this initial phase, the aim was to represent the concept of the transmission system under study, examining the spaces utilised, their layout, and the optimisation of the remaining space.

The model consists mainly of the cover, to which various supports for the entire actuation system have been attached. The motor and gearbox of all 5 systems have been mounted within frames to eliminate lateral movement, whilst to prevent axial movement, it was decided to flange the top of the gearbox using a flange connected to the frame and two M1.6 screws. To ensure correct alignment of the bevel gear with the pinion and the cable reel pulley, a through-shaft was used for all four systems, creating an interlocking system with the cover, albeit without any additional fastenings. Its sole purpose is to provide structural support for the system; consequently, it must be secured so that it does not rotate, whilst ensuring that the gear and pulley can rotate. As for the connection between the wheel and the pulley, 1.5 mm diameter holes have been drilled in both parts, allowing them to be joined using a 1.5 mm x 6 mm pin. The aim is to ensure that the wheel and pulley rotate in unison, guaranteeing direct transmission of motion to the pulley without the need for additional transmission components.

The fifth motor in the Bebionic hand was used to enable the rotation and positioning of the thumb on the palm and back of the hand.

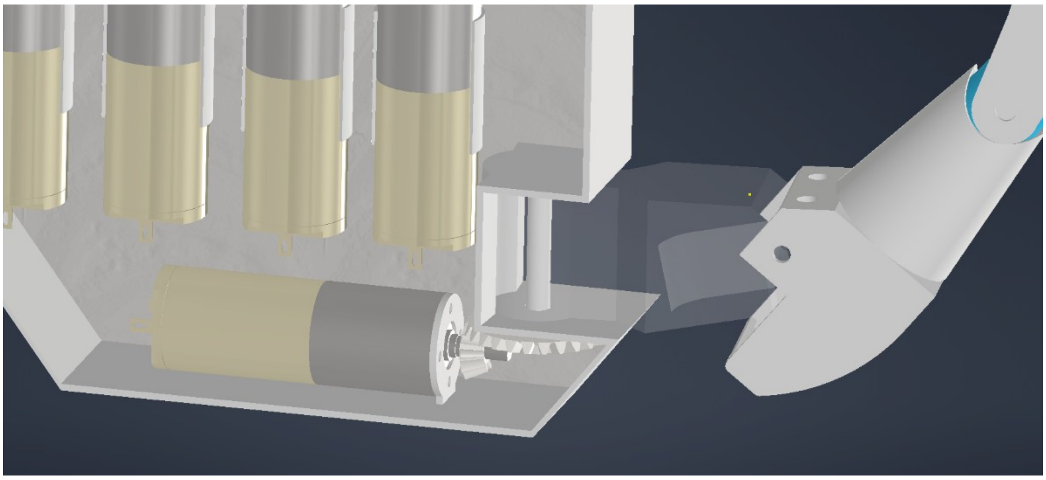

Figure 13: thumb rotation mechanism

Following the conical connection, a shaft with a flanged end was inserted into the wheel to create the conical connection, whilst at the opposite end a preliminary sketch was drawn up for the shaft-tongue coupling, a detachable mechanical connection that joins a rotating shaft to a component – in this case, the thumb connection. The tongue, a steel parallelepiped, is inserted halfway into a groove on the shaft and halfway into the hub, transmitting movement via lateral thrust. Contact occurs solely on the sides of the tongue. A small amount of play is maintained in the upper radial section (between the back of the tongue and the bottom of the hub groove), thus preventing eccentricity in the coupling.

3.1.1 Finger holder frame – first model

In this model, the finger holder frame was manufactured separately from the cover, creating a single piece for all four fingers. With a view to producing an aluminium model, it was decided to create multiple parts, thereby simplifying the machining required using CNC machines. As can be seen from the figure… slots have been created on the model's frame, specifically four slots per side, ensuring that each pulley has two symmetrical slots. Their purpose is to allow the wires to pass through, ensuring correct alignment from the pulley to the first pin in the finger's wire configuration; another consideration was to ensure minimal wire exposure once the model is closed, limiting the possibility of slackening that could cause the mechanism to jam during repeated cycles.

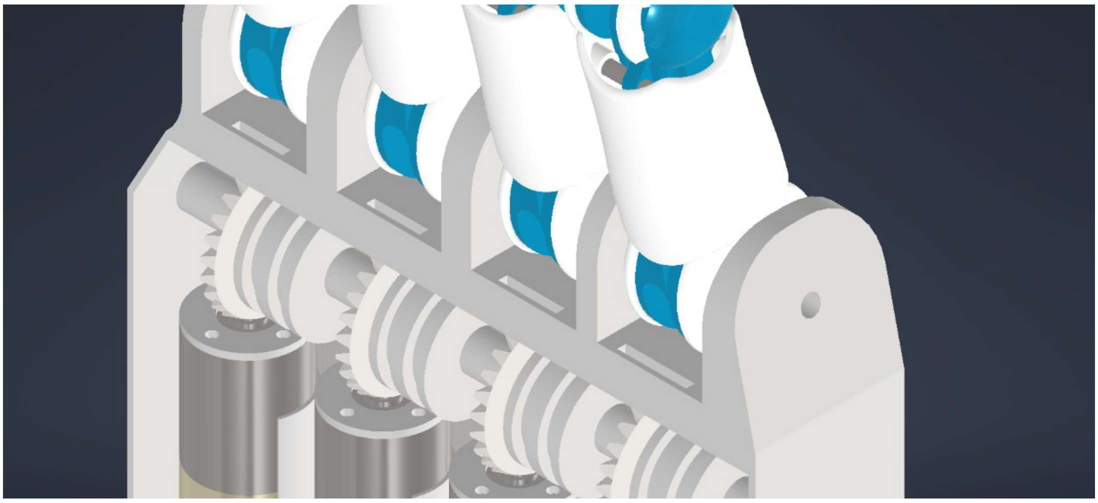

Figure 14: view of the finger holder in position

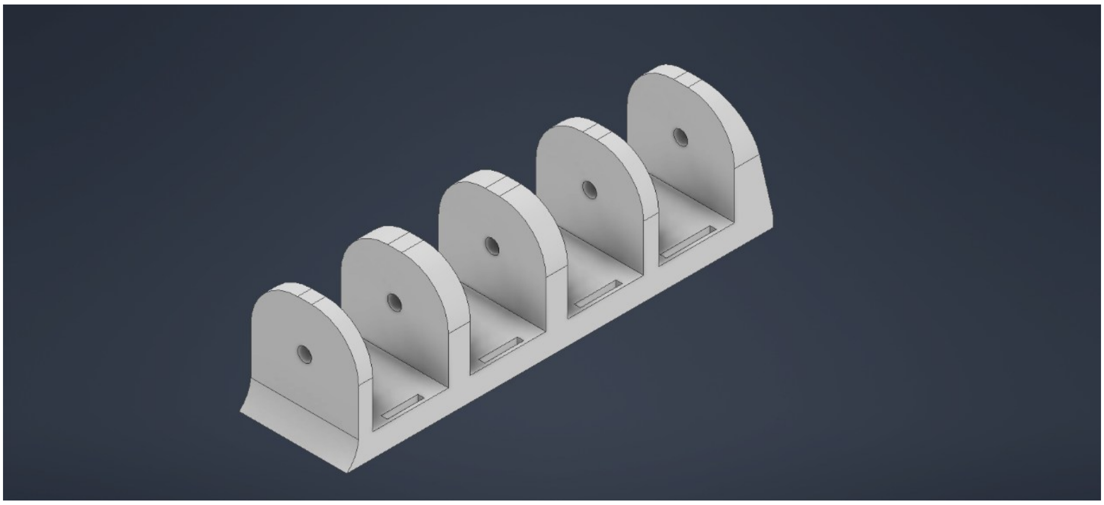

Figure 15: view of the finger holder

It was decided not to give the frame an anthropomorphic orientation of the fingers, precisely because of the hand’s non-anthropomorphic nature and, primarily, due to the chosen drive system; this system runs vertically, resulting in a perpendicular alignment between the main shaft and the pulleys, which consequently will have the same angle of inclination as the frame and, by extension, the fingers. To create the fingers at a specific angle of inclination rather than perfectly ‘straight’, each pulley would have had to be inclined in turn, making it impossible to have a single shaft passing through all four systems, which would have created considerable problems in the construction of the supports. Another issue is the coupling between the shaft and the cover, which has not yet been studied in this model but will be reviewed in future ones.

3.1.2 First thumb design

The design of the thumb warrants a separate discussion, as its movement and structure

differ from those of the other fingers. Having used the fifth motor to create the mechanism that allows rotation towards both palms, the idea of using a pulley as in the other systems was no longer a viable option, partly due to the dimensional constraints that had to be met. Since the thumb is positioned in opposition to the fingers on both sides, the function of flexing like the other fingers was no longer necessary, thereby simplifying the concept of the thumb and making it anthropomorphic. This allows us to adopt actuation mechanisms similar to those of other prosthetic hands.

The basic idea was to create an irreversible system so that, even without a reduction and speed system matching the others, it could still guarantee a grip. In this first model, only an aesthetic form with some details was sketched out, but it was irrelevant to the mechanical aspect of actuation. This will be explored in greater depth in subsequent models.

3.2 Second model

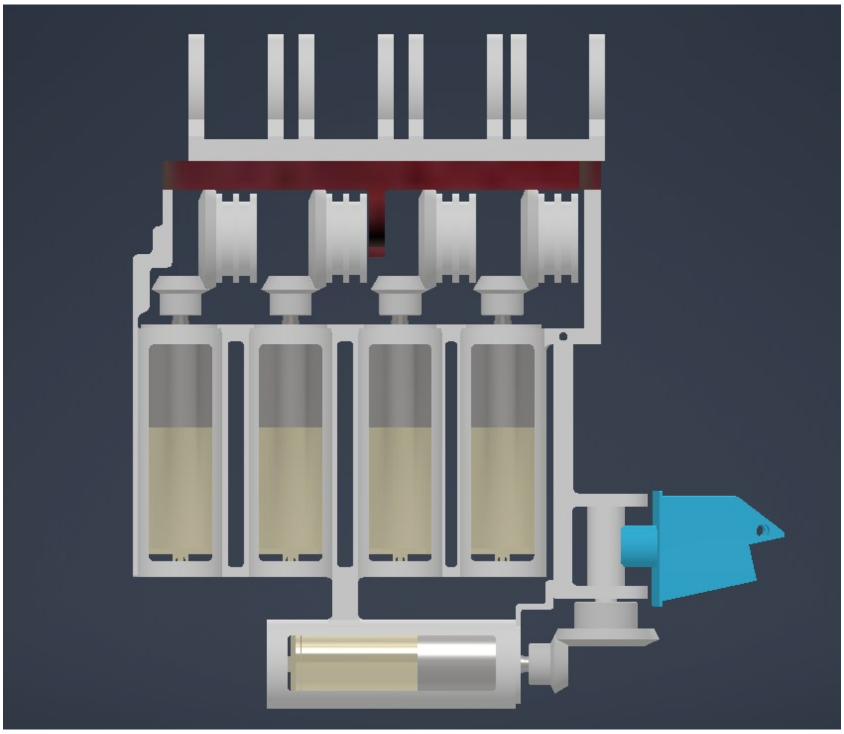

Figure 16: view of the mechanism and the frame

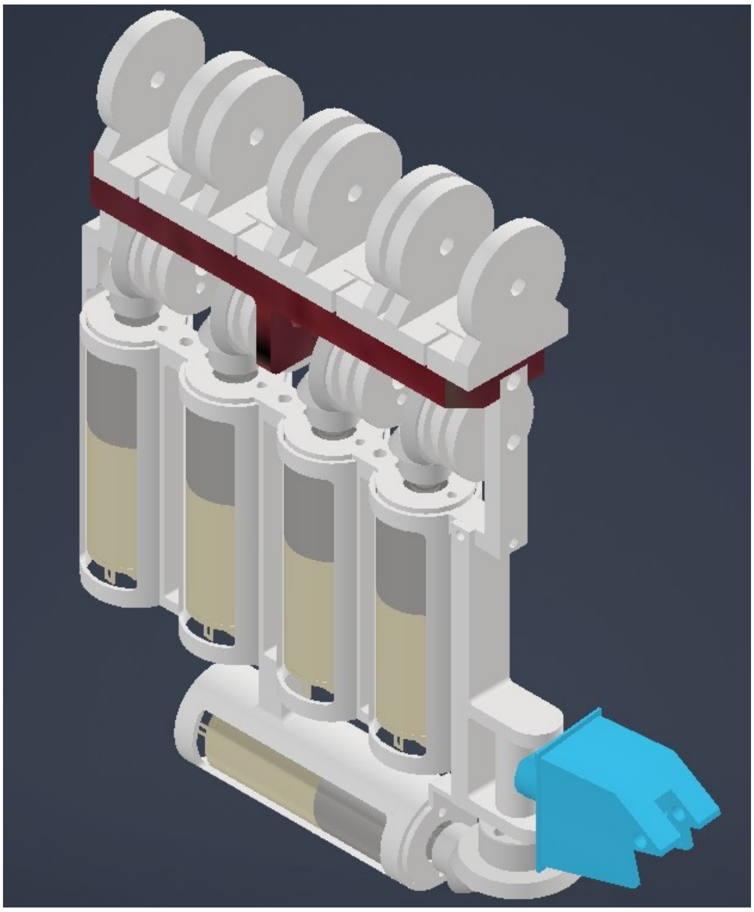

Figure 17: view of the mechanism and the frame

The figures 16 and 17 above illustrate the second model proposed following a redesign.

It can be seen that the model has changed drastically compared to the first proposed model. The first model had several problems; the actuation systems were, in fact, connected via brackets directly to the cover, which had to withstand the stress caused by the tensions of the mechanical components and the loads borne by the hand itself. This led to several critical points and was not as efficient in operation, given that it was initially intended to be produced using 3D printing. In order to further reduce the space required and make better use of it, we decided to take inspiration from other robotic hands on the market and design an initial prototype of a lightweight yet sturdy frame to support the structure.

Upon examining the assembly, one can see a new central frame designed to support all four motors; it consists of four hollow cylinders with a centre-to-centre distance of 21 mm, ensuring the correct assembly and spacing of the reduction systems at a later stage. The motor responsible for wrist rotation has been positioned at a height of 16.5 mm between the base of the four hollow cylinders above and the centre-to-centre distance of the cylinder below, ensuring compliance with the anthropomorphic dimensions of a hand and guaranteeing the correct alignment of the actuation system with the thumb attachment. It has been designed so that the motor-gearbox unit can be inserted from the top of the hollow cylinder, flanged at the end directly onto the remaining part of the frame. The fifth motor below has been flanged to another frame component that will support the base of the thumb and the structure above.

The frame also features two extensions at the upper end, designed to create a connection between the main frame and the structure above, ensuring the connection between the finger holder frame and the intermediate frame.

Figure 18: frame for flanging the 4 gear motors

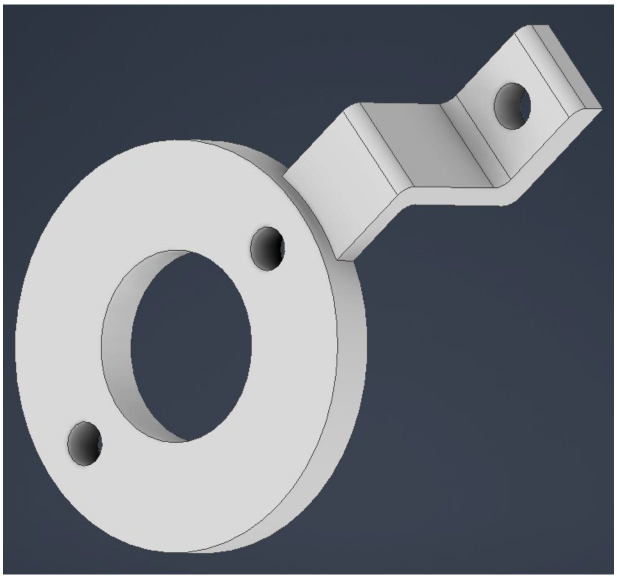

Figure 19: frame for flanging the fifth engine

It was decided to divide the frame into several parts with a view to machining them in the workshop rather than using 3D printing, ensuring parts that are easier to machine, at a lower cost, and suitable for mass production. At the end of this model, the main issues encountered during the design phase will be explained.

An additional component has been designed on the side of the main frame to simplify future machining, creating a connection between the frame, thumb and tool holder. Its threefold function enables a flanged connection between the gearbox below and the base of the component, preventing the system inside the hollow cylinder from rotating.

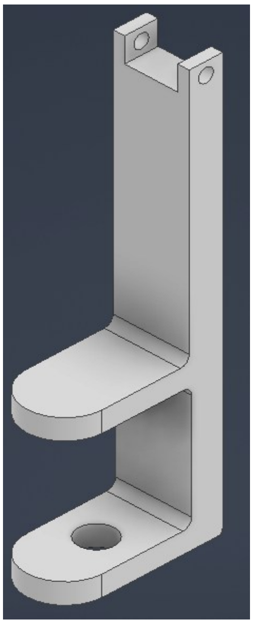

Figure 20: frame for side mounting

The piece features a 4mm hole at the bottom of the block and a recess of the same size at the top. The aim was to create a shaft-tongue connection, thereby ensuring the rotation of the initial thumb frame (shown in blue in the figure 21).

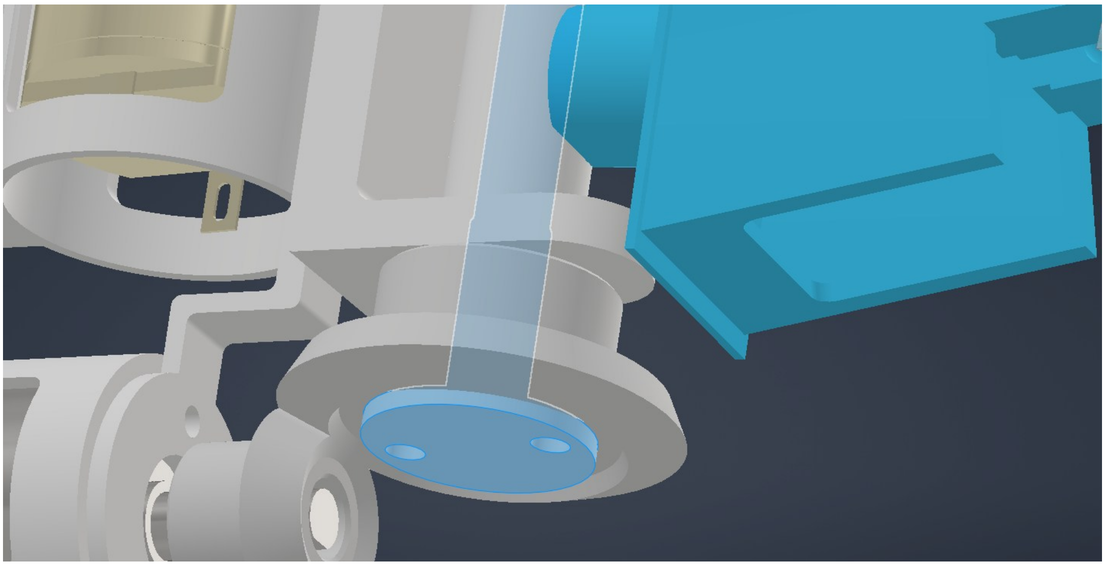

Figure 21: thumb rotation mechanism

As shown in the figure 21 the bevel gear has been connected to the shaft via one of its flanged ends, using two M1.6 screws, thereby ensuring that torque and speed are transmitted directly to the shaft.

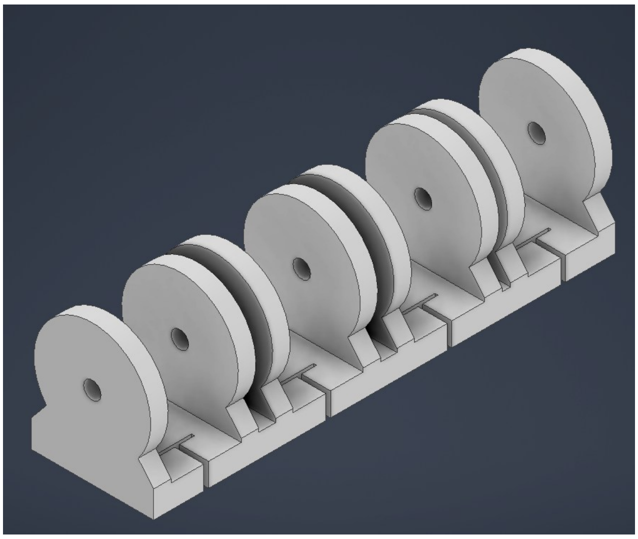

Figure 22: finger holder

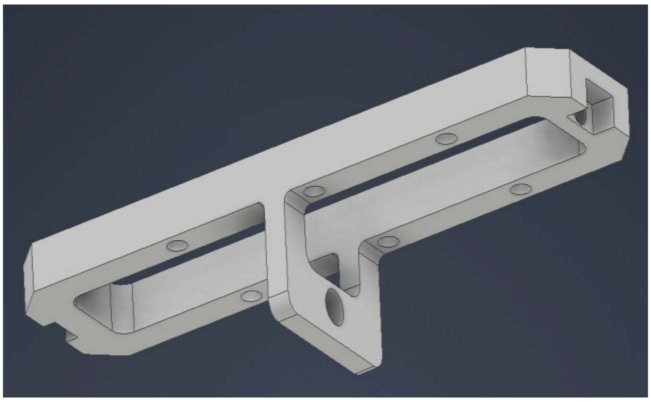

Figure 23: upper support frame

The figure 22 and 23 shows the revised frame of the finger and the support attached to it.

The upper frame features a series of three holes on each side, designed to connect to the finger holder frame using M2 screws. At each end, it has two recesses, each containing two threaded holes for M3 screws, designed to connect to the main frame below. It also features a central support designed to hold the main shaft, preventing any bending at the centreline. The finger holder frame has been remodelled to follow the lines of the prototype finger covers, creating small slots that allow the wires from the pulley to pass through the upper frame and be inserted from the outside via the openings, thus preventing the part from opening up due to wire slackening and jamming.

Following an initial print using a powder bed printer, various defects in this model were noted. It transpired that the structure was too slender, causing it to deform due to its extremely small dimensions, leading to the breakage of a section of the main frame. The ends connecting to the upper frame were also too thin, creating an unstable joint that deforms easily. The dimensions of the drive chain for thumb rotation were similarly insufficient, causing the structure to fail and unable to support the thumb block.

3.3 Third model

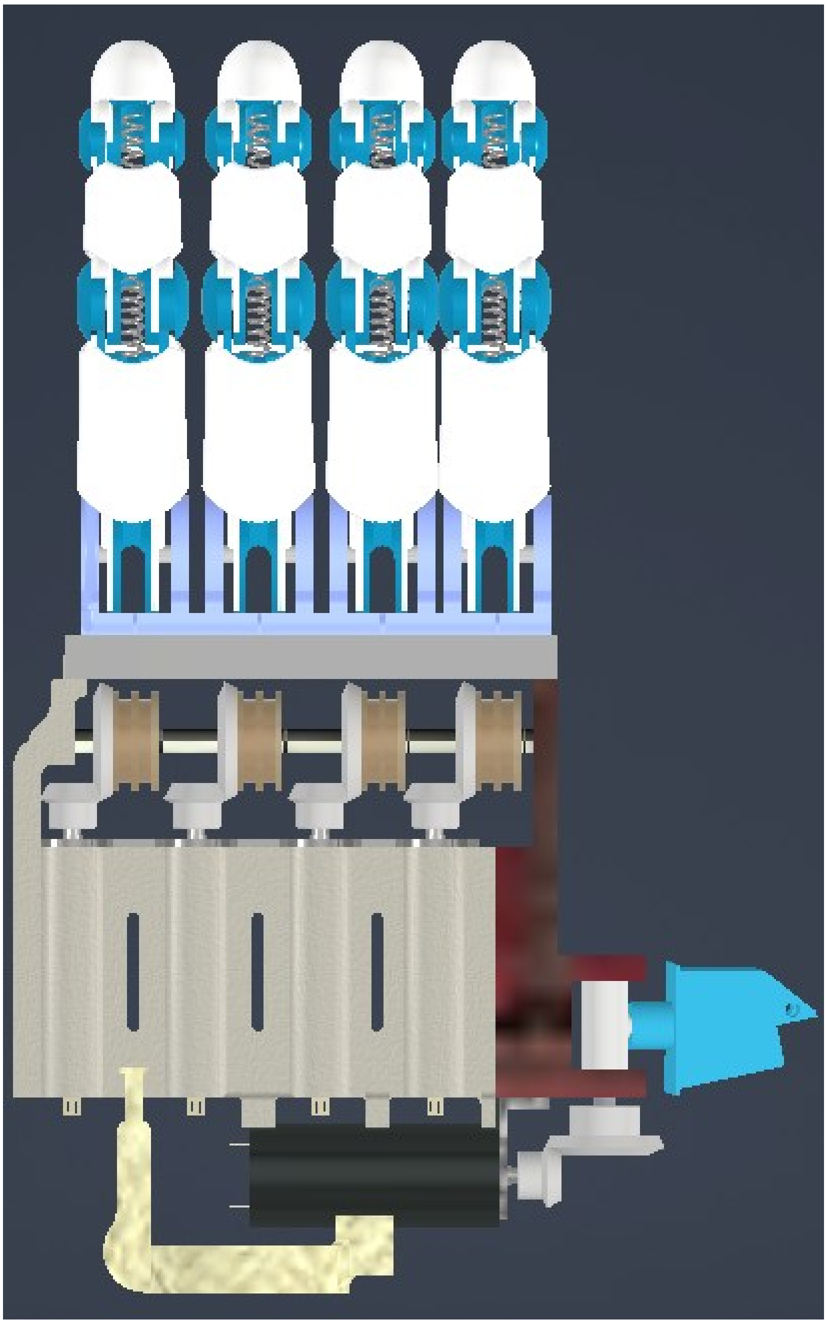

Figure 24: front view of the third model

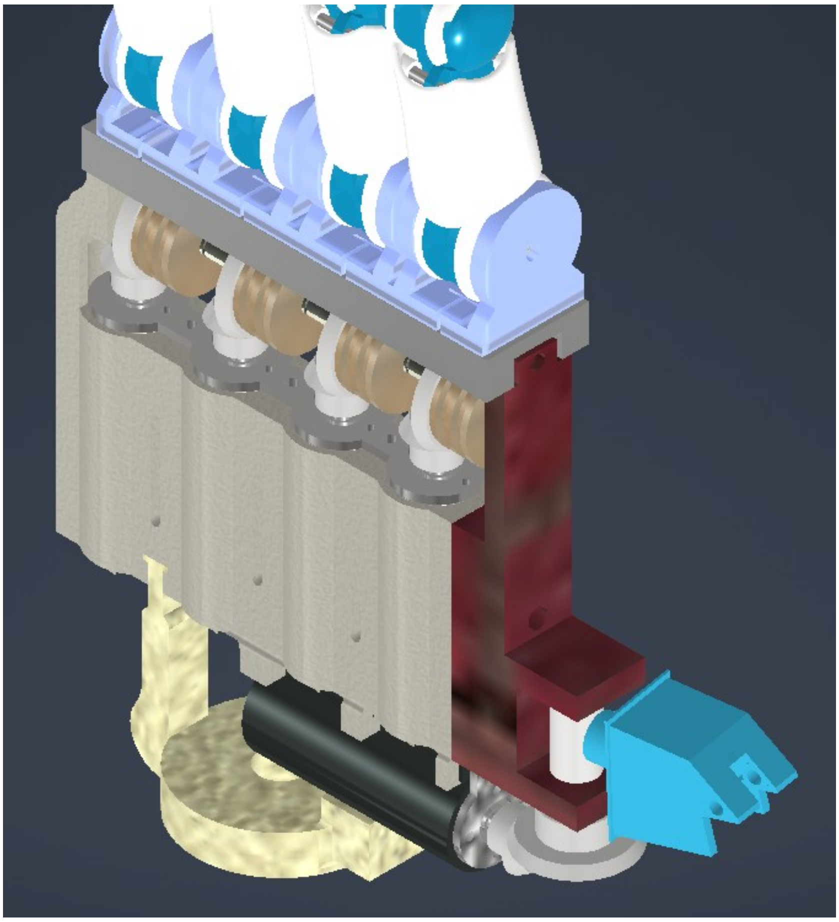

Figure 25: side view of the third model

The figure 24 and 25 provide an overview of the structure of the third model.
Following the problems encountered during the design of the second model, significant changes were made to the structure and components were optimised for the most critical interfaces.
From the third model onwards, the components will be analysed in greater detail, given their design and the characteristics they possess.

Figure 26: main frame

The figure 26 shows the main frame. As can be seen, compared to the previous model, the structure has been reinforced due to its slender dimensions, with a thickness of 1.5 mm for the hollow cylinders that will house the motor-gearbox unit, and a thickness of 10 mm between the centres of the hollow cylinders. This has enabled the structure to be connected to other structures via threaded holes for assembly.

The frame features three M2 holes at the top designed to connect with the frame for flanging the gearboxes, as shown in the figure 26; it also features an M3 hole for connection with the frame of the second side chassis section and an M2 hole for connection with the upper chassis frame. It features an additional 4 mm hole in the side extension for coupling with the main shaft, which supports the pulleys and bevel gears. This coupling will be discussed in the final model, given its delicate design. In this model, it was decided to use a threaded hole and, at the same time, to thread the shaft externally.

The lower section features three projections designed to accommodate the motor mount frame, as this will be fitted once the four upper motors have been secured. There is also a hole to create a snap-fit connection for the rough-cut frame of the wrist attachment. It was found that both the motor mount connection and the wrist required precision machining to achieve an interlocking fit; these methods could be replaced by screw-based connections, which are more suitable for this stage of the design process. The frame was deemed too labour-intensive to machine, given its geometric complexity due to the left-hand appendage, both in terms of cost and the amount of scrap material produced. It is acceptable for 3D printing, but the design is intended for production using machine tools.

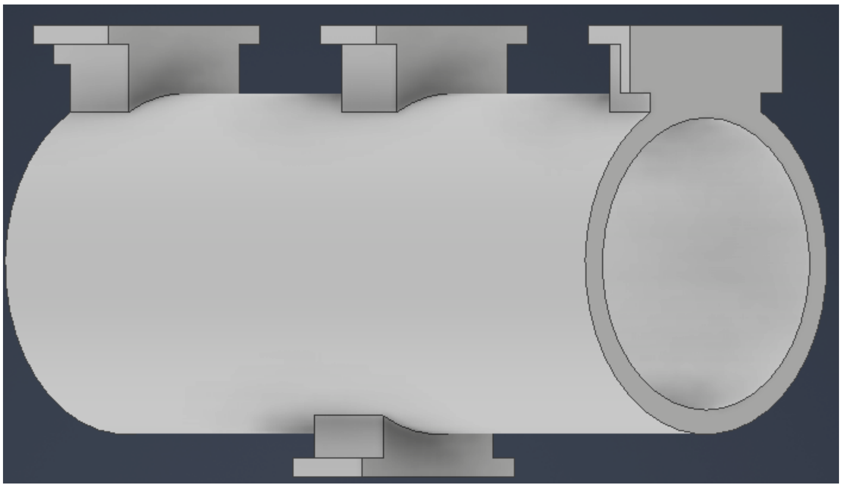

Figure 27: fifth motor support frame

The figure 27 shows the engine mount frame at the base of the palm; for design reasons, it was decided to manufacture it as a separate component, thereby also simplifying machining operations. The main frame has an internal diameter of 15 mm and an external diameter of 17.5 mm; it has four ends: three upper ends to connect with the main frame and the lower end designed to connect with the wrist block. All these connections are of the interlocking type, an assembly method in which two or more components are joined by combining a protrusion (male element) with a complementary cavity or slot (female element). Stability is ensured by the precision of the shape and the friction generated between the parts.

As with the frame described above, this type of coupling is not feasible for this project at present.

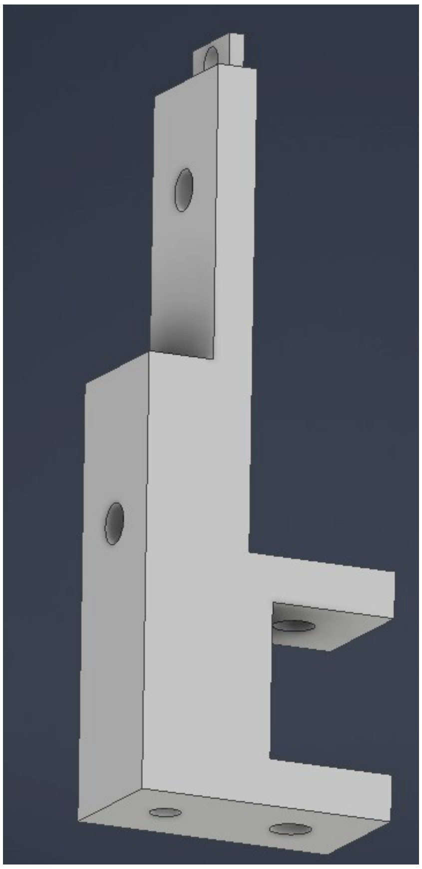

Figure 28: side frame

Improvements have been made to the frame shown in the figure 28 compared to the previous model; the structure has been reinforced, bringing the frame to a thickness of 14 mm and a height of 74 mm, ensuring proper support for the thumb attachment and the connection between the shaft and the tab. The thumb rotation mechanism in this model remains similar to that of the previous model.

In this frame, there is a hole for an M4 screw to connect it to the main chassis, whilst at the upper end there is a hole to create a press fit with the main shaft and a hole for an M3 screw to connect it to the upper chassis.

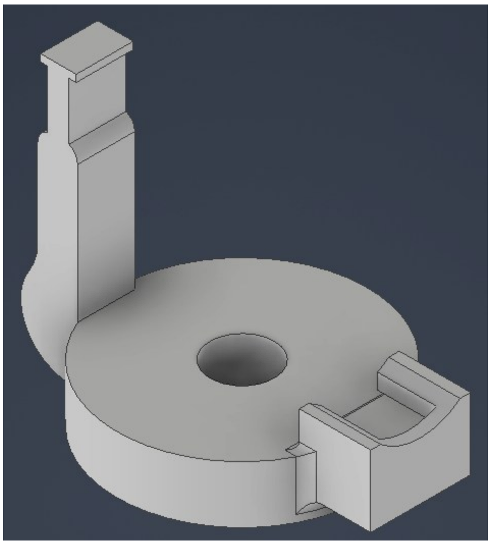

Figure 29: sketch of the frame for the wrist attachment

In this model, a draft wrist assembly with a diameter of 35 mm has been created for insertion into the model; the aim was to provide an initial assessment of the space required and the potential interfaces needed. The figure shows the upper end and the recess along the length of the cylinder, designed to create an interlocking connection with the main frame and the fifth motor frame.

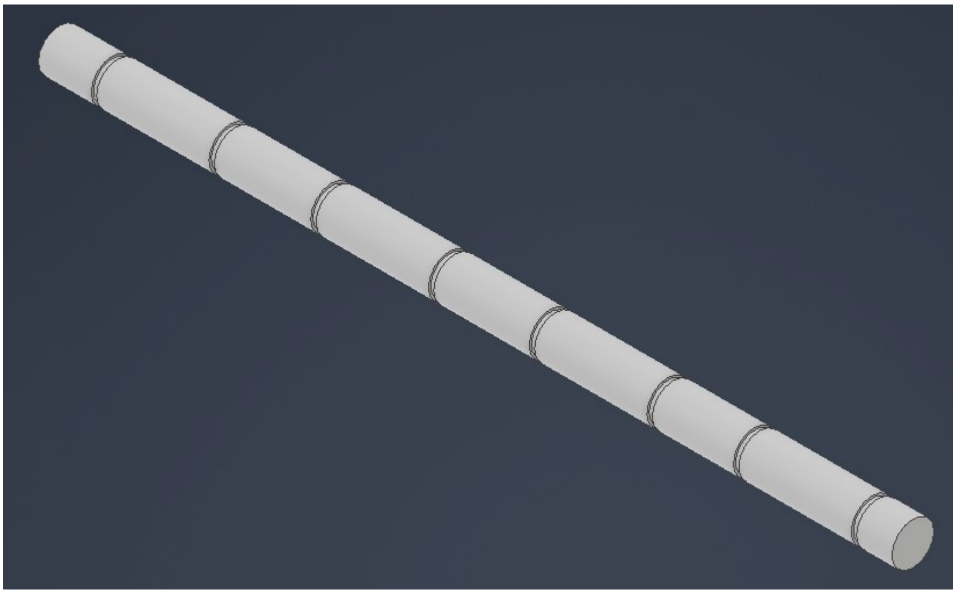

Figure 30: main support shaft with grooves for Seeger rings

More detailed assessments were carried out for the design of the main support shaft. As previously explained, it plays a key role in the operation of the robotic hand, as any misalignment of this shaft leads to the failure of the bevel gear pair, resulting in the system locking up. The figure shows a cross-section of a rod that will be manufactured from 4 mm diameter stainless steel with a total length of 81 mm. As this is a short component, even though the diameter-to-length ratio is approximately 1:20, it was assumed that, given the forces involved, it would not undergo significant deformation at its centre; consequently, the upper frame support was removed, as in the previous model.

In this model, the couplings, assembly and fastening of the components were analysed in greater depth; in particular, how to secure the coupling between the bevel gear and the pulley so that it rotates freely on the shaft without axial slippage. It was decided to use DIN 471 external Seeger rings, spring-loaded retaining rings **specifically designed for use on (external) shafts**. These are used to lock mechanical components such as bearings, gears or pulleys axially within their housings, preventing them from slipping out.

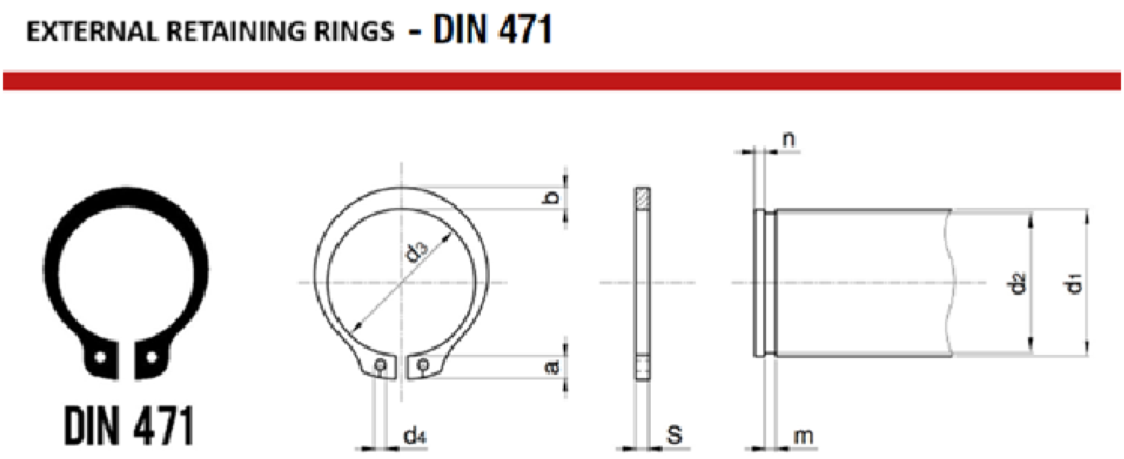

Ø SHAFT d1 mm	s mm	d3 mm	a mm	b mm	d4 mm	d2 mm	m mm	n mm	INOX	CODE
4	0,4	3,7	2,2	0,9	1	3,6	0,5	0,3		ES4
									✓	ES4I
5	0,5	4,7	2,5	1,1	1	4,8	0,7	0,3		ES5
									✓	ES5I
6	0,7	5,6	2,7	1,3	1,2	5,7	0,8	0,5		ES6
									✓	ES6I
7	0,8	6,5	3,1	1,4	1,2	6,7	0,9	0,5		ES7
									✓	ES7I

Figure 31: Technical data sheet for external Seeger rings

The frame shown in the figure 30 features recesses designed to house the Seeger rings; these have been designed in accordance with the standards and dimensions specified for the diameter of the shaft used.

During the assembly phase, it was noted that this type of ring must be inserted one at a time from the ends, as they cannot expand to a width at both ends equal to d2; consequently, to reach the innermost cavities, one must pass through all the previous cavities, increasing the risk of component breakage and adding to the complexity of assembly, as a bevel gear and pulley must be inserted before each Seeger ring, which is then closed by the next Seeger ring.

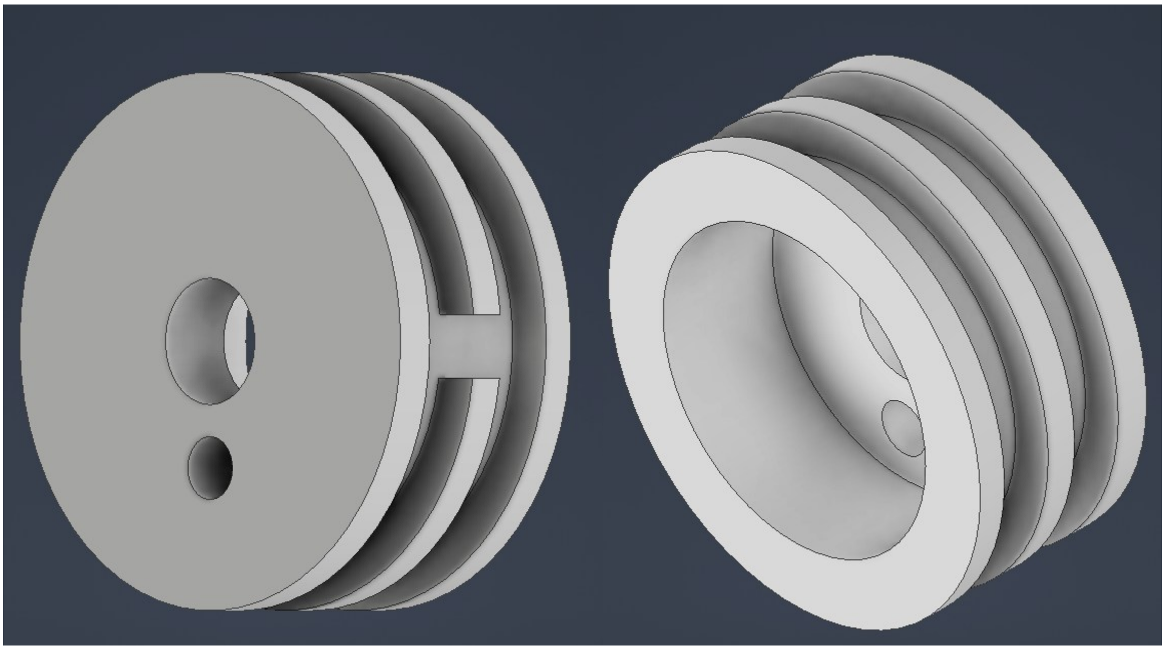

Figure 32: cable-winding pulley

The figure 32 shows the frame of the cable reel pulley, a component produced using powder bed 3D printing. The wires will be placed inside the two 2 mm wide guides with a radius of 7 mm, a key parameter for calculating the performance to be achieved. There is a recess in the central section designed to connect the two guides for winding the cables, whilst the structure itself has a radius of 8.5 mm. The frame features a main hole with a diameter of 4 mm for the passage of the main shaft, and a hole at the rear with a radius of 6 mm and a depth of 5 mm, designed to house the main body of the bevel gear, creating a connection via a 2 mm diameter pin. This connection is achieved through machining on the base of the bevel gear and on the pulley, as can be seen in the figure…, which shows a 2 mm hole on the face intended for the pin.

Pin coupling in mechanics (or plug coupling) is a fastening or positioning system that joins two components. It uses cylindrical, conical or shaped pins inserted into corresponding mating holes to ensure correct alignment and, in some cases, to transmit shear or rotational forces. Its main functions are the alignment of frames, fastening and the transmission of power without additional elements in the drive chain. In this case, elastic cylindrical pins were used.

3.4 Fourth model

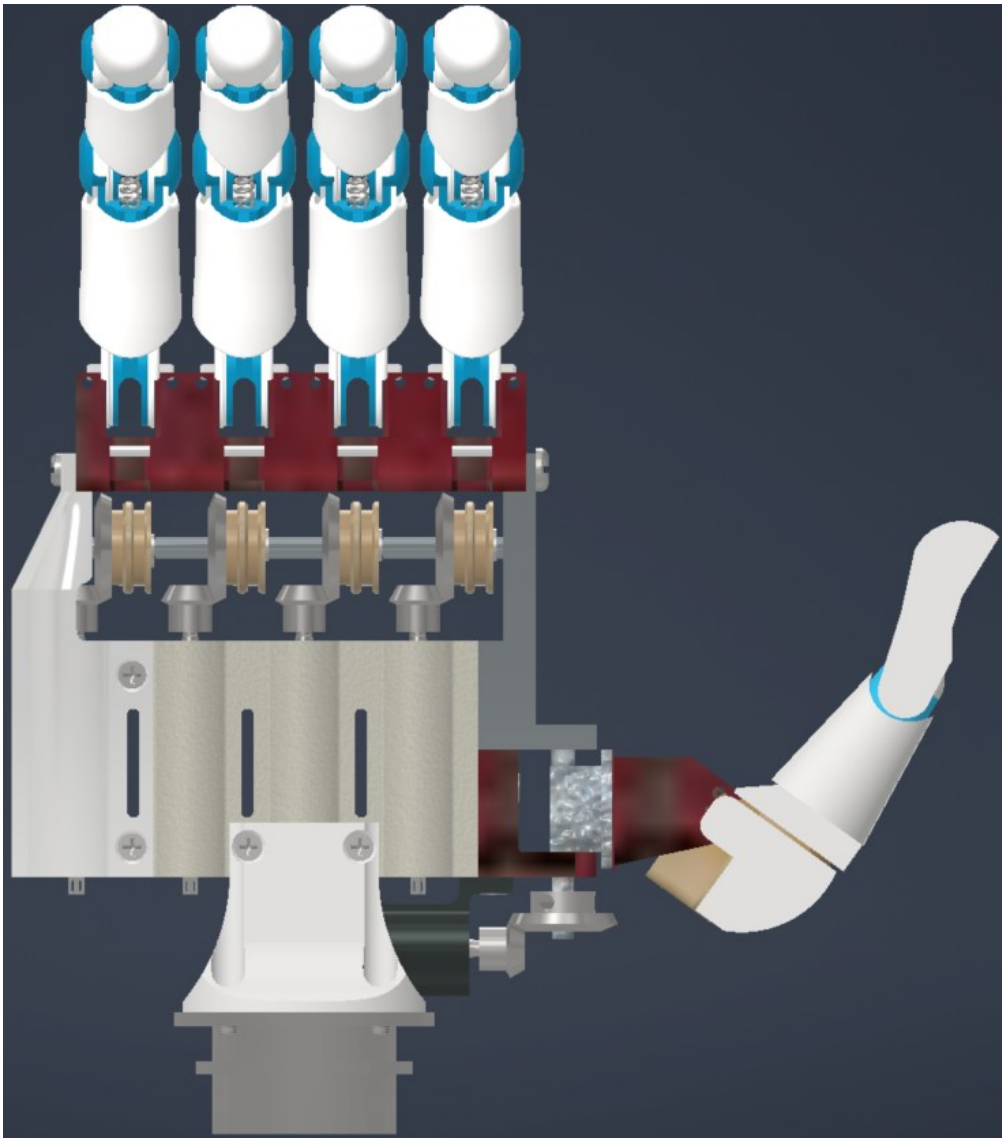

Figure 33: front view of the fourth model

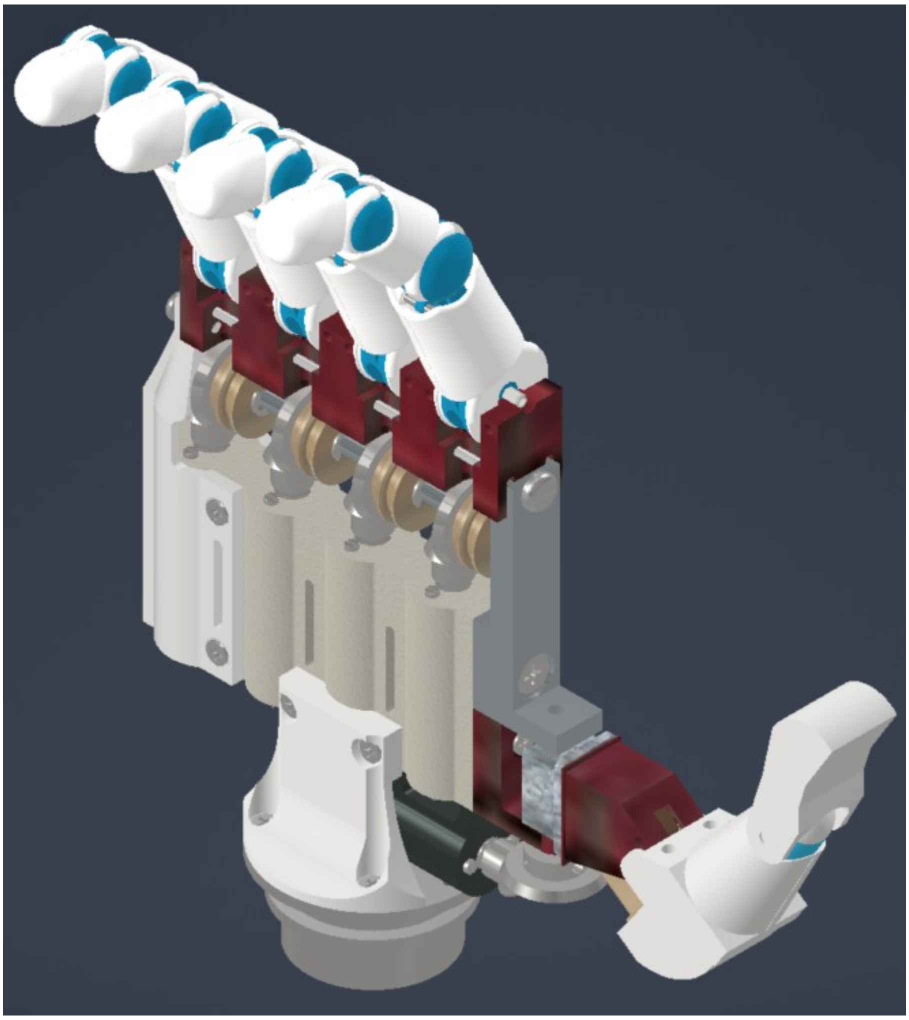

Figure 34: side view of the fourth model

Following the results obtained from the third model, a number of modifications and corrections were made to the model, as it contained significant design flaws. At this stage, having already produced a draft of the hand's structure, the project entered a more detailed phase, involving a frame-by-frame analysis to assess the design and the interfaces between them, with particular attention paid to dimensions and future machining operations using machine tools.

Particular attention was paid to simplifying the parts, with the aim of reducing production costs and simplifying assembly, as there are many connections that must follow a specific assembly sequence.

Figure 35: side view of the main frame

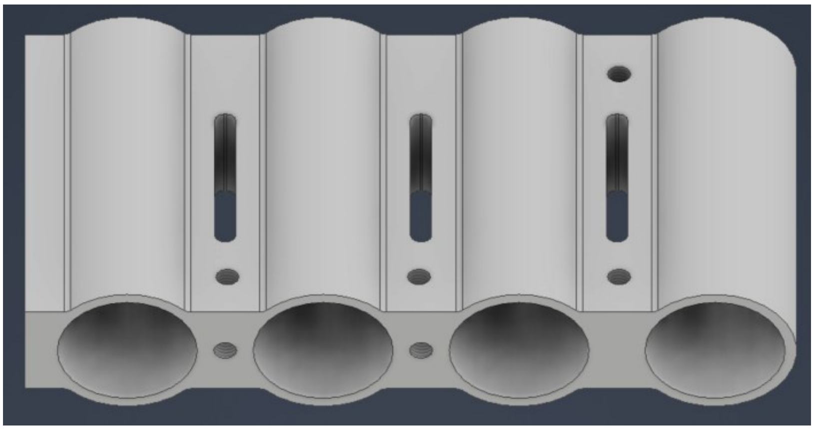

Figure 36: bottom view of the main frame

The figures 35 and 36 show the new main frame, which will serve to support the entire structure of the hand via specific couplings. It measures 82.75 mm in length, 43.5 mm in height and 12 mm in thickness; the centre-to-centre distance between the hollow cylinders is 21 mm, giving the structure a symmetrical design. Consequently, one can start with a block of aluminium and machine it to produce minimal waste. Compared to the previous model, for practical and functional reasons, the frame has been joined to flange the gearboxes directly to the chassis, creating a single piece. The frame has therefore been increased by 1.5mm at the top, where 8 holes for M1.6 screws have been created to secure the gearboxes and motors, thus preventing them from rotating in their mountings. The frame consists of three slots, each 2.2 mm wide and 20 mm high, designed to accommodate the cables for the controls and electronic boards that will be produced. Near the slots there are holes for M3 screws, which are required for assembly with other components that we will explain in detail later. On the flat section at the end, starting from the bottom, there is a hole for an M3 screw, a hole for an M4 screw and two holes with a diameter of 4 mm and a depth of 2.5 mm, which are necessary to align the supporting structure of the upper frame (see the dark grey frame in the figure…), thus preventing the rotation and wobbling that can occur when using only a screw connection. On the lower part of the frame there are two holes for M3 screws, designed to create a connection with the motor mount frame below.

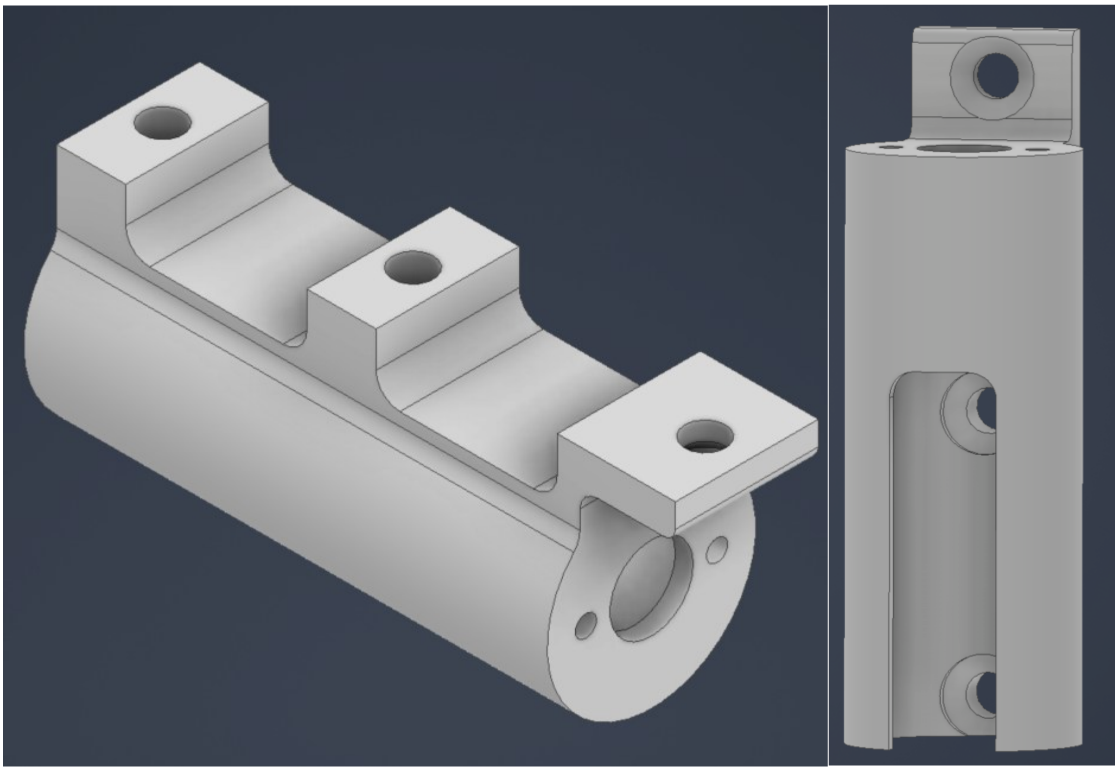

Figure 37: fifth motor support frame view

Significant changes have been made to the design of the frame housing the motor and gearbox responsible for thumb rotation. The structure has been adapted to the new assembly specifications and optimised for industrial production using machinery. As with the main frame, the gearbox is flanged directly onto the frame using two M1.6 screws.

The model features three countersunk holes for M3 screws, positioned at the frame's ridges, designed to create a connection with the main chassis. The purpose of the recess is specifically for assembly; the screws are tightened using a screwdriver, after which the motor-gearbox unit is inserted and flanged to the part. During the design process, particular attention was paid to ensuring the screws were positioned correctly so as not to cause obstructions when inserting the motor into the 15mm diameter hole. Grooves have been left in the space between the ridges to accommodate the motor encoders and the cables emerging from them. The outermost ridge is connected to another frame section.

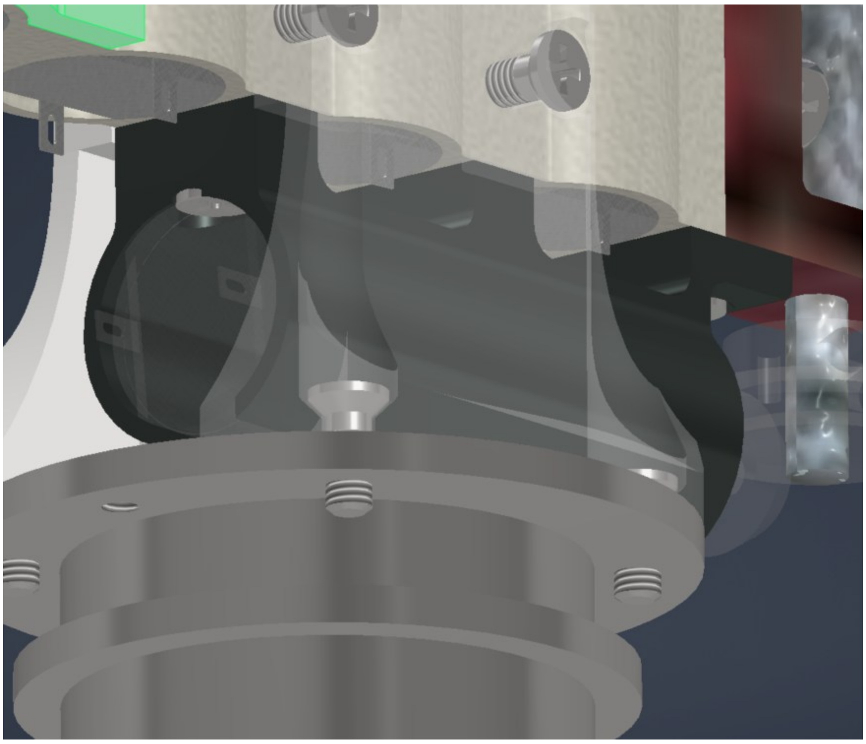

Figure 38: view of the connection to the main frame

3.4.1 New connection component

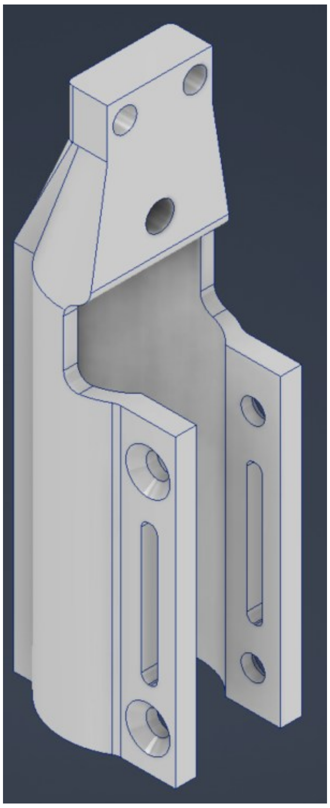

Figure 39: side support frame near the little finger

In previous models, another function of the main frame was to connect the lower structure to the upper structure, whilst also serving as a support for the main shaft; however, due to the complexity of the machining processes, this was no longer a viable option. In the initial drafts, the idea was to recreate a connection similar to that at the thumb side, but this would have required additional joints and exceeded the space allocated for the frame, resulting in an excessively wide structure.

The frame shown in the figure 39 represents the solution to this problem. To avoid further complicating the main frame and to remain within the set limits, a frame was created designed to follow the lines of the main frame. Thanks to its structure, which is 2 mm thick on each side and 3.5 mm thick at the rear, the frame can be inserted from the top of the main frame, thereby restricting the rotation and longitudinal movement of the part. There are two slots corresponding to the slots in the main frame and two countersunk holes on each side for M3 screws, which are designed to secure the frame; this will constrain the part axially, creating stability for the component and making it a solid structure to support the shaft and the finger holder frame.

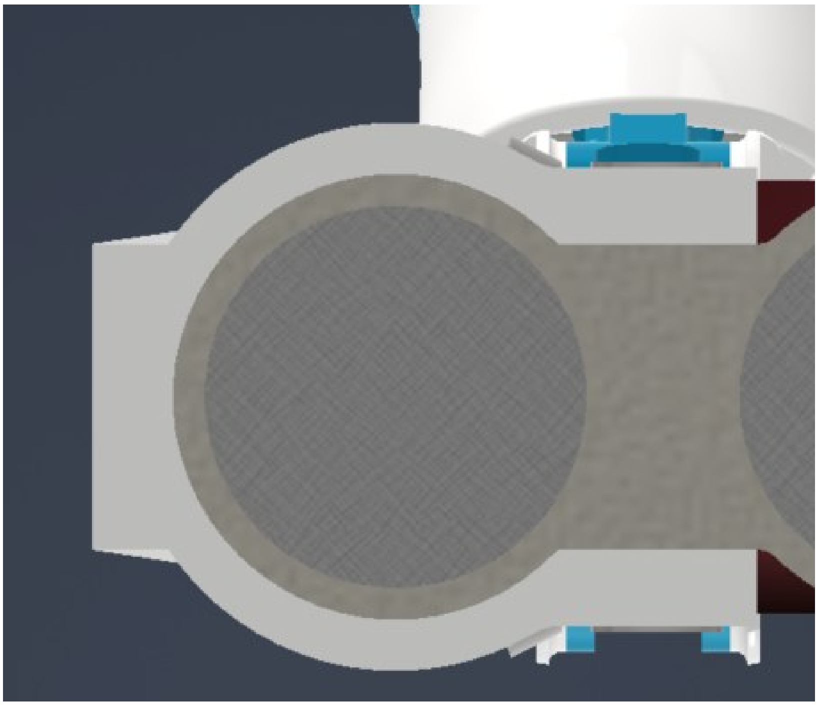

Figure 40: bottom view of the frame fitted onto the central frame

At the top of the structure there is a recess designed to house the pinion, whilst also adding thickness to the frame, a significant feature given the slender dimensions we are working with. There is a 4mm diameter hole, required to create a snap-fit connection with the main shaft, and two holes for M2 screws, intended for attachment to the frame that will support the fingers.

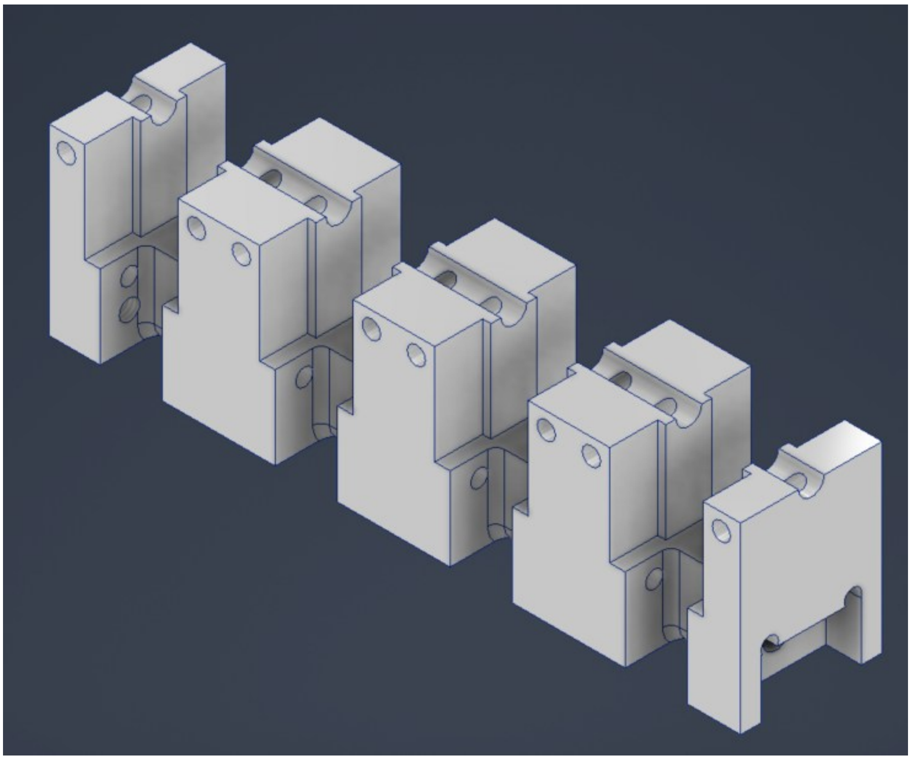

Figure 41: view of the final design of the finger holder

The frame shown in the figure 41 represents the final design of the finger holder, featuring elements that combine the frame with the upper chassis of the previous model. In this prototype, the upper chassis has been removed and integrated into the frame, thereby eliminating an extra component and avoiding further unnecessary connections.

The finger housing has been redesigned to accommodate the base of the fingers and mount it together with its support covers, secured via the 2mm holes on the upper sides of the figure. It was decided to use a 2mm shaft secured at both ends to connect all four fingers. In the cavity provided for the fingers, there is a 3mm diameter hole designed to allow the cables to pass through, which will provide sensor feedback along the length of the finger.

At the left end, there are two threaded holes designed to connect to the previous frame, whilst at the opposite end there is a threaded hole for M4 screws designed to connect to the complementary frame section. Two-millimetre holes have been drilled along the lower sides of the figure at the connection points; these will be fitted with two 2mm steel shafts, designed to guide the wires exiting the pulleys. They are aligned with the radius of the pulleys, creating a zero-degree angle between them, ensuring the outgoing wire is perfectly aligned.

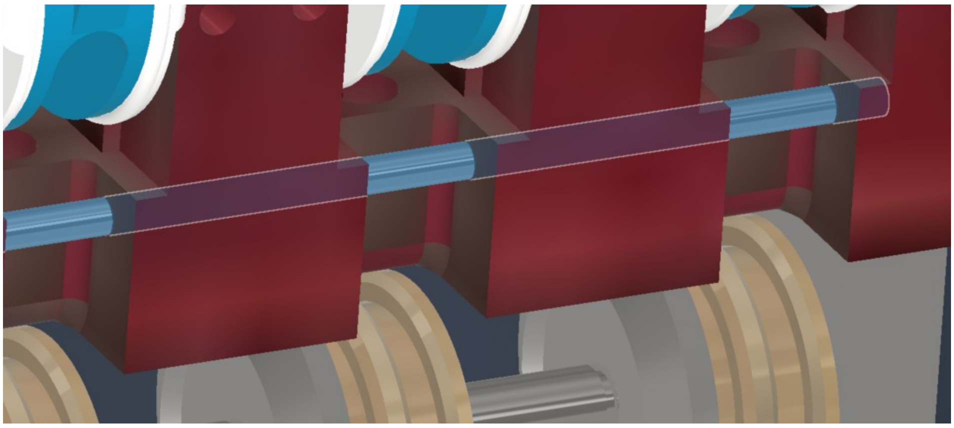

Figure 42: shaft for the wire guides

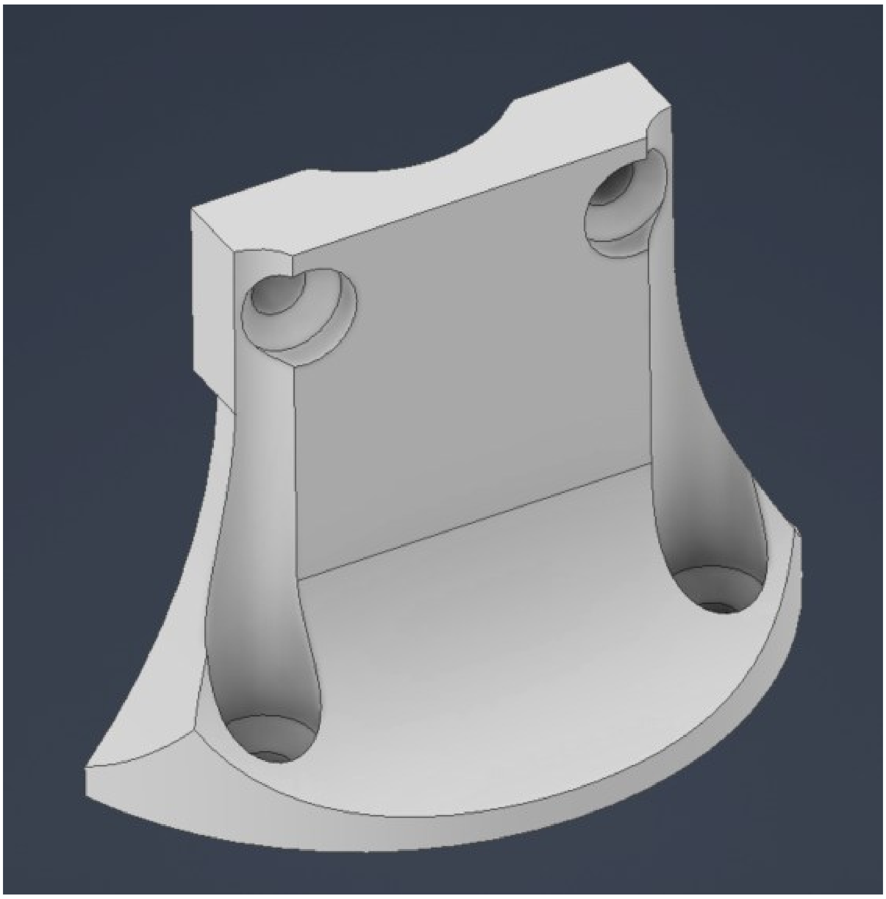

Figure 43: wrist attachment frame

The figure 43 shows the wrist attachment frame. To achieve a more streamlined design with the prototype, this intermediate component was created to connect the main frame to the wrist. For the wrist, the most commonly used wrist module was selected: Ottobock's Quick Disconnect, which, as it is a standard component, is also used in the Hannes hand (a hand developed in collaboration between INAIL and IIT). Starting from this, the drawings with the geometric dimensions were obtained and modelled in CAD to assess the dimensions within the assembly. Subsequently, based on these dimensions, a frame was created to form the connection with the main frame. At the top, there are two countersunk holes for M3 screws, whilst at the base there are two further holes with the same characteristics, designed to form the connection with the wrist module. This part is symmetrical on both sides of the main chassis, enclosing between them the motor chassis frame shown in the figure 37.

The base has a diameter of 48 mm, whilst the upper base has a length of 27.5 mm, reaching a total height of 35 mm.

3.4.2 Thumb

This sub-section will explain the mechanism used for the thumb. The thumb was one of the most challenging aspects to design for the prototype, as depending on the method of coupling with the system for its palmar and dorsal rotation, the thumb could have different closing mechanisms. In previous models, a few prototypes of little significance were sketched out, but it was taken into consideration from this model onwards.

Figure 44: thumb mechanism

Following the design of the actuation system to position the thumb in both palms, it was found that the thumb does not need to be able to close on both sides, as, by rotating on a fixed axis positioned at the end of the frame, it will always position itself opposite the fingers to form a grip. This eliminates any issues related to bilateral closure and allows for the development of a more traditional mechanism.

The figure 44 illustrates the mechanism designed for closing the thumb. To simplify the model, it was decided to make only the metacarpophalangeal (MCP) joint movable, using it as a pivot, thereby ensuring the closure of the entire thumb block. In an initial draft, the interphalangeal (IP) joint was to be fitted with a cord-operated closure mechanism, driven by the mechanism described below. It was subsequently decided to make it fixed, creating a 20° angle between the proximal and distal phalanges. This is because when the thumb opposes the other fingers, the IP joint has a reduced range of motion. By fixing it in this way, we will achieve a stiffer structure, capable of withstanding greater loads.

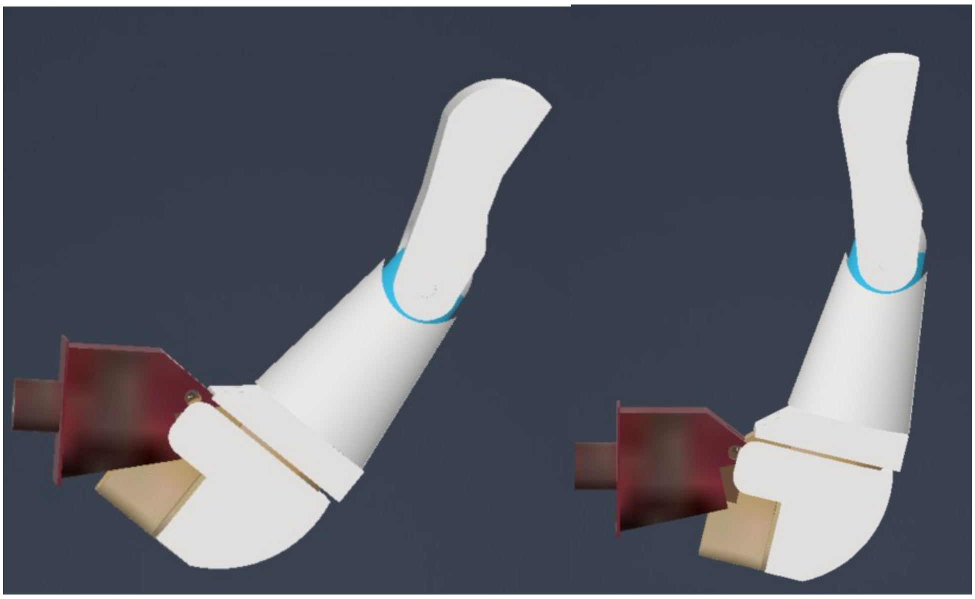

Figure 45: view of the thumb in the open and closed positions

Due to the reversibility of the four three-phalanx fingers selected for the prototype, a mechanism was chosen that would ensure the irreversibility of the thumb, thereby guaranteeing a secure grip, as the four opposing fingers generate a greater overall torque.

Let’s now look at the mechanism, starting from the motor and moving on to the pivot point where the closure is generated.

Starting with the motor, a Maxon Motor 327533 DC gearmotor has been used; It consists of a brushed micromotor and a planetary gearbox, factory-assembled for high-precision applications and powered by a 3 V supply. This is a custom product manufactured by the company, capable of achieving a reduction ratio of 1:35, with a diameter of 10 mm and an overall length of 41 mm.

The gearbox is screwed to the main thumb frame and secured with threadlocker, which allows for axial and rotational locking whilst keeping the gearmotor in place. To transfer motion from the output shaft to another shaft positioned perpendicularly, a coupling using straight-toothed bevel gears was used, with a module of 0.5 and 15 teeth. The result is therefore a coupling without reduction.

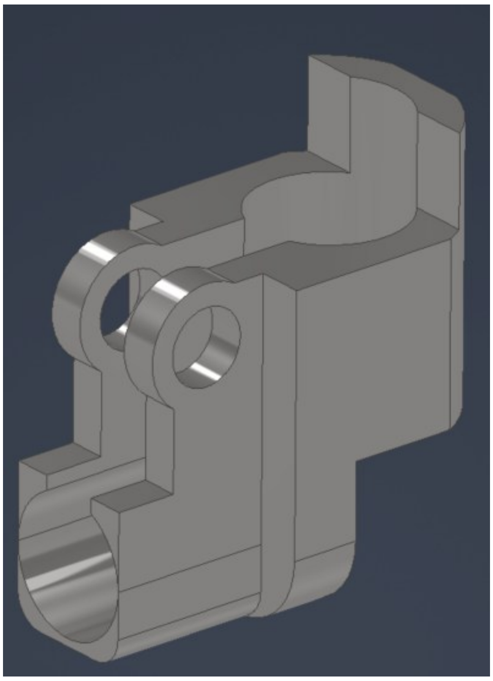

Figure 46: view of the thumb central metal support

At the bottom of the frame shown in the figure 44, a worm screw approximately 8 mm long will be coupled to the bevel gear. The complete assembly will consist of the bevel gear, a ball bearing, a 6.5mm diameter bronze washer, the worm screw, another ball bearing, another bronze washer and a Seeger ring for DIN 472 bores. To complete the mechanism, the worm screw engages with a helical gear section fixed to the secondary frame, which connects to the thumb attachment and has its pivot point aligned with the holes in the upper part of the main frame. This is where the pin is located, around which the entire system will rotate; the two parts will be secured by a pin that acts as a locking mechanism.

The I-Limb prosthetic hand mechanism was used and described in this bilateral hand prototype.

Figure 47: view of worm gear

Figure 48: view of the gear frame

3.4.3 Connection between the thumb and the frame

Once the design of the thumb was complete, the frame connecting the thumb assembly to the main frame was defined. The final component of the thumb performs two main functions; the first is to connect to the next frame via a 6mm diameter cylinder with a hole for M3 screws at the rear, the second is to carry the motor power supply via two cables that run through the entire thumb and are soldered to two connectors, which are in turn inserted into the part and exit at the rear.

It was therefore necessary to design a component that meets these specifications, whilst also taking into account the loads to which it will be subjected.

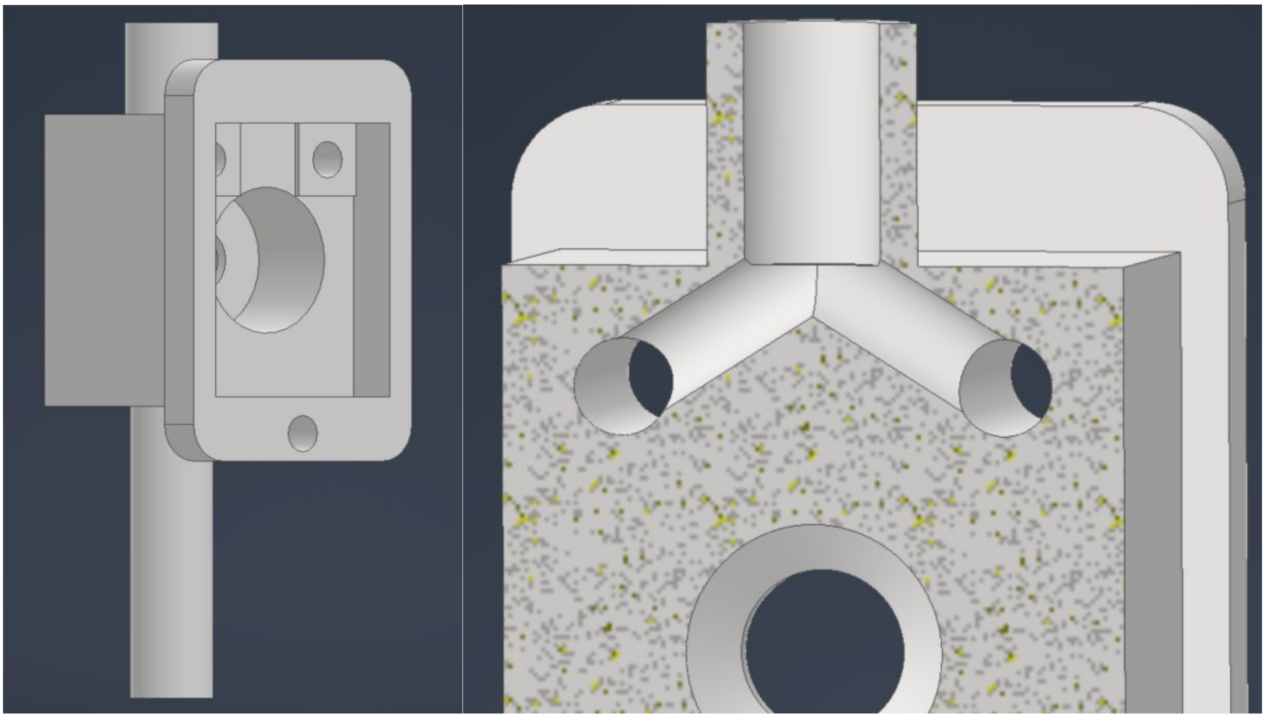

Figure 49: view of the intermediate frame for the thumb attachment

The figure 49 shows a detailed view of the frame and its internal structure. Starting from the front, the frame features a 12mm x 15mm recess designed to house the thumb component. There is an 8mm-diameter hole intended to allow for screw fastening, with the screw to be inserted into the rear of the component. At the top of the recess there are two 2mm diameter holes, housing two conductive pins to which the power cables will be soldered. Due to the continuous rotation of the component from the front to the back of the hand, the cables may become tangled or risk breaking; for this reason, it was decided to route the cables directly out through the upper central hole, passing through part of the side frame, thereby avoiding the problem. Two 2mm-diameter channels have been created near the pins, which will merge into the central channel with a diameter of 3mm. Each cable will have its own dedicated channel, with pins soldered to the ends, which in turn will be secured with resin inside the hole.

The frame features two shafts: the upper shaft is designed to route the cables and to interlock with the adjacent frame, whilst the second shaft passes through the adjacent frame to interlock with it, and then engages with the bevel gear via a set screw, as the gear is fitted with a tapped hole, thereby ensuring a stable connection and the transmission of the desired torque and speed.

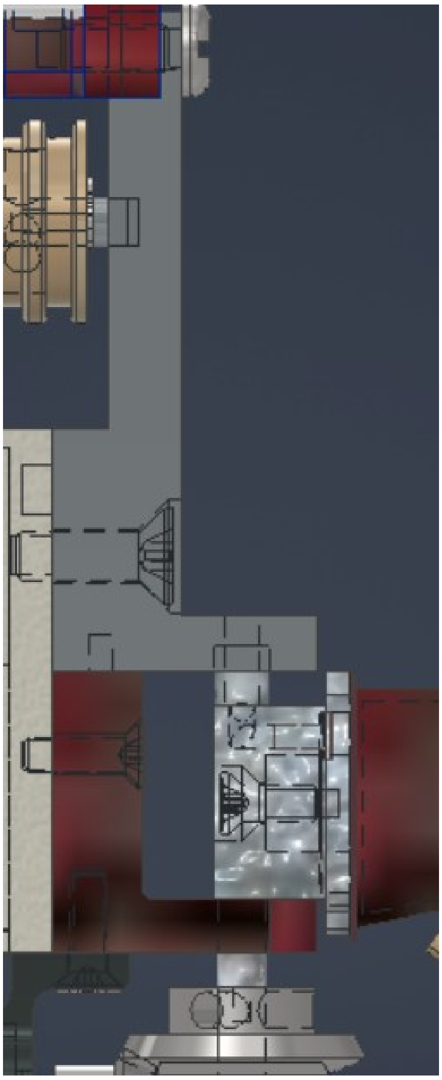

Figure 50: view of the thumb rotation mechanism with its couplings

A significant update to the model has been made to the thumb-grip block; in fact, to simplify the production of the parts and improve assembly efficiency, the frame has been divided into two sub-assemblies. As can be seen in the figure 50 the frame analysed previously will first be inserted into the burgundy block, which connects via an M3 screw to the frame shown in black at the bottom. The frame is attached to the main chassis using a countersunk screw and features a 2mm diameter, 3mm high extrusion designed to align with the upper part, which is also attached to the main chassis using a flanged screw. In the figure, we can see that the two frames described above have a hole designed to accommodate the two cylinders of the light grey frame, creating a guide in which it can rotate with its centre line positioned precisely near the holes. As it is enclosed by the two frame sections, it will be clamped in a vice, preventing axial movement and allowing rotation only about the main axis.

The upper frame protrudes 11.3 mm from the main section; this dimension has been calculated to accommodate the recess into which part of the upper shaft fits, and to ensure that it does not come into contact with the frame during rotation, which could cause it to jam.

3.5 Fifth model

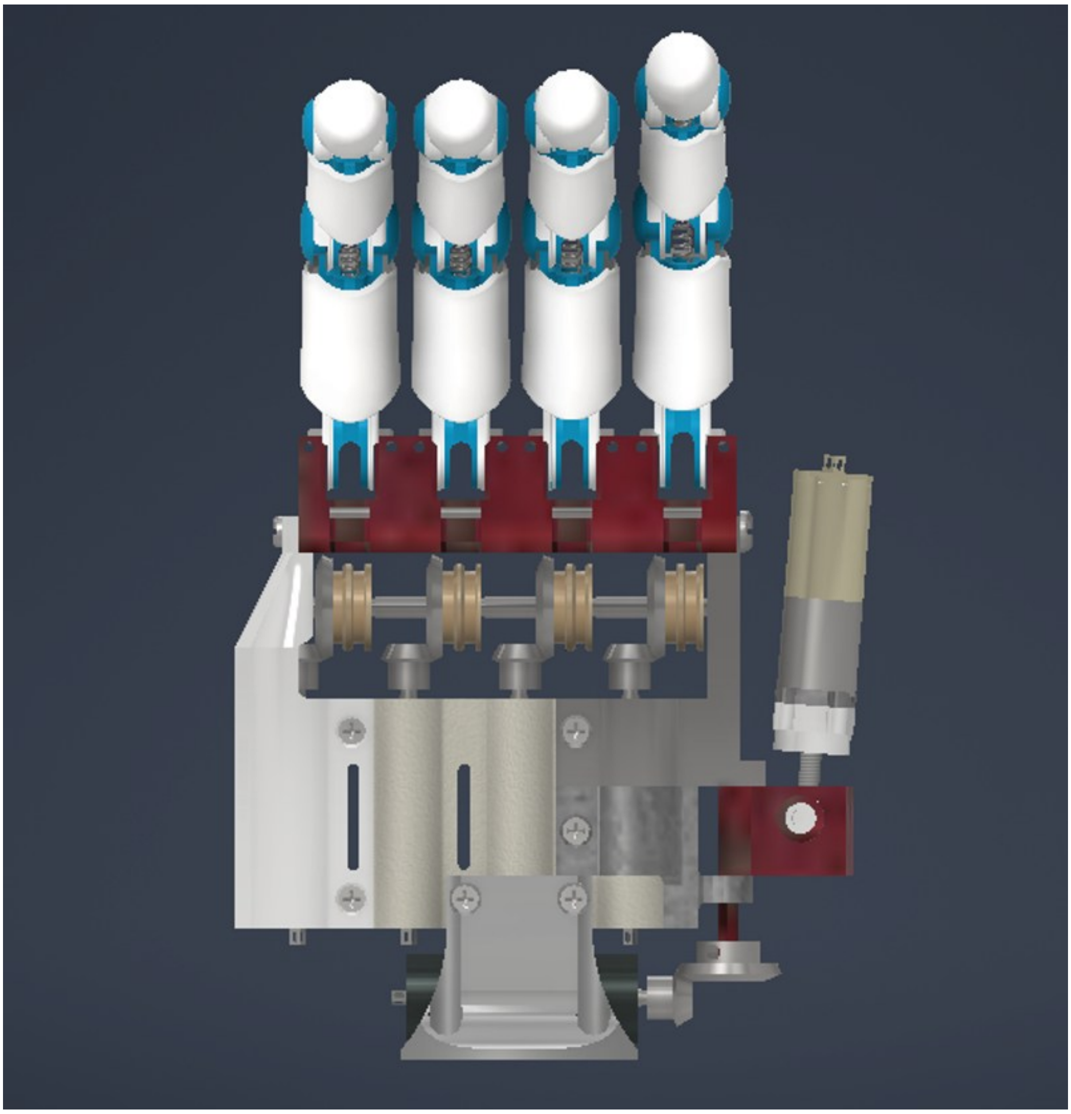

Figure 51: front view of the fifth model

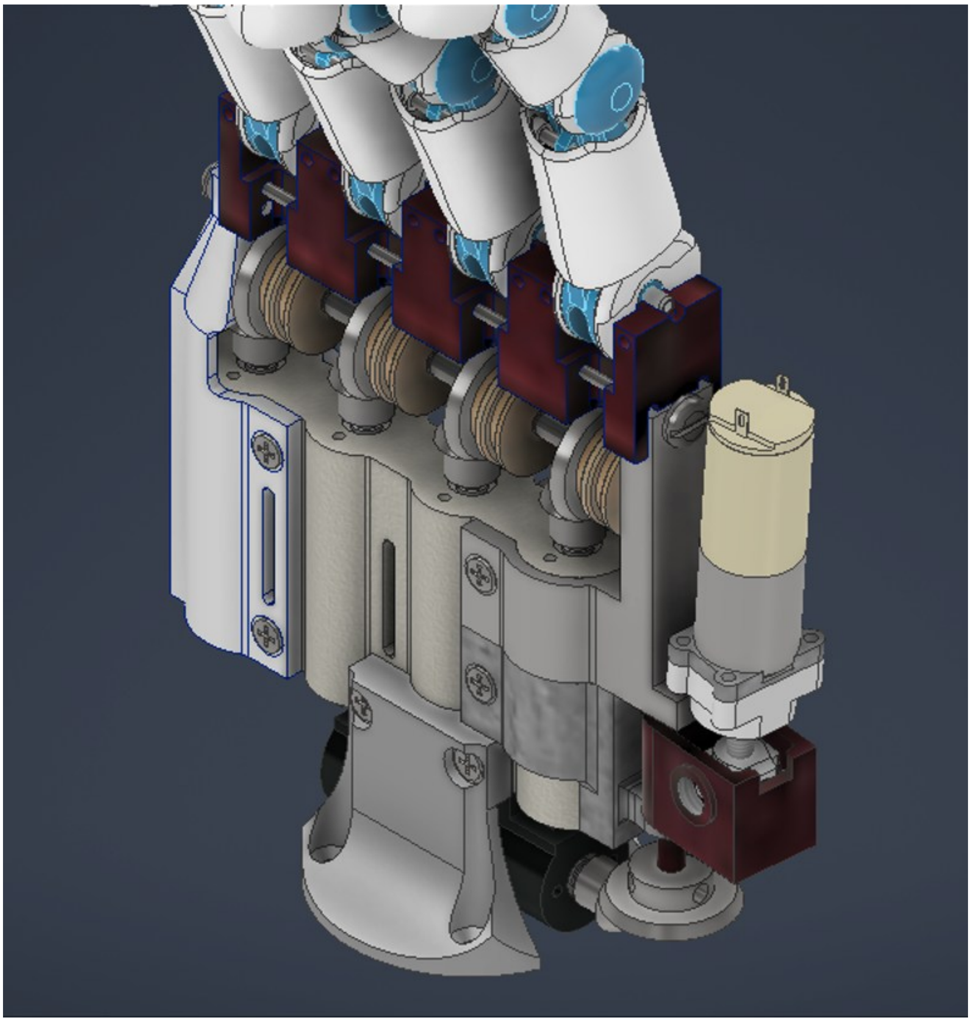

Figure 52: side view of the fifth model

In this prototype, we will illustrate the significant changes made to the frame regarding the thumb mount and the connection to the upper frame. With the exception of the main frame, which has been modified to feature M3 screw holes for coupling with the components to be described, the other components will remain unchanged.

Following a moulding and assembly test, it became apparent that the system lacked stability due to the couplings, the frame dimensions and the load generated by the thumb block. Due to the assembly methods, different frames were required, and because of the moulding processes associated with the powder bed printer, it was not possible to achieve the precision needed for a successful assembly.

It was therefore decided to improve the mounting strategy so as to adapt it to 3D printing during an initial prototyping phase. Building on this, inspiration was drawn from the design of the block at the opposite end of the main frame, using a frame that partially wraps around the main frame to make the most of the couplings and make them more stable.

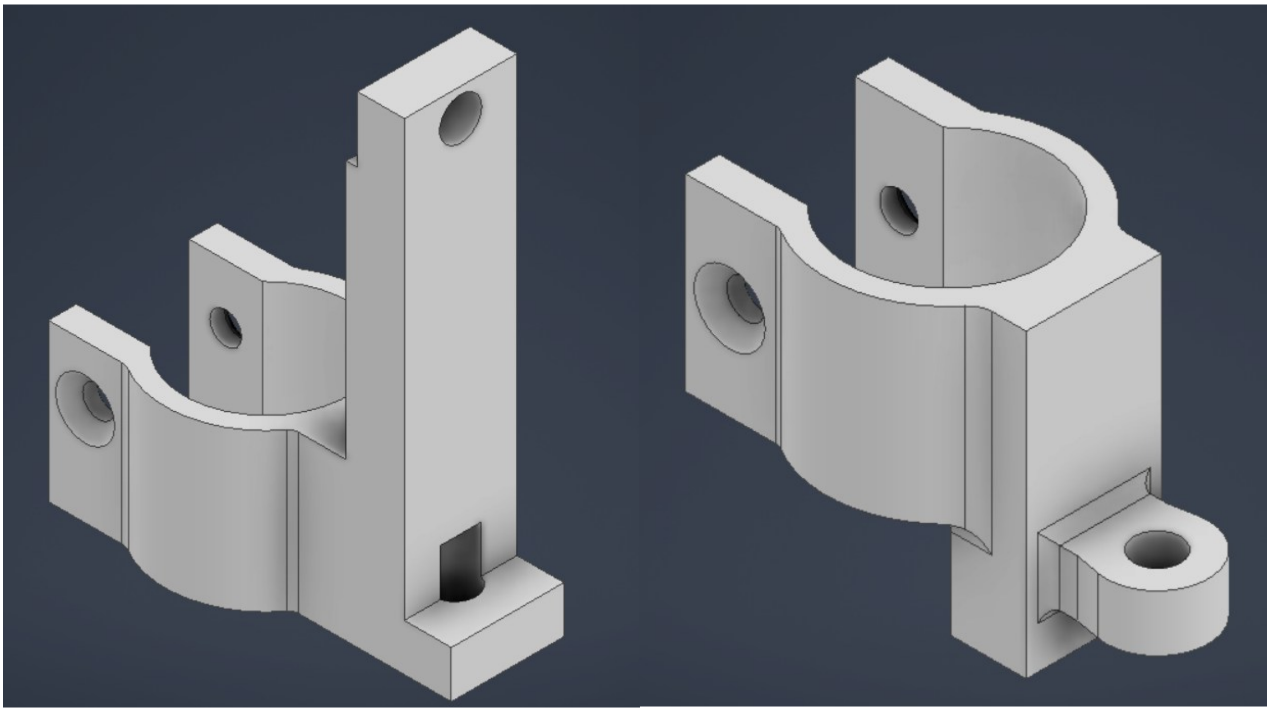

Figure 53: view of the upper and lower frames fitted to the main frame

As can be seen from the figure 53 and from the overview of the complete model, two frames have been created with a central structure of the same dimensions as that used for the frame on the opposite side, with the height varying by 16.75 mm for each. The same mating dynamics as the aforementioned part have been retained. The first figure illustrates the frame for supporting the upper needle holder and the interlocking support for the main shaft. At the upper end, there is a hole for M4 screws for assembly. At the lower end, there is a 4.5mm diameter hole which serves the same function as in the previous model, both for cable routing and for aligning the frame shaft attached to the thumb.

The second figure, on the other hand, shows the frame that supports the thumb block. The model features the same type of machining as the adjacent part, except that the end has been extruded by 22 mm to achieve the required height for the connection. There is a ring with an internal diameter of 4 mm that performs the function of the frame analysed in the previous model. Compared to the fourth model, this system is aesthetically cleaner, with a more robust structure capable of withstanding loads whilst saving 10 mm in width, making the overall frame sleeker. Following these modifications, a further four threaded holes for M3 screws were added to the main frame to connect the parts and remove the slot located in the space between the two motor centre lines.

3.5.1 Thumb

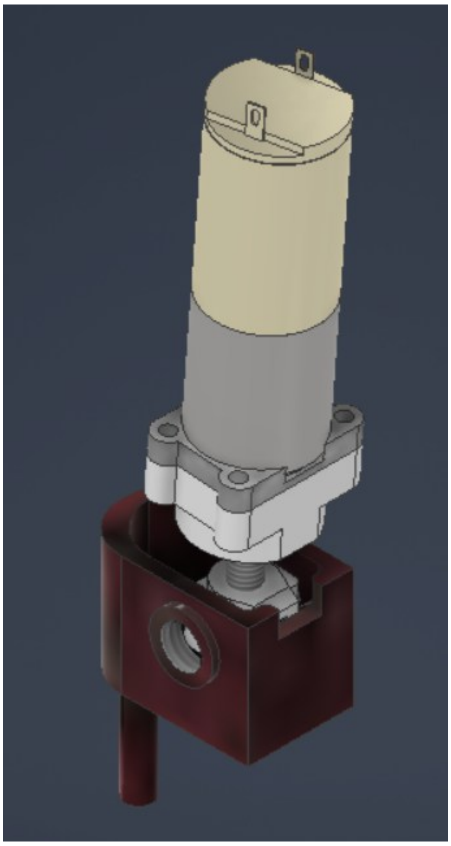

Figure 54: view of the new thumb mechanism

In the model described, new thumb mechanisms have been outlined for comparison with the mechanism analysed in the previous paragraphs. The figure shows the mechanism without the thumb cover, in order to illustrate its components and operation. Compared to the model discussed, this mechanism bases the closing of the finger on the principle of rigid links and the study of the quadrilateral. The gearmotor block is flanged to a steel ring nut, which in turn is flanged to a worm screw with a total length of 16 mm and a diameter of 4 mm. The output shaft from the gearmotor is inserted directly into this frame, creating a pin-coupled connection between the shaft and the bore. The worm screw is housed in a frame measuring 10 mm x 10 mm x 12 mm, which in turn is free to rotate within its support via two 4 mm diameter pins on either side. During operation, the screw will bring the piece closer to the support, which, via a rod connecting the burgundy piece and the worm gear frame, will create a quadrilateral that draws the piece closer, creating a bending motion. In turn, through the use of custom-made covers, the approach will bring part of the cover into contact with the support, pushing the section of the cover upwards so that its extension allows the distal phalanx to flex. The end-of-travel limits for thumb flexion are determined by the constraints imposed by the support. Compared to the previous model, this one is more complex, involving an in-depth analysis of the quadrilaterals and movement via rigid constraints.

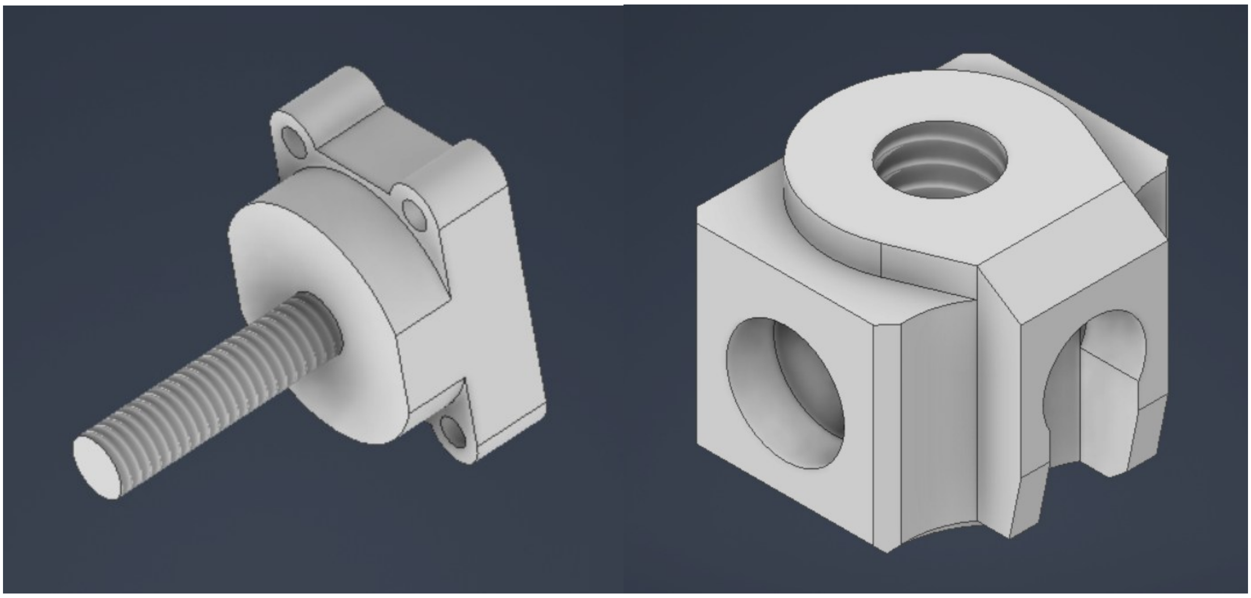

Figure 55: view of the pin onto which the worm screw is screwed

Following a more detailed assessment, it was decided to abandon this approach, as it required greater attention to detail; however, due to the tight development schedule, the previous model was chosen instead. Nevertheless, it remains a viable alternative with potential for future development.

3.6 Sixth model

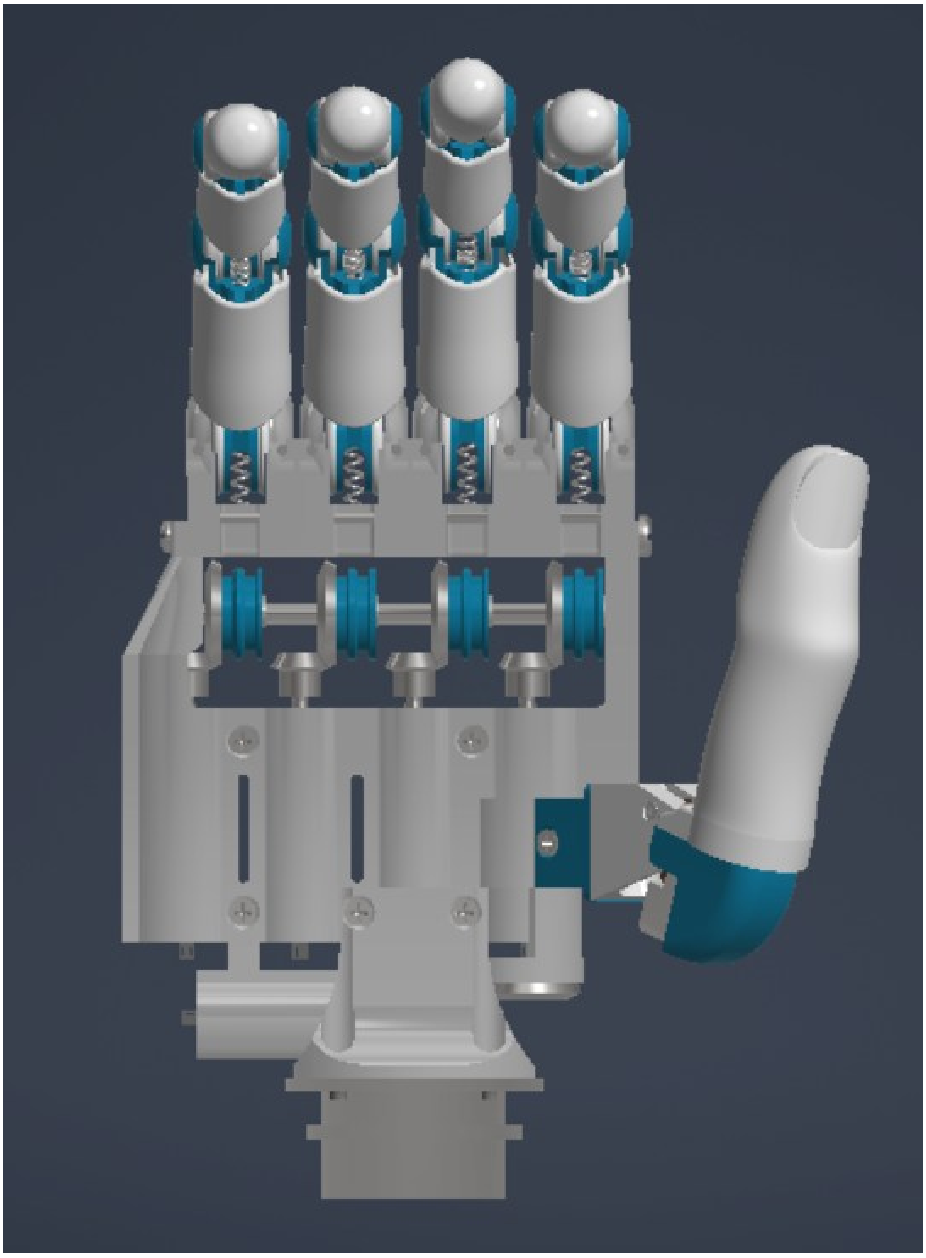

Figure 56: front view of the sixth model

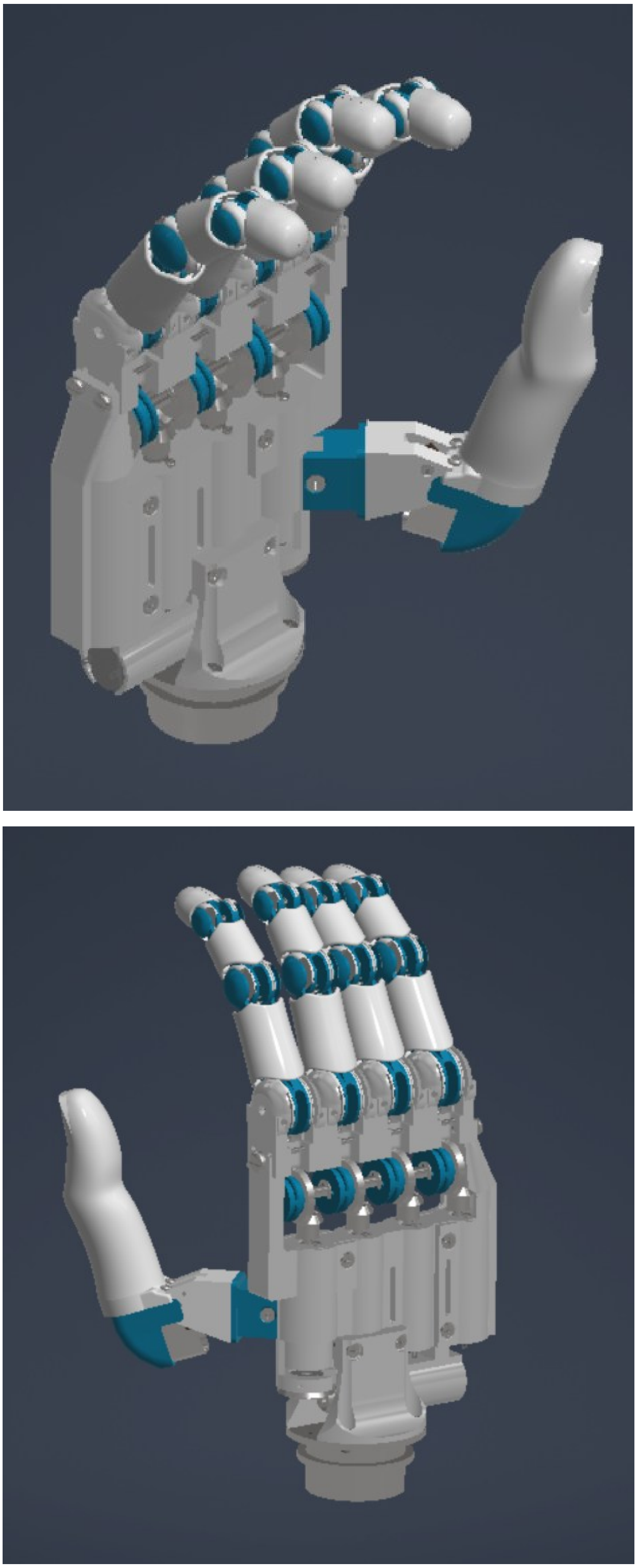

Figure 57: side views of the sixth model

The figures 56 and 57 above show the final model, complete with all fittings and components. The colour and material of each individual part have been incorporated into the model, with the total mass and characteristics calculated. The frame material used is 6061 aluminium; C45 carbon steel was used for the conical gears; stainless steel was used for the main shaft and secondary shafts; whilst 3D powder-bed fusion prints were used for the remaining components, including covers and pulleys.

The model includes all the components and connections required for construction and assembly, which will be listed below. In this prototype, changes have been made to the thumb connection to the main frame and the finger holder design has been improved.

3.6.1 thumb

During the development of the fifth prototype, a problem was identified that was preventing the hand from closing properly. Due to the position of the thumb rotation pin, located adjacent to the index finger axis, during rotation from both the palmar and dorsal sides, the thumb did not reach the required position; consequently, during closure, the fingers only partially opposed each other with the index finger, leaving the other three fingers without any contact. This led to a misalignment of forces which, when grasping an object, caused it to rotate without ensuring a secure hold.

During the analysis of other robotic prosthetic models, attention focused on the position of the thumb's axis of rotation, which is situated at the base of the artificial metacarpal, with a pivot passing through the body of the prosthesis in a palmar-dorsal and slightly oblique direction, geometrically replicating the CMC. However, this solution is suitable for anthropomorphic hands with palmar closure only. In the current model, this inclination would have caused significant design problems.

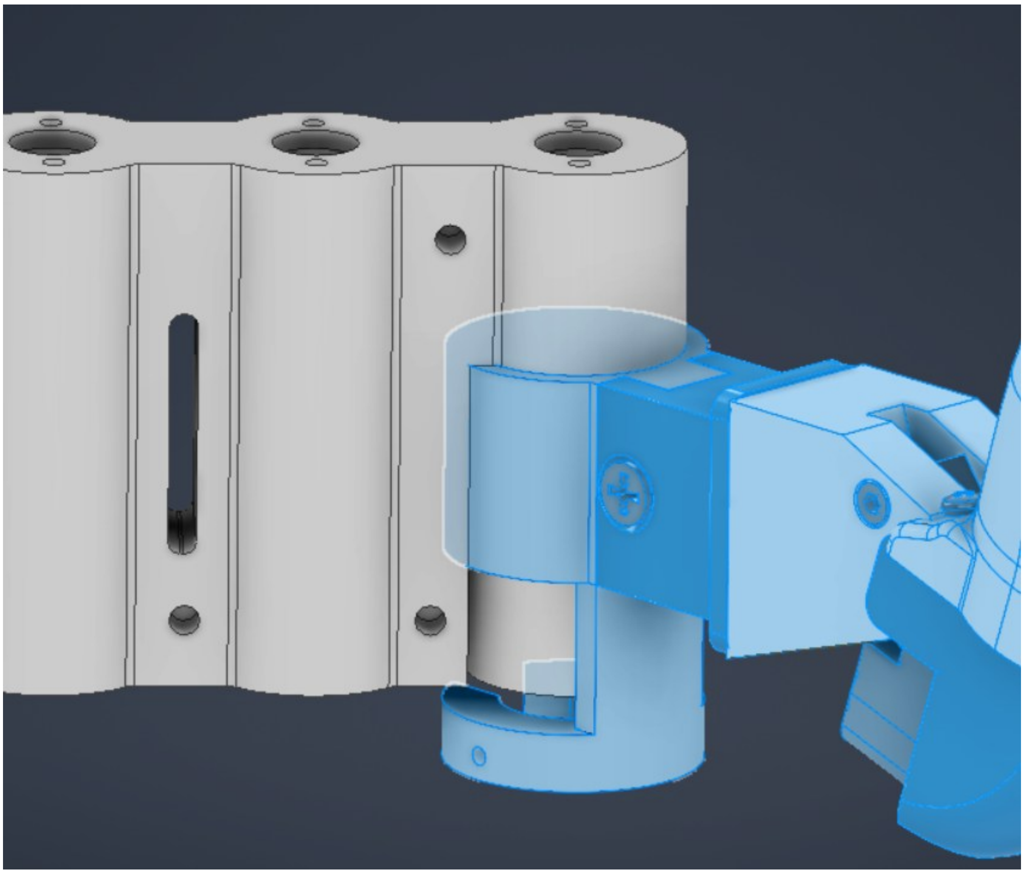

Figure 58: thumb rotation frame with matching paired thumb piece

In light of these considerations, the pivot point for our model had to coincide with the axis running through the centre line between the index and middle fingers. This axis corresponded to the centre distance of our hollow cylinder, which housed the gear motor responsible for actuating the index finger. We considered a mechanism that could resolve this issue, with its fulcrum located directly on the main frame.

As illustrated in the figure 58 a mechanism was created, using the same principle as the other frames, which exploits the shape of the main frame and its rigidity.

The main frame has been modified to create a 1.75 mm gap between the 17.5 mm diameter section, designed to house the gear motor, and the rest of the frame; this gap has been used to insert a 1.75 mm thick, 16.75 mm long hollow cylinder, which acts as the pivot point for the thumb's rotation whilst maintaining the specified centre distance. To connect to the bevel gear and ensure the transmission of torque and speed, a further 17 mm extension was created to reach the gear's mounting position. To ensure a secure fit, two 1.5 mm diameter holes, 3 mm deep, were machined into the wheel, with corresponding holes on the frame extension shown, designed to be fitted with two pins of the same diameter, each 6 mm long. Another significant issue was the axial locking of the frame along its sliding axis; even a slight shift would have caused the bevel gear to move closer to or further away from the pinion, thereby causing the system to jam. As can be seen in the diagrams of the complete model, the frame is locked axially at the top by the chassis frame that connects to the needle holder, whilst at the bottom, once inserted into its cavity, it is locked by the two frames designed to attach to the wrist. This allows the frame to rotate only along its axis without any translational movement. The extension was created using a section of the cylinder so that, once the thumb reaches its maximum position, it is stopped by the extension, which acts as a limit stop against the wrist attachment frame on both sides.

As for the mechanism for closing the thumb, the initial model created was retained, with modifications made to the attachment to the new system and the creation of a cover.

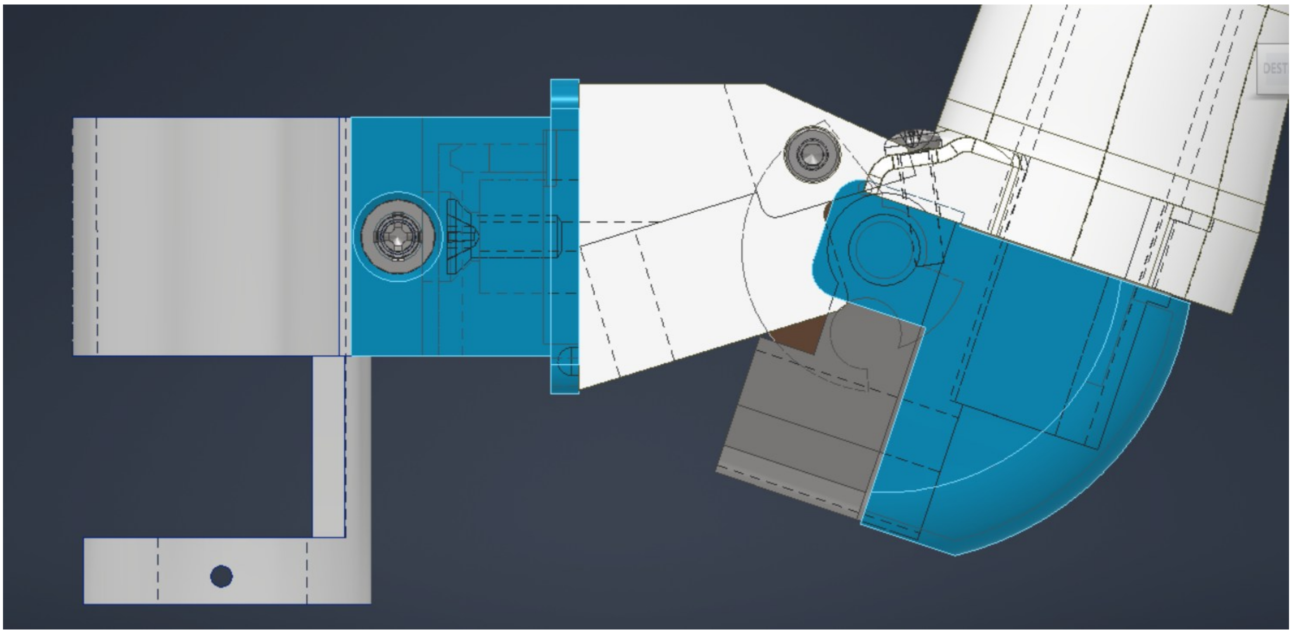

Figure 59: thumb assembly with visible couplings

Modifications have been made to the intermediate frame that connects the aluminium frame to the thumb. Due to the design of the frame responsible for attaching the thumb and the need to use an M3 screw to secure it to the rest of the assembly, the blue intermediate frame is an essential component for the assembly. Drawing on the original frame, a connection has been created using a cavity-and-projection fit between the aluminium frame and the component, which is then secured by two M3 screws that hold it in place. The model shows the cavities where the two conductor pins are inserted, in this case extending them towards the lower part of the frame, as there is no longer a need to route the cables through a cylinder. The aim of this change was to group all the power cables for all 6 motors in the lower part of the model, without creating any obstruction among the moving mechanical parts.

In the illustration 59, we can see two M3 hex head screws, two M3 Phillips screws and a pin that acts as a pivot point at the centre of the thumb mechanism. The two Phillips screws are used to secure the cover inside the central steel block, with an additional internal support within the cover that will slot into the rear of the steel frame, ensuring stability and preventing any rotation or movement.

The thumb cover is produced using powder bed 3D printing, forming a single block between the proximal and distal phalanges. The decision was made to simplify the design, giving the joint a 17° angle between the two phalanges and achieving a total height of 70 mm. As this is a thumb with an anthropomorphic, non-bilateral function, a design was chosen that mirrors a traditional finger.

3.6.2 Further changes

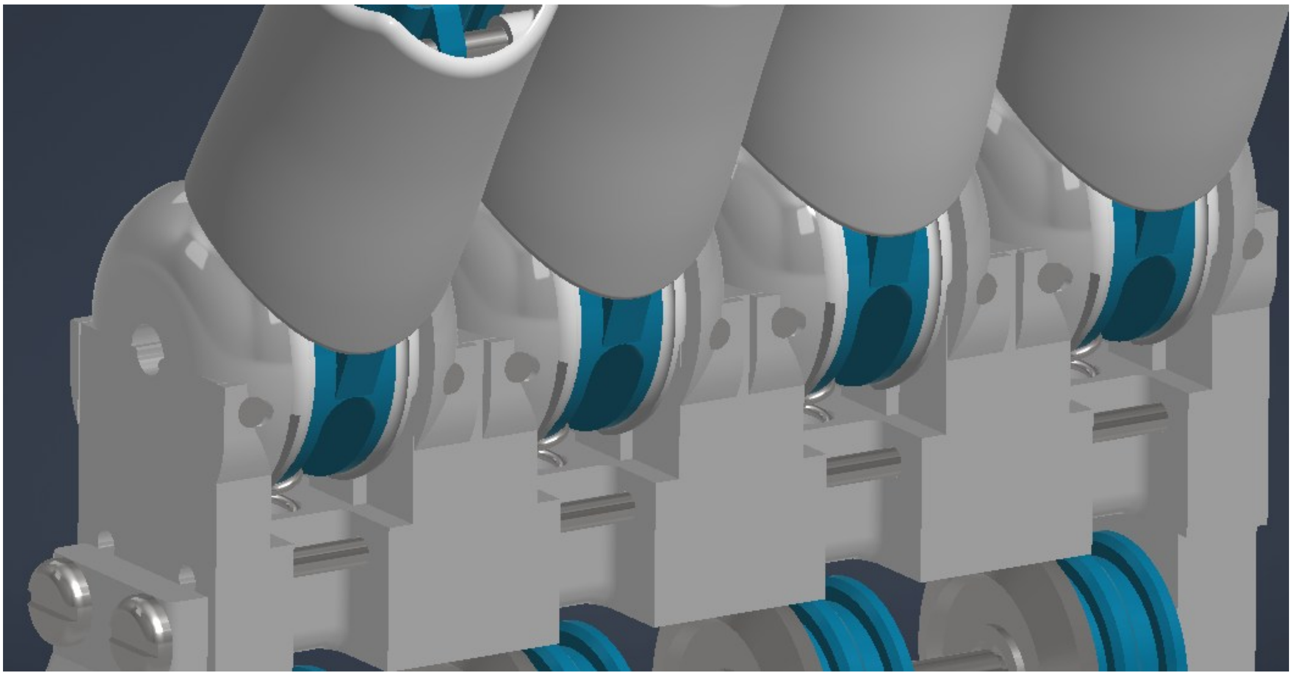

Figure 60: full view of the top of the model

The attachment of the fingers to the frame has been redesigned, with the addition of elements that serve both a decorative and functional purpose. As shown in the figure 60 two covers have been added to the end of each finger near the metacarpophalangeal joint, secured to the frame by two 2mm-diameter pins. During the 3D powder printing phase, it was decided to treat them as a single piece of the frame, due to the size of the covers and their fragility if considered as individual parts. The fingers are connected via a shaft passing through the aforementioned joint, allowing rotation about it whilst preventing translation and rotation about the other axes. The covers serve as supports for a 2mm-diameter, 83mm-long shaft passing through all the covers, which will support all four fingers.

Following a number of tests, it became apparent that the springs were in the way when the aforementioned shaft passed through, causing the springs to twist to one side, which will result in a different spring return depending on which side the spring has moved to. It was decided to cut the steel bar into 13.5mm pins, except for the two outer covers where the pins will be 6mm, with the aim of inserting them into the supports in such a way as to replicate the functions of the through-bar for all fingers whilst leaving the spring's passage unaltered, thus achieving an equivalent spring return. In the initial testing phase, this is not particularly significant, but in a more advanced phase it can result in significantly different fuel consumption and performance.

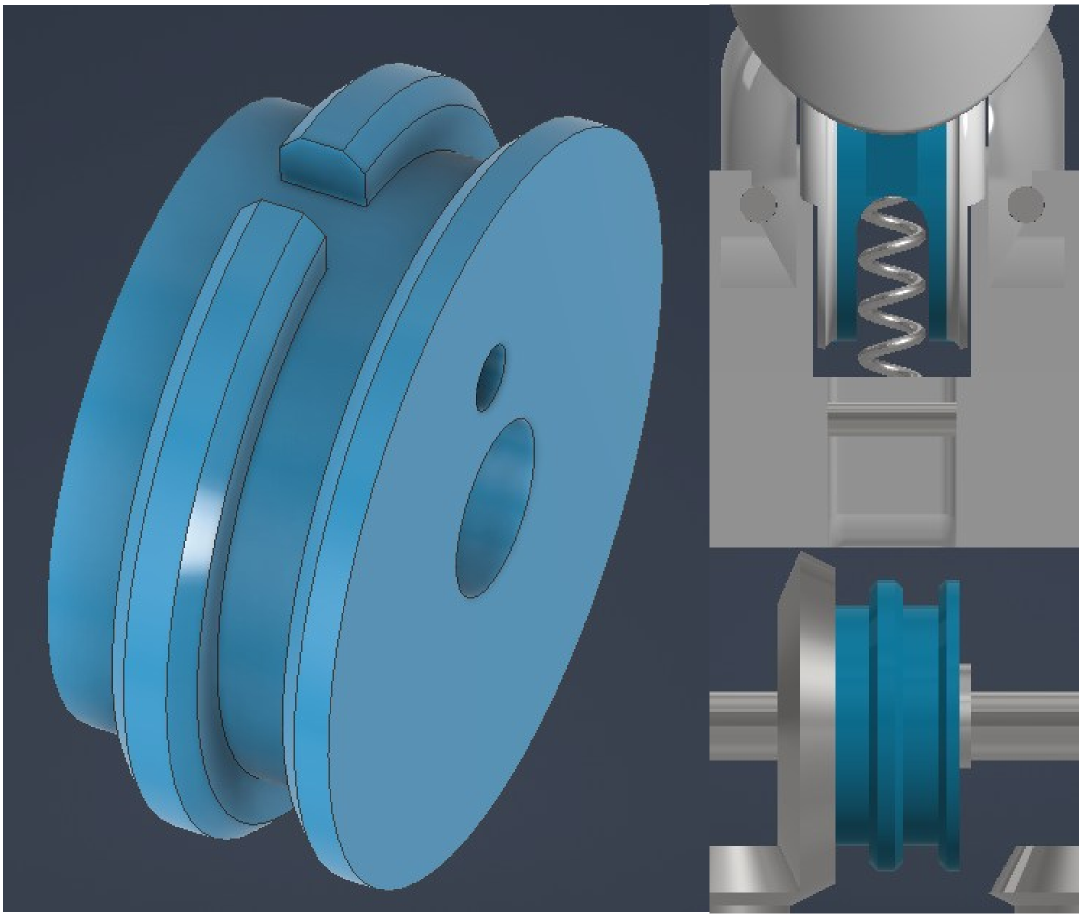

Figure 61: cable-winding pulley aligned with the finger

Minor changes have been made to the frame of the cable reel pulley compared to the previous model. Due to the positioning of the actuation systems and the fingers, the pulley's position is determined by the contact between the pinion and the bevel gear, as the pulley is coupled to the latter. The pulley was found to be on the same centre line as the fingers; however, its dimensions are smaller than the space between the two cables passing through the first joint. It was decided to chamfer the edges of the pulley by 0.5 mm where the cable channels are located, in order to ensure smooth movement even when climbing at an angle, thereby avoiding contact tension between the edge and the cable which could cause the cable to break or damage the frame.

3.6.3 Other components

In order to assemble and operate the hand, other components were required, such as the screws and bearings mentioned in the previous paragraphs. The table below provides a list of these, specifying their quantity, dimensions and the position in which they are used.

component	dimension	standard	quantity	position
Countersunk flat-head screw with cross-recess	M3x0.5x8mm	IFI 513	10	connections between the frames and the main frame
Countersunk flat-head screw with cross-recess	M3x0.5x10mm	IFI 513	6	connections between the frames and the main frame
Round-head screw with slotted head	M3x8mm	AS 1427	2	connections between the fifth engine frame and the main frame
Round-head screw with slotted head	M4x10mm	AS 1427	1	connection between the finger holder frame and the right-hand side frame
Slotted pan head screw	M1.6x5mm	BS 4183	10	connections between the gear motors and the main frame
Countersunk cross-recessed screw	M2x0.4x8mm	ANSI B18.6.7M	2	joints in the thumb mechanism
External Seeger	4mm(shaft diameter) 3.2mm(groove diameter)	DIN6799	8	used on the main support shaft

spacers	11.5 mm x 4.5mm (internal diameter)	/	3	used on the main support shaft as an alternative to Seeger rings
washers	1mm width	/	2	used on the main support shaft as an alternative to Seeger rings

Table 1: list of components used to assemble the hand

To ensure the success of the bevel gear couplings, machining work was carried out by the mechanical workshop of the DEII at the University of Padua. With regard to the couplings between the bevel gear and the pulley, a 1.5 mm diameter hole 3 mm deep was milled into the base of the gear, designed to accommodate a spring pin of that size. As for the fifth gear wheel used to connect to the frame for thumb rotation, two holes were drilled, 180° apart, 1.5 mm in diameter and 2.5 mm deep, perpendicular to the base of the wheel. This machining is intended for coupling via two pins, designed to rotate the wheel and the frame in unison.

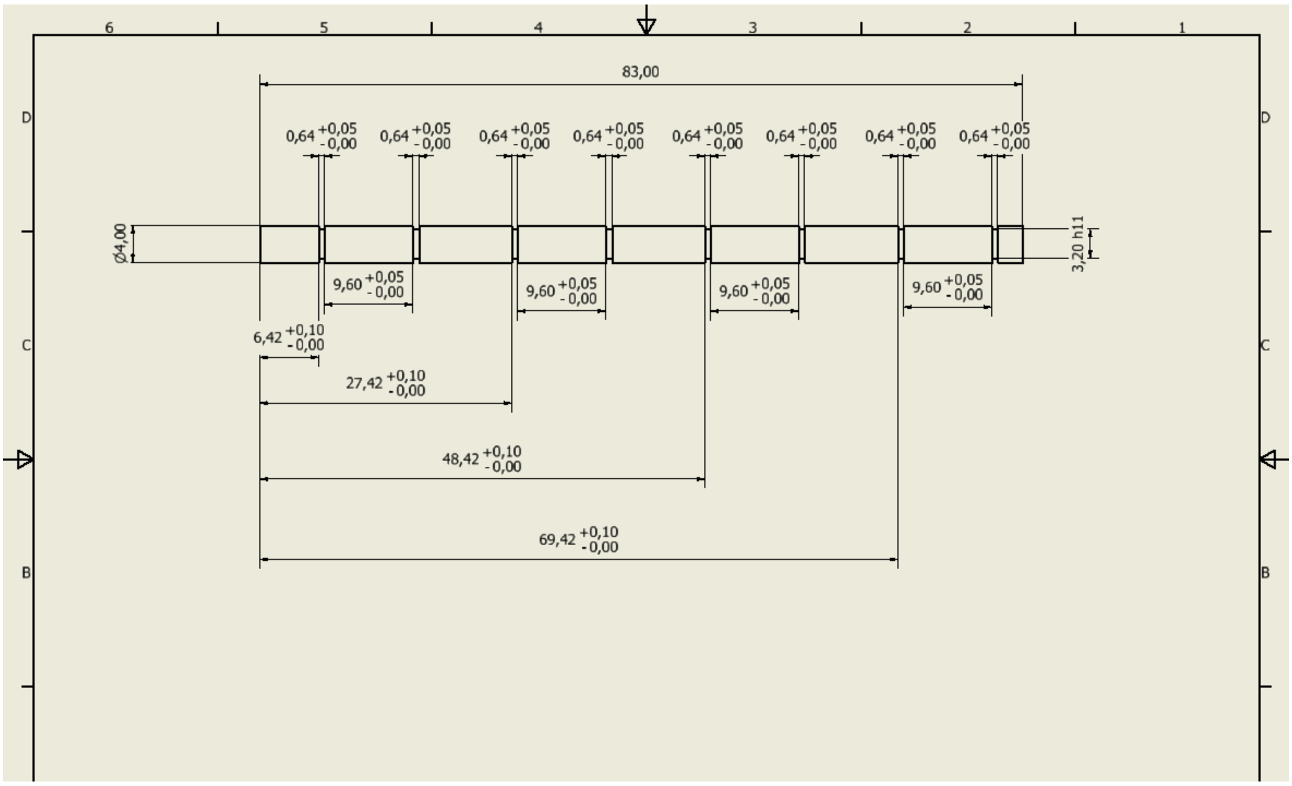

Figure 62: technical drawing illustrating the machining operations on the main shaft

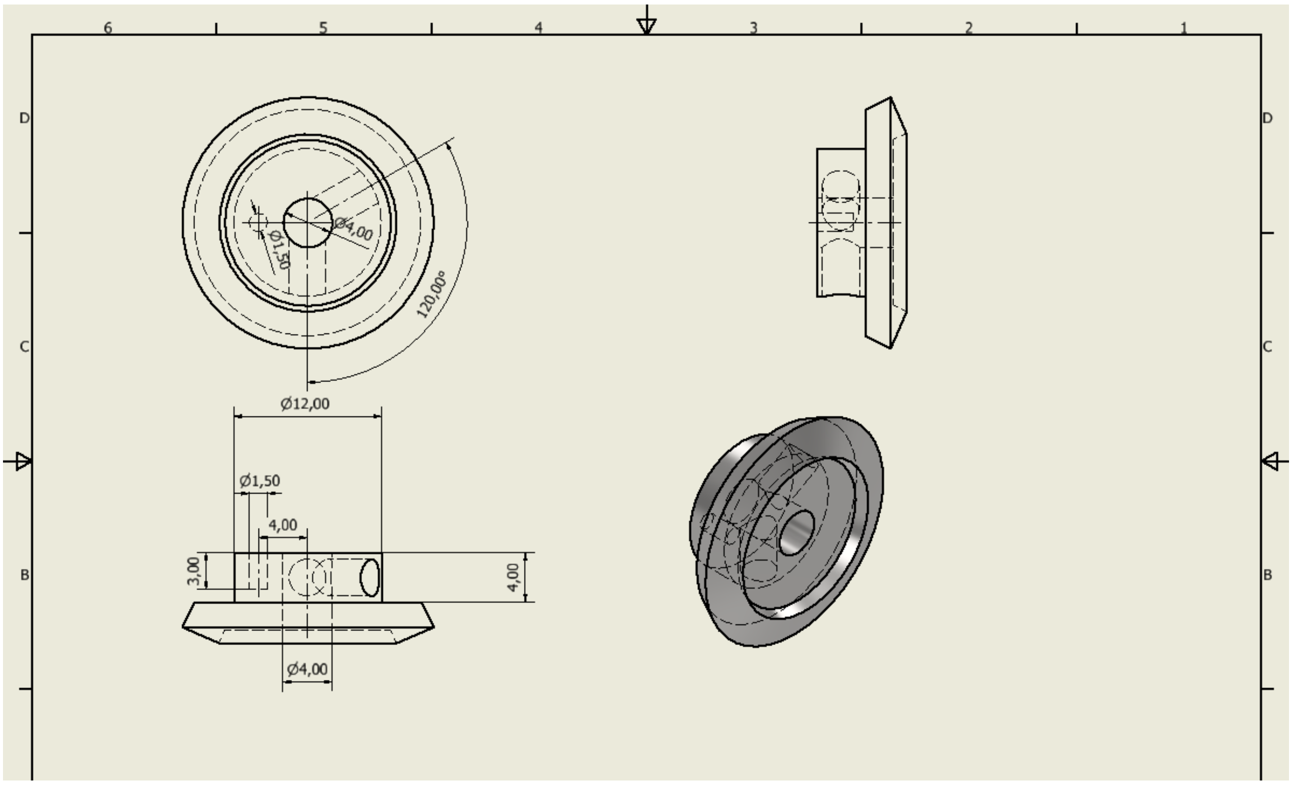

Figure 63: technical drawing illustrating the machining operations on the four bevel gears

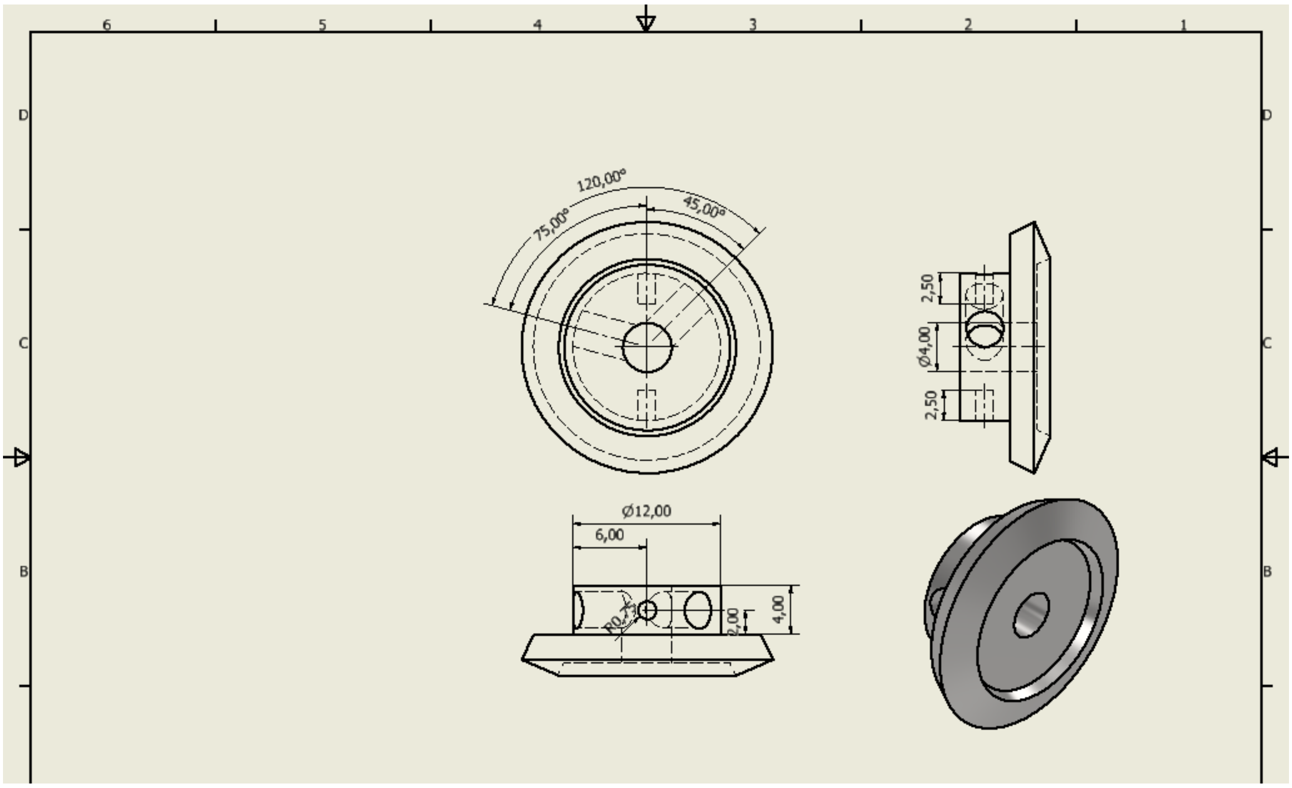

Figure 64: technical drawing illustrating the machining operations on the fifth wheel for thumb rotation

Chapter 4

Results

Bearing in mind the initial aim namely, to conduct a feasibility study of a bilateral-grip robotic prosthetic hand, this chapter will present the results obtained in order to determine whether or not the set objectives have been achieved. The assembly procedure will be described, highlighting the final issues encountered and the possible solutions. The tests carried out using test specimens will be reported.

4.1 Assembly and considerations

Following the production of the rapid prototyping parts, those machined on CNC machines and the purchase of the additional components required, the assembly process began. Due to malfunctions with the powder bed printer, the assembly and various tests took longer to complete.

During the design of this model, several assembly options were considered, creating connections that would not unduly complicate maintenance in the event of disassembly and replacement. The first step involved mounting the four gear motors onto the main frame.
Due to the powder-bed 3D printer, using a hole diameter matching that of the gear motor caused insertion difficulties, although this ensured a secure fit without wobble. If this 3D printing technique is used, it is not recommended to enlarge the hole by 0.1–0.2 mm to facilitate insertion. The gear motors will be flanged to the main frame using eight M1.6 screws, securing them in place. The motors are fitted with two cables at the lower end to supply power to the motor following an initial test, which caused minor complications during the assembly of subsequent parts. We then proceed with the assembly of the fifth motor's frame; the frame will be secured using two M3 screws at the bottom of the main frame. Thanks to its lower slot, it was possible to tighten the screws by inserting them from below the frame and screwing them into its countersunk holes, allowing them to be concealed. The gear motor was then fitted and flanged into position, just like the other four. The next step was to mount the pinions onto the output shafts of the gearboxes. Each pinion and bevel gear is fitted with two holes at right angles to the base, spaced 120° apart, with dimensions of M2.5 and M3 respectively, which can be secured using a grub screw supplied in the pack. The pinion will

be coupled to the output shaft via one of these holes using an M2.5 grub screw. Although the shaft is grooved, the axial positioning of the pinion is not identical for all shafts, as they are inserted and coupled manually. This coupling must be checked when fitting the wheels onto the shaft, as the height of the pinion is crucial for coupling with the wheel and the transmission of motion.

Once all the sprockets have been adjusted to the same height, the next step is to fit the frame responsible for the thumb's rotation. As it will be locked axially, it will be inserted via its guide at the bottom, and then secured from below by the mirror-image frames for the wrist attachment. Whilst this operation is being carried out, the pinion on the shaft will be connected in the same way as the others, whilst the bevel gear will be secured to the frame using two M3 screws, utilising the existing tapped holes. Once secured, we will connect the base of the mirror-image frames to the wrist module, thereby closing the lower assembly. One point to bear in mind is the motor power cables, as these may cause problems during assembly; it was decided to route all the cables to the lower section opposite the thumb, passing them between the mirror-image frames, above the motor mount frame of the fifth motor.

For the next step, the bar will be inserted into the side frame near the little finger, where the wheels and pulleys, already coupled by pins, will be fitted, effectively 'packing' the structure, which will then be closed by the opposite side frame. During assembly, it was not possible to source a shaft with grooves for the Seeger rings; consequently, the following components were fitted in sequence: a 1.25mm-thick washer between the frame and the first wheel, followed, after the first pulley, by three powder-moulded spacers with an external diameter of 8mm, an internal diameter of 4.5 mm and a length of 11.3 mm, positioned between the wheel-pulley assemblies. Finally, a 0.7 mm thick washer was inserted between the last pulley and the frame; this created the correct alignment that would have been achieved using the Seeger rings. Once the assembly is complete, the two side frames will be inserted onto the main frame via their guides, and then secured to the frame using M3 hexagon socket head cap screws. In this way, the bevel gears, having levelled the pinions, will all form a stable coupling supported by the main steel shaft, without any axial movement. Once assembly is complete, the needle-bearing frame will be positioned at the top and secured at each end by two M3 screws and one M4 screw.

The crucial step in this assembly process was fitting the fingers and positioning the filament, a task that took a long time due to the constant adjustments required during this phase. We will describe the assembly of one finger, as the procedure is the same for the other three. As only a powder-and-filament 3D printer was available, the finger model was made thicker to address its fragility.

Following the assembly of the three phalanges using two 2mm-diameter pins at the joints, a spring was positioned at the base, which will subsequently slot into the end opposite the frame. Once this is done, the initial pulley will be secured to the frame using two 2mm pins, so that it can rotate only along this axis. Multiple pins were used to secure the fingers to the frame rather than a single shaft, due to the presence of springs along the path; as the finger moves, these springs would shift to one side, causing asymmetrical spring returns for both directions of finger closure.

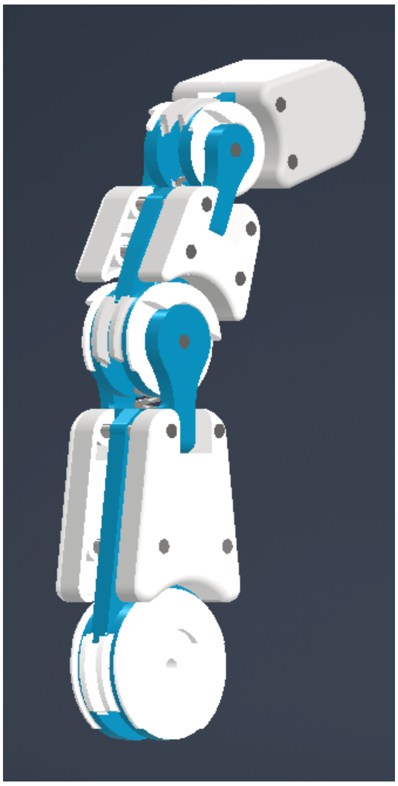

Figure 65: frame of the new finger

During the tests carried out to close the cables, it was noticed that the cables on the pulley were slipping due to excessive speed and low friction; as a result, the finger would not close. The pulley was reconfigured so that the wires were fed inside it and, using the wheel's axle, were pressed together in the middle, thus creating a restraint that prevents slipping. It was refitted onto the frame to change the wheels and reassembled, confirming that the solution worked.

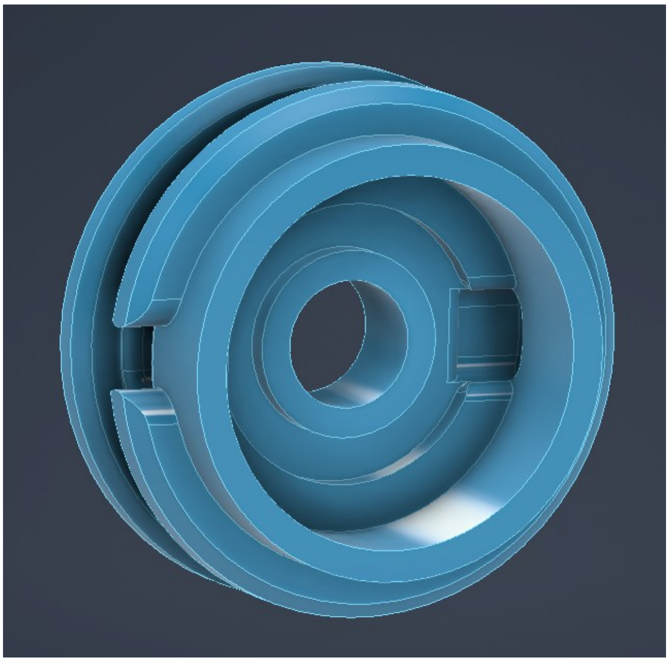

Figure 66: frame of the cable reel fitted

The biggest problem remained the bending of the finger, as after fitting the pins and the redesigned covers, the finger would not close as intended, due to friction and difficulties in routing the cables – caused both by loss of tension and the finger pulleys coming out of their guides. Due to the lack of a resin printer for producing the first finger as designed, the use of the new finger has resulted in closure defects that have not yet been resolved, given the limited time remaining. Again, due to printer-related issues, it was not possible to complete the printing of the other three fingers.

Due to these setbacks, it was not possible to carry out tests on the complete hand; instead, tests were conducted on the individual finger, the thumb, and its rotation into palmar and dorsal positions. All systems meet the pre-set calculation targets; therefore, the objective has been achieved.

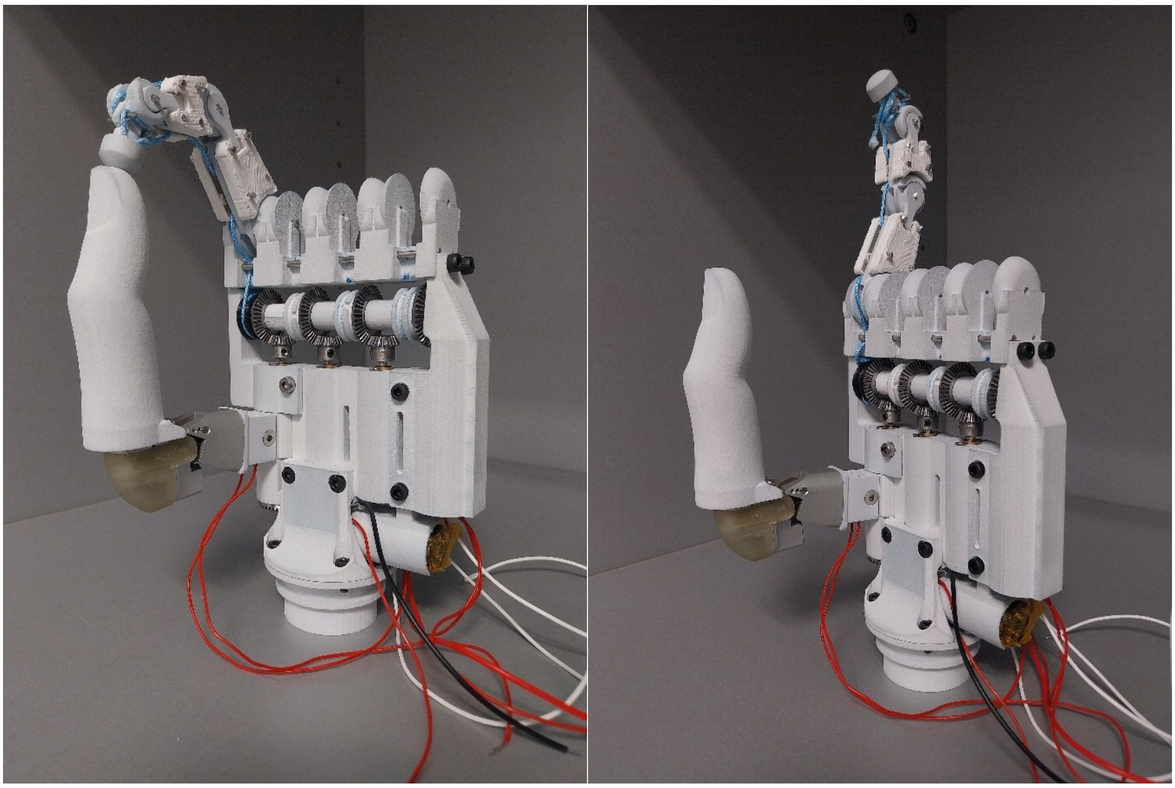

Figure 67: oppositional mechanism between the index finger and the thumb

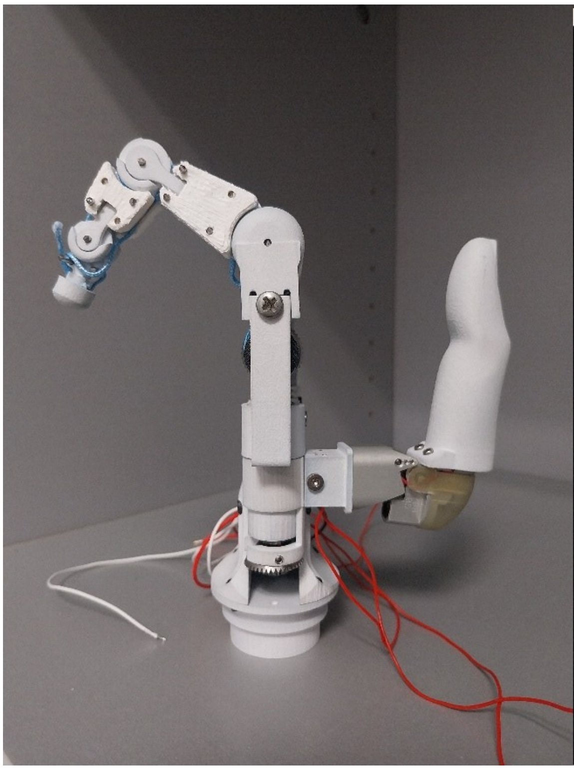

Figure 68: illustration of the bidirectional movement of the fingers and the rotation of the thumb from the palmar side to the dorsal side

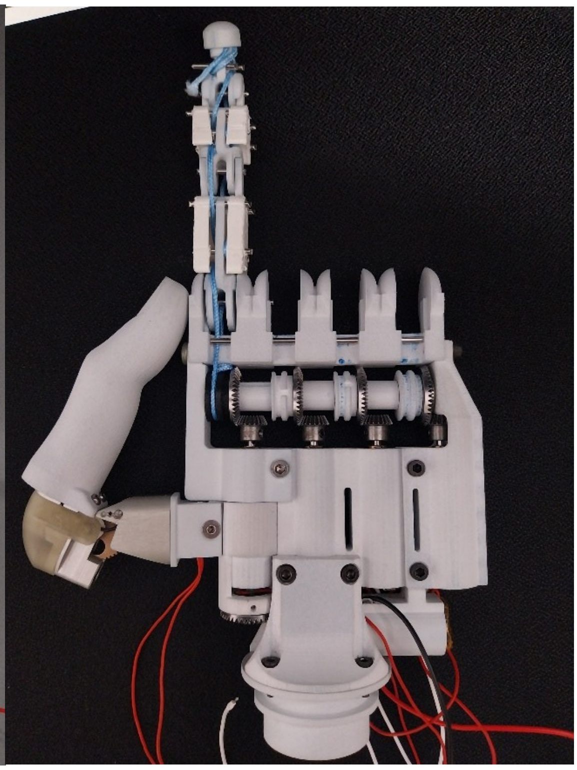

Figure 69: front view of the hand

In the figures, we can see the complete robotic hand, with the exception of the three remaining fingers, whilst the index finger is not fully formed. Tests were successfully carried out on finger bilaterality and the rotation of the thumb from the palm to the back; as these are complex movements, they require different control signals, since the rotation of the thumb takes place in a shorter time than that of the fingers and the closing of the thumb. In Figure 69, we can see how the thumb can perform an adduction movement towards the index finger. This movement was observed during thumb rotation but has not yet been studied; in future, it could be evaluated as an additional grip type alongside those already studied.

4.2 Performance Testing

Once all the calculations had been performed to determine the performance specifications required for the prosthetic hand, a simpler version was simulated, keeping the gearmotor and reduction ratio unchanged, in order to verify the accuracy of the results.

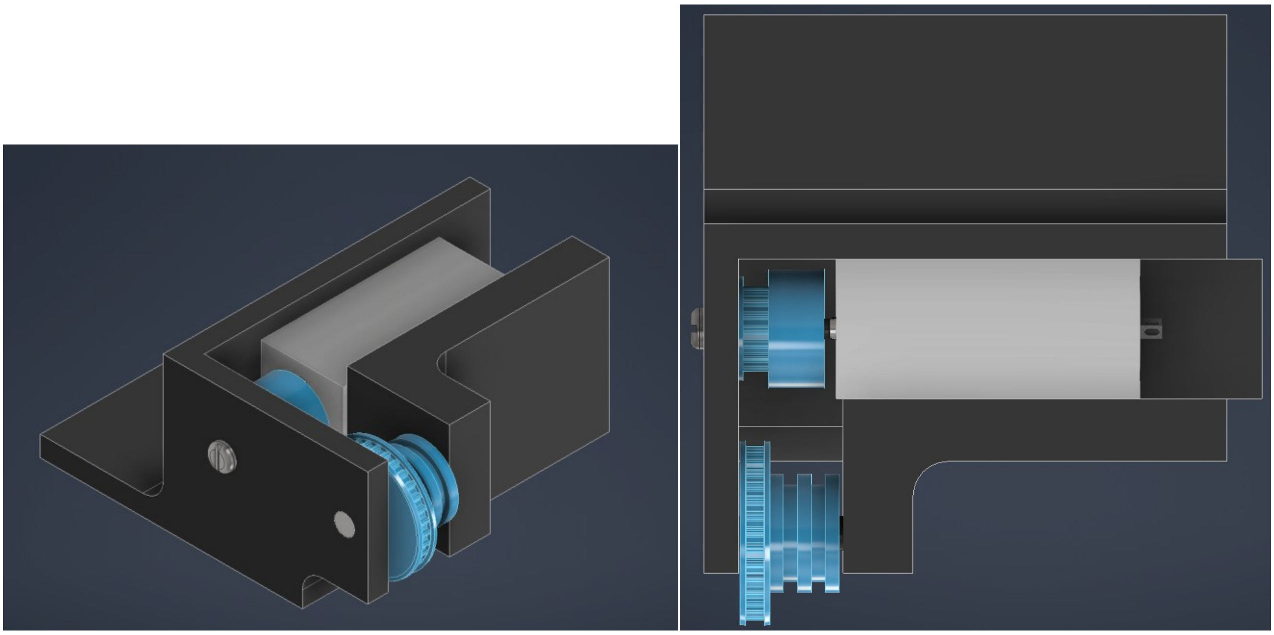

Figure 70: Side and front views of the test assembly

Figure 70 shows the test setup designed for this purpose. To replicate the same reduction system, since the bevel gears were not yet available at the time of the test, we opted for a reduction using a synchronous pulley with a 1:2 ratio, connected to the output shaft of the gearmotor. The figure shows the main frame designed to support the structure, which will be secured to a table using a vise at the rear end, so that the cable is free to move without obstruction. Next is the frame designed to house the motor, using the same technique as in the hand prototype, flanged at the end with two M1.6 screws. At the output, there are two pulleys designed to create the reduction system via a toothed belt; both pulleys were produced using filament 3D printing, while the other components were produced via powder bed fusion. For the synchronous belt stage, a T2.5 belt 120 mm long and 2 mm wide was selected; the driven pulley was then designed with a diameter of 25 mm and 32 teeth. The center distance between the two pulleys is 29.3 mm. The output pulley of the gearmotor is coupled via a snap-fit connection. The shaft is forced into a 3-mm hole, slightly deforming the cavity and ensuring a secure fit. The wheel is then mounted via a bushing on which it will rotate freely; this bushing is in turn flanged to the frame using an M3 screw. The driven pulley will be free to rotate on a 3.9 mm shaft, since a 4 mm steel shaft is not yet available, to ensure a 0.1 mm clearance that prevents friction from affecting the accuracy of the performance test. Finally, a string was attached to the pulley to replicate the string on the finger.

Figure 71: pulley winding speed test

As a first test, we conducted an experiment to verify the finger's closing speed. Calculations indicated that the cable would need to wind 32.2 mm in 0.5 seconds to fully close the finger.
For practical purposes, we conducted the test by rounding the value to 3.2 cm; based on a total cable length of 16 cm, the cable should have reached the mark on the wire after 2.5 seconds.
After several measurements taken by timing the process manually, the result was a no-load winding time of 0.5 seconds, while using a mass of 0.853 kg resulted in a time of 2.4 seconds.

Figure 72: torque test

A load greater than the set limit of 0.8 kg was used, completing the closure in a maximum of 2.4 seconds; this indicates a performance slightly better than expected. An additional test was conducted with 1.2 kg, but the system stalled halfway through the ascent, establishing a lower limit than that weight. During the load test, it was noted that the fully unwound cable had difficulty winding back up, as it slipped on the pulley. Starting with three turns of rope, enough friction was created to prevent the cable from slipping and ensure it gripped the pulley, thereby pulling the load upward.

These tests constitute an experimental trial to verify the set objectives. Due to problems with the 3D printers, it was not possible to carry out grip tests on various objects using the complete hand. These tests serve to validate the research conducted in this thesis, confirming its potential application in the fields of robotics and prosthetics. The next steps involve producing the fingers using resin 3D printing and assembling them, thereby enabling the hand to function and allowing the tests to be carried out.

The forthcoming tests will involve verifying the hand's bilateral grasping ability by grasping objects on both sides, ranging from large items such as a water bottle to smaller objects such as a pen or a sheet of paper, thereby demonstrating the precision of the grasp. Due to the large number of motors involved and their different functions, a setup with multiple power supplies will need to be created, as the rotation of the thumb will take place more quickly than the flexion of the fingers on the opposite side. A support will be created to which the wrist can be secured, in order to keep the hand in position and ensure the accuracy of the results. To achieve smoother, more precise and synchronised control, once these preliminary tests have been carried out, control electronics will be developed to resolve the issues listed, so that the functionality of the hand can be verified under continuous cycles.

Conclusions

The objectives set for this thesis were partially achieved, verifying the design and manufacturing feasibility of a bilaterally actuated robotic hand.

The concept behind this hand represents an innovative idea, distinct from all other robotic prosthetic hands currently available, as it breaks away from traditional anthropometric models. This work began with an idea developed by Engineer Emanuele Gruppioni, a researcher at the INAIL Prosthetics Center, who designed an initial functional two-finger prototype. Building on this, the finger concept was adapted to develop a fully functional hand capable of performing both palmar and dorsal grips, thereby eliminating the distinction between the palm and the back of the hand.

The feasibility study, which consisted of mechanical design using CAD software, fabrication via rapid prototyping and traditional CNC machining, and subsequent partial testing, showed that this type of actuator is feasible with certain design considerations and opens up potential future applications in the fields of robotics and prosthetics. In fact, in the first case, a drive of this type could prove useful, for example, in automation processes, while in the field of prosthetics, it would allow for a single hand usable by both right- and left-handed patients, or, an even more interesting alternative, a device that expands the grasping capabilities of the human hand within a prosthetic framework that prioritizes dexterity and functional recovery, even at the expense of natural movement.

However, since this was a project started from scratch, in terms of both design and the actuation system, the purpose of this thesis was to conduct a feasibility study on the design and actuation of the hand itself. Due to technical constraints and the challenges encountered, it was not possible to produce a fully functional prototype; however, it was verified that the main features, namely, the bilateral movement of the fingers and the rotation of the thumb from the palmar to the dorsal side, functioned as intended. This lays the groundwork for future work, based on a functional concept with dimensions comparable to those of an adult male hand. Furthermore, the development of dedicated electronics will allow for simpler and more functional actuation and will resolve some of the problems encountered, foremost among them the misalignment of the fingers during the reversal of motion, through the use of appropriate sensors.

In conclusion, we can state that this thesis has yielded excellent results in terms of mechanical design and actuation systems, enabling bilateral functionality in a robotic hand, a development that could serve as a starting point for further improvements and for use in robotic and prosthetic applications.

Bibliography

[1] D. Farina et al., “The Extraction of Neural Information from the Surface EMG for the Control of Upper-Limb Prostheses,” *IEEE TNSRE*, 2014.

[2] M. R. Cutkosky, “On Grasp Choice, Grasp Models, and the Design of Hands for Manufacturing Tasks,” *IEEE TRA*, 1989.

[3] T. Feix et al., “The GRASP Taxonomy of Human Grasp Types,” *IEEE Trans. Human-Machine Systems*, 2016.

[4] M. Catalano et al., “Adaptive Synergies for a Humanoid Robot Hand,” *IJRR*, 2014.

[5] A. Bicchi, V. Kumar, “Robotic Grasping and Contact: A Review,” *ICRA*, 2000.

[6] R. Deimel, O. Brock, “A Novel Type of Compliant and Underactuated Robotic Hand,” *IJRR*, 2016.

[7] C. Gosselin, F. Pelletier, T. Laliberté, “An Anthropomorphic Underactuated Robotic Hand with 15 DOF and a Single Actuator,” *ICRA*, 2008.

[8] L. Birglen, T. Laliberté, C. Gosselin, *Underactuated Robotic Hands*, Springer, 2008.

[9] C. Laschi et al., “Soft Robot Arm Inspired by the Octopus,” *Advanced Robotics*, 2012.

[10] A. M. Dollar, R. D. Howe, “The Highly Adaptive SDM Hand,” *IJRR*, 2010.

[11] H. In et al., “Exo-Glove: A Wearable Robot for the Hand with a Soft Tendon Routing System,” *IEEE Robotics & Automation Magazine*, 2015.

[12] S. Polygerinos et al., “Soft Robotic Glove for Combined Assistance and Rehabilitation,” *Robotics and Autonomous Systems*, 2015.

[13] A. Bicchi, “Hands for Dexterous Manipulation and Robust Grasping: A Difficult Road Toward Simplicity,” *IEEE Trans. Robotics and Automation*, 2000.

[14] A. Bicchi, V. Kumar, “Robotic Grasping and Contact: A Review,” *ICRA*, 2000.

[15] R. M. Murray, Z. Li, S. S. Sastry, *A Mathematical Introduction to Robotic Manipulation*, CRC Press, 1994.

[16] S. Cordella et al., “Literature Review on Needs of Upper Limb Prosthesis Users,” *Frontiers in Neuroscience*, 2016.

[17] D. Atkins et al., “Comprehensive Overview of Prosthetic Socket Design,” *Journal of Prosthetics and Orthotics*, 1996.

[18] D. Farina et al., “Man/Machine Interface Based on the Discharge Timings of Spinal Motor Neurons,” *Nature Biomedical Engineering*, 2017.

[19] K. Horch et al., “Artificial Sensory Feedback for Limb Prostheses,” *IEEE TBME*, 2011.

[20] F. Ilievski et al., “Soft Robotics for Chemists,” *Angewandte Chemie*, 2011.

[21] D. Dahiya et al., “Tactile Sensing—From Humans to Humanoids,” *IEEE Trans. Robotics*, 2010.

[22] E. Gruppioni, "From multi-jointed to over-jointed robotic prostheses and manipulators," *Bio-medical campus University of Rome*, 2019.